

1-1-2010

# The Development Of A Piezoelectric Fuel Injector For Diesel Engine

Kei S.A. Chiu  
Ryerson University

Follow this and additional works at: <http://digitalcommons.ryerson.ca/dissertations>

 Part of the [Mechanical Engineering Commons](#)

---

## Recommended Citation

Chiu, Kei S.A., "The Development Of A Piezoelectric Fuel Injector For Diesel Engine" (2010). *Theses and dissertations*. Paper 1283.

This Thesis is brought to you for free and open access by Digital Commons @ Ryerson. It has been accepted for inclusion in Theses and dissertations by an authorized administrator of Digital Commons @ Ryerson. For more information, please contact [bcameron@ryerson.ca](mailto:bcameron@ryerson.ca).

**THE DEVELOPMENT OF A PIEZOELECTRIC FUEL INJECTOR  
FOR DIESEL ENGINE**

by

Anthony Siu Kei Chiu

Bachelor of Engineering, Ryerson University, 2008

A thesis

presented to Ryerson University

in partial fulfillment of the  
requirements for the degree of  
Master of Applied Science  
in the Program of  
Mechanical Engineering

Toronto, Ontario, Canada, 2010

©Anthony Siu Kei Chiu, 2010

## **Author's declaration**

I hereby declare that I am the sole author of this thesis.

I authorize Ryerson University to lend this thesis to other institutions or individuals for the purpose of scholarly research.

---

Anthony Siu Kei Chiu

I further authorize Ryerson University to reproduce this thesis by photocopying or by other means, in total or in part, at the request of other institutions or individuals for the purpose of scholarly research.

---

Anthony Siu Kei Chiu

# **Abstract**

The Development of a Piezoelectric Fuel Injector for Diesel Engine

Master of Applied Science, 2010

Anthony Siu Kei Chiu

Mechanical Engineering, Ryerson University

Stringent emission levels challenge automotive industries to come up with innovative ways of improving existing technologies. In advancing diesel engine technology, the key factor lies in further developing a piezoelectric fuel injector in the common-rail system. A direct acting piezoelectric fuel injector prototype for the common-rail system was developed to preserve the lifetime of the actuator, achieve an adequate needle lift, and response quickly. Through analytical work and ANSYS simulations, problems were encountered on the initial designs. These problems were overcome with successive design improvements. Simulations and analytical estimations provide evidence on the potential performance on these improvements. After design iterations, a prototype was fabricated according to the final design. Experimental work further validated that the fuel injector designed is capable of meeting the requirements. Problems with the test results are discussed for further improvements on the design.

# Acknowledgement

I want to thank the following. The two supervisors who provided me with valuable guidance and advice through the duration of this project:

Dr. Siyuan He (Ryerson University)

Dr. Ridha Ben Mrad (University of Toronto)

Also, the technical officer who showed great patient throughout the process of designing and fabricating the prototype:

Mr. Joseph Amankrah (Ryerson University)

Last but not least, my family who encouraged and supported me during this period:

Mr. Alfonso Chiu

Mrs. Teresa Chiu

Ms. Fiona Chiu

Rev. Hoang Ho

# Table of Contents

<b>Author’s declaration</b> .....	<b>ii</b>
<b>Abstract</b> .....	<b>iii</b>
<b>Acknowledgement</b> .....	<b>iv</b>
<b>Table of Contents</b> .....	<b>v</b>
<b>List of Figures</b> .....	<b>vii</b>
<b>List of Tables</b> .....	<b>ix</b>
<b>Nomenclature</b> .....	<b>xi</b>
<b>Chapter 1 Introduction</b> .....	<b>1</b>
1.1 Background .....	1
1.2 Fuel Injector Concept.....	3
1.2.1 Piezoelectric Actuator .....	4
1.2.2 Servo Circuit Fuel Injectors .....	6
1.2.3 Direct Acting Fuel Injectors .....	7
1.3 Existing Fuel Injectors .....	8
1.3.1 Denso.....	8
1.3.2 Midé .....	10
1.3.3 Delphi.....	12
1.4 Thesis objectives.....	13
<b>Chapter 2 Fuel Injector Designs</b> .....	<b>15</b>
2.1 Generation 1 Concept .....	15
2.1.1 Objective .....	15
2.1.2 Setup.....	15
2.1.3 Assembly Procedures .....	17
2.1.4 Limitations .....	18
2.2 Generation 2 Concept .....	19
2.2.1 Objective .....	19
2.2.2 Setup.....	19
2.2.3 Assembly Procedures .....	23

2.2.4 Limitations .....	25
2.3 Generation 3 Concept .....	25
2.3.1 Objective .....	25
2.3.2 Setup.....	25
2.3.3 Assembly Procedures .....	28
2.3.4 Limitations .....	30
<b>Chapter 3 Injector Components Design .....</b>	<b>31</b>
3.1 Piezoelectric Multi-layer Stacked Actuator .....	31
3.2 Telescopic Stack Actuator .....	34
3.3 Disc Spring.....	35
3.4 Needle Design.....	37
3.5 Fuel Pressure Balance .....	38
<b>Chapter 4 Analytical Models .....</b>	<b>41</b>
4.1 Generation 1 Injector .....	41
4.1.1 Precompression .....	41
4.1.2 Needle Lift Estimation .....	44
4.2 Generation 2 Injector .....	46
4.2.1 Mechanical Amplifier Analysis .....	47
4.3 Generation 3 Injector .....	50
4.3.1 Hydraulic Amplifier .....	50
4.3.2 Precompression .....	51
4.3.3 Needle Lift Estimation .....	56
<b>Chapter 5 Simulations .....</b>	<b>59</b>
5.1 Generation 1 Injector .....	59
5.1.1 Static Simulation .....	59
5.1.2 Dynamic Simulation.....	64
5.2 Generation 2 Injector .....	66
5.2.1 Static Simulation .....	66
<b>Chapter 6 Design of Experiments.....</b>	<b>71</b>
6.1 Prototype and Fixture Design .....	71
6.1.1 Design .....	71
6.1.2 Assembly.....	73

6.2 Prepressed Piezoelectric Actuator Performance Test .....	80
6.3 Actuator with Hydraulic Amplifier Test.....	82
6.4 Hydraulic Amplifier Performance Test .....	84
6.5 Piezoelectric Injector Static Test .....	86
<b>Chapter 7 Experimental Results .....</b>	<b>89</b>
7.1 Prepressed Piezoelectric Actuator Performance Result.....	89
7.2 Actuator with Hydraulic Amplifier Result .....	90
7.3 Hydraulic Amplifier Performance Result.....	93
7.4 Piezoelectric Injector Static Result.....	96
<b>Chapter 8 Conclusions and Recommendations for Future Work .....</b>	<b>98</b>
<b>Appendix A Technical Drawings.....</b>	<b>102</b>
<b>References .....</b>	<b>116</b>

## List of Figures

Figure 1 Solenoid injector in operation [2].....	3
Figure 2 Piezoelectric stack with electrodes.....	5
Figure 3 Delphi's direct acting fuel injector [3].....	7
Figure 4 Configuration of piezoelectric fuel injector from Denso [4].....	9
Figure 5 Configuration of piezoelectric unit injector from Midé [8] .....	10
Figure 6 Mechanical amplified piezoelectric actuator from Midé [7].....	11
Figure 7 Cross-sectional drawing of generation 1 injector.....	16
Figure 8 Generation 1 injector component connections diagram .....	17
Figure 9 Cross-sectional drawing of generation 2 injector.....	20
Figure 10 Initial idea of mechanical amplifier indicating input forces and output displacement.	21
Figure 11 Final modification of mechanical amplifier .....	22
Figure 12 Generation 2 injector component connections diagram .....	24
Figure 13 Cross-sectional drawing of generation 3 injector.....	26
Figure 14 Cross-sectional view of the hydraulic amplifier.....	27

Figure 15 Generation 3 injector component connections diagram .....	29
Figure 16 Characteristic plot of piezoelectric actuator and spring .....	32
Figure 17 Cross sectional view of single disc spring with references .....	35
Figure 18 Common diesel injector nozzle design.....	38
Figure 19 Fuel pressure balance diagram .....	39
Figure 20 Pre-compression of stack actuator.....	42
Figure 21 Simplified schematic for estimating the extra prepress distance needed to overcome the fuel pressure for design 1 .....	43
Figure 22 Schematic of the interface plate indicating forces exerted by other components in the system .....	44
Figure 23 Gen 2 injector serpentine spring diagram.....	47
Figure 24 Gen 2 injector input force and reaction forces shown on beam .....	48
Figure 25 Gen 2 injector serpentine spring geometry.....	48
Figure 26 General hydraulic amplifier diagram.....	50
Figure 27 Simplified schematic for compressing the return disc spring at load step 2 for design 3 .....	52
Figure 28 Simplified schematic for generating sealing force at load step 3 for design 3.....	53
Figure 29 Forces acting on hydraulic amplifier of design 3 .....	56
Figure 30 Gen 1 injector component diagram in ANSYS .....	60
Figure 31 Gen 1 injector under sealed state simulated in ANSYS .....	62
Figure 32 Gen 1 injector under lifting state at high pressure case simulated in ANSYS .....	63
Figure 33 Gen 1 injector under lifting state at low pressure case simulated in ANSYS .....	64
Figure 34 Gen 1 injector modal analysis fixed locations.....	65
Figure 35 Geometrical model of the serpentine spring built in ANSYS .....	67
Figure 36 Gen 2 injector geometrical model done in ANSYS .....	68
Figure 37 Gen 2 injector static analysis with low pressure fuel in ANSYS .....	69
Figure 38 Gen 2 injector static analysis with high pressure fuel in ANSYS .....	70
Figure 39 Isometric and cross-sectional drawing of prototype with test rig.....	72
Figure 40 Diagram showing all the components in the fuel injector prototype.....	73
Figure 41 Diagram showing all the components of the hydraulic amplifier .....	75
Figure 42 Cross-sectional drawing of the hydraulic amplifier .....	75

Figure 43 Capacitive sensor mounting diagram for location 1 .....	79
Figure 44 Capacitive sensor mounting diagram for location 2 .....	80
Figure 45 Presentation of how equipments are connected for actuator performance test .....	81
Figure 46 Physical arrangement of the prototype and test equipments for actuator test .....	82
Figure 47 Physical arrangement of the prototype and test equipments for hydraulic amplifier test with actuator.....	83
Figure 48 Hydraulic amplifier performance test configuration .....	84
Figure 49 Presentation of how equipments are connected for hydraulic amplifier performance test.....	85
Figure 50 Physical arrangement of the prototype and test equipments for hydraulic amplifier performance test.....	86
Figure 51 Injector static test configuration .....	87
Figure 52 Presentation of how equipments are connected for injector static test.....	87
Figure 53 Graphical test result of actuator performance .....	90
Figure 54 Graphical test result of actuator with hydraulic amplifier showing the input and output displacement .....	91
Figure 55 Graphical test result of actuator with hydraulic amplifier showing the amplification factor .....	92
Figure 56 Graphical test result of average input and output displacement of hydraulic amplifier.....	95
Figure 57 Graphical test result of hydraulic amplifier showing the amplification factor.....	95

## List of Tables

Table 1 Specifications of two sample stack actuator from Sensor Technology .....	5
Table 2 Dimensions of actuators, coupler, and needle for design 1 .....	46
Table 3 Material properties used in estimating needle lift for design 1.....	46
Table 4 Estimated results using analytical model for design 1.....	46
Table 5 Dimensions of the serpentine spring for design 2.....	49
Table 6 Results of the serpentine spring analytical model for design 2 .....	49
Table 7 Quantities used to estimate precompression for design 3 at HP .....	55

Table 8 Overall compression of the actuator, prepressed disc spring, and return disc spring at HP .....	55
Table 9 Quantities and overall compression of various components at LP .....	55
Table 10 Dimensions and properties of the stack actuator in design 3.....	58
Table 11 Estimated results using analytical model for design 3.....	58
Table 12 Simulated results using ANSYS .....	64
Table 13 Simulated results of serpentine spring.....	67
Table 14 Gen 2 injector tabulated static simulation results from ANSYS .....	68
Table 15 Bill of material for hydraulic amplifier.....	74
Table 16 Bill of material of all the components for the fixture .....	77
Table 17 List of componenets required for actuator performance test .....	80
Table 18 Piezoelectric actuator properties [5] .....	89
Table 19 Piezoelectric actuator performance test results under various preloads .....	89
Table 20 Actuator with hydraulic amplifier test result under preloads of 1000 N and 2000 N....	90
Table 21 Actuator with hydraulic amplifier test result under preloads of 3000 N and 4000 N....	91
Table 22 Five sets of results of the hydraulic amplifier test.....	93
Table 23 Average of input distance, output distances, and amplification ratio of amplifier test .	94

## Nomenclature

$d_{33}$	Piezoelectric strain constants in the 33 direction
$D_{CI}$	Inner diameter of the coupler element
$D_{CO}$	Outer diameter of the coupler element
$D_{II}$	Inner diameter of the inner stacked actuator
$D_{IO}$	Outer diameter of the inner stacked actuator
$D_{OI}$	Inner diameter of the inner stacked actuator
$D_{OO}$	Outer diameter of the outer stacked actuator
$D_{nb}$	Diameter of the bottom portion of the needle
$D_{nt}$	Diameter of the top portion of the needle
$E$	Young's modulus
$EDC$	Electronic diesel control
$L_A$	Actuator length
$L_C$	Length of the tubular portion of the coupler element
$L_{nt}$	Length of the top portion of the needle
$L_{nb}$	Length of the bottom portion of the needle
$t_L$	Layer thickness of the stacked actuator
$\epsilon_{33}^T$	Relative Dielectric Constant
$\epsilon_0$	Vacuum Permittivity

# Chapter 1 Introduction

## 1.1 Background

The automotive industry is constantly challenged to overcome the demands of lower engine emission level, more efficient fuel economy, and quicker vehicle response time with innovative designs and technologies. These demands are especially critical in the area of the internal combustion engine, with the use of diesel fuel as the driving agent criticized for loud noise and dirty emissions. To meet these challenges, a recent idea that has been implemented is to separate the pressure generation system from the fuel-injection system. To accomplish this, the common-rail system was introduced into the automotive sector in 1997 [1]. Soon after, in 2000, a vehicle equipped with the common-rail system, in conjunction with the piezoelectric actuator, was introduced. The implementation of these technologies into diesel engines had brought many breakthroughs in meeting stringent emission level and power output standards.

The advantage of using the common-rail system lies in the ability to vary injection pressure and timing over a broad scale [2]. High injection promotes a very fine spray atomization resulting in emission reduction [3][4]. The common-rail system is controlled by the electronic diesel control (EDC) which allows flexible control of actuating mechanisms and sub-systems to produce an optimized combustion. The EDC enables fuel injectors to spray fuel into the combustion chamber multiple times within one combustion cycle. This multi-injection feature greatly reduces the noise level produced by the combustion and also aids in mixing of fuel particles and compressed air. Without the multi-injection feature, fuel is sprayed all at once into the combustion chamber causing a rapid and high pressure rise [2]. When fuel is injected

before the main injection, fuel particles can mix better with the compressed air in the chamber producing a more complete combustion with less unwanted particulates. Post injections can also be applied to reduce soot emission by reburning the soot particles with small amounts of diesel fuel. These elements have led diesel engines to achieve the global demands for cleaner emission, higher fuel efficiency, and faster response time.

Within the common-rail system, a heavy emphasis is placed on the fuel injector especially on the responsiveness of the actuator because it directly affects the overall performance of the engine. Not only within the area of the diesel engine but also other areas such as gasoline and hydrogen engines are applying piezoelectric actuators in the fuel injector to achieve a quicker response [1].

This project focuses on the design of the fuel injector using a piezoelectric actuator within the common-rail system in a diesel engine. A piezoelectric actuator poses high force generation and fast response time; thus, it can be a great asset to the fuel injector if implemented successfully. With the piezoelectric actuator and EDC, a high number of multiple injections within a combustion cycle can be achieved allowing an efficient combustion to occur. An efficient combustion emits cleaner exhaust and generates higher power output [2]. Multiple injections also lower the noise level generated by the combustion because of a gradual rise in temperature as opposed to a sharp rise [2]. The following session provides a summary of fuel injectors and the operational mechanisms that are currently in this field of research. The requirements to be achieved for this design project are presented at the end of the chapter.

## 1.2 Fuel Injector Concept

The current fuel injectors that are being used in the common-rail system consist of several basic components. Figure 1 shows the components of these injectors in 3 positions: a) sealed, b) lifting, and c) closing.

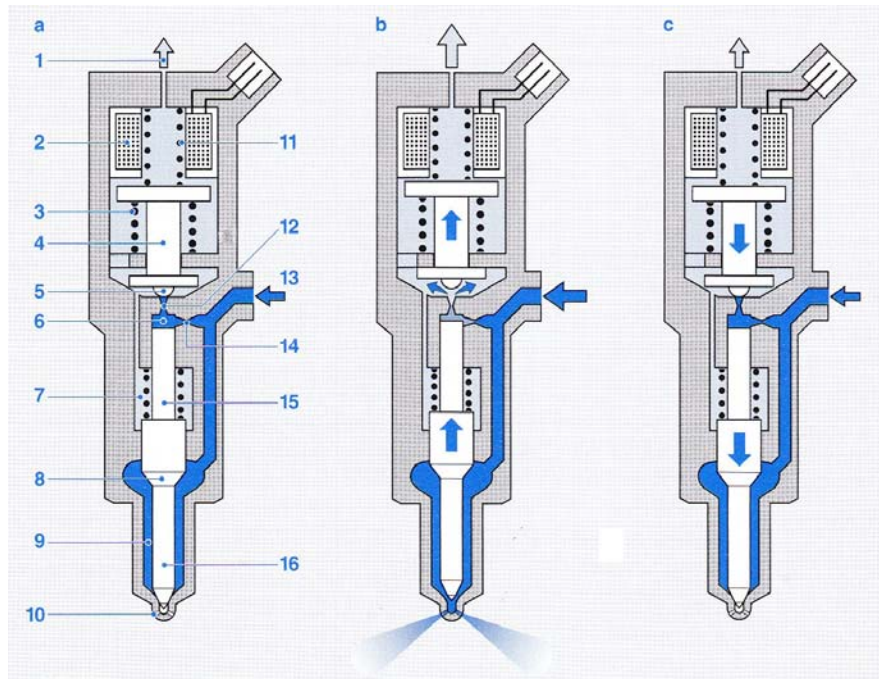


Figure 1 Solenoid injector in operation [2]

Fuel return line (1) is where unused fuel returns back to the fuel tank. The pressure within the fuel return line is lower than that of the high-pressure fuel line (13). With the aid of the overstroke spring (3), the solenoid coil (2) pulls the solenoid armature (4) in the upward direction once it is energized as shown in b). The valve ball (5) is attached to the solenoid armature, and as the armature lifts, the valve ball is no longer in contact with the outlet restrictor (12). The high pressure fuel escapes through the outlet restrictor causing the valve-control chamber (6) to depressurize. Though the high pressure fuel continues to enter the pressure chamber through the inlet restrictor (14), pressure difference exists due to the small cross-sectional area of the inlet

restrictor. As the armature is lifted, the solenoid valve spring (11) is compressed in the upward direction. Depressurizing the chamber causes the valve plunger (15) to be pushed by the high pressure fuel within the chamber volume (9) at the pressure shoulder of nozzle needle (8). This high pressure fuel force overcomes the downward force provided by the nozzle spring (7). Once the nozzle needle (16) is lifted, high pressure fuel is sprayed from the injection orifice (10) into the combustion chamber.

Once the solenoid coil is de-energized, the solenoid valve spring overcomes the force from the overstroke spring and seals the outlet restrictor with the ball valve. Once this occurs, the pressure within the control chamber builds up again through the high pressure fuel flow at the inlet restrictor. As the pressure within the control chamber builds up, the needle assembly is sent in the downward position where the injection orifice is sealed shut.

The fuel injector shown above is solenoid based. There are other fuel injectors that use a similar configuration but the solenoid actuator is replaced with a piezoelectric actuator. Other than this usual configuration of making use of the fuel pressure to lift the needle, there are other injectors that use a different configuration to perform the same task. Following sections will discuss the advantageous characteristics of piezoelectric actuator over the solenoid actuators and the available types of configurations available for fuel injectors.

### **1.2.1 Piezoelectric Actuator**

The piezoelectric actuator is a smart material that undergoes mechanical deformation when an electrical load is applied. The type of piezoelectric actuator that is used for fuel injection is the multi-layer stack, which consists of many thin layers of piezoelectric material bonded together, as depicted in Figure 2. The stack actuator comes in prismatic form as shown,

circular cross-section, and ring cross-section. Each layer is made of lead zirconate titanate (PZT), a ceramic solid material.

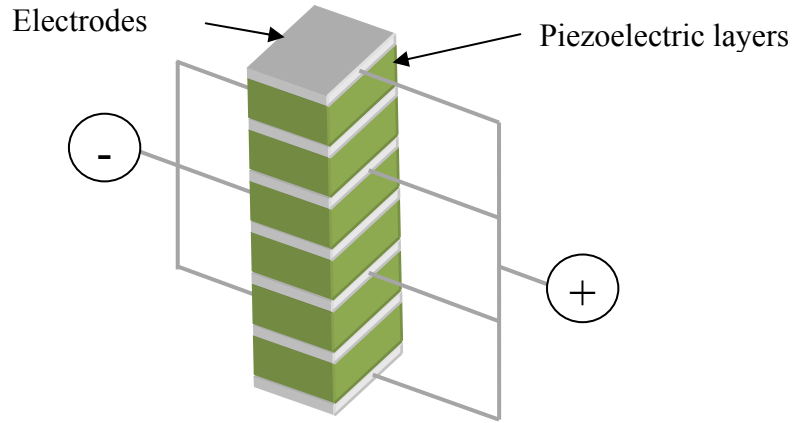


**Figure 2 Piezoelectric stack with electrodes**

Between the piezoelectric layers lie the electrodes where current passes through to generate the electrical stress on the actuator. In this stacked configuration, the displacements of each of the piezoelectric layers are superimposed together. The force generated is very high, and the response time is very fast. The following table shows some of these specifications of two sample stack actuators from SensorTech Ltd [5].

**Table 1 Specifications of two sample stack actuator from Sensor Technology**

Part No.	Area	Height	Displacement @ 200V	Blocked Force @ 200V	Response Time
	mm <sup>2</sup>	mm	μm	N	μs
SJ12-15-1010-00	10x10	15	22.4	6000	100
SJ12-30-1010-00	10x10	30	44.8	6000	100

Even though the displacements are added together through the stacked configuration, the stack still suffers from producing small stroke. However, the superior characteristics of the response time and force generation are promising attributes for the replacement of the solenoid actuators.

Other than suffering from the weakness of small displacement, the maximum stress that these actuators can withstand is limited. Even though the maximum stress that this ceramic material can take is 250 MPa, the actual compressive stress that the actuator can withstand is only 20 to 30% of the maximum mechanical limit [6]. At this load limit, the actuator starts to depolarize, at which the actuator starts losing the ability to deform under electrical stress. The tensile stress that a non-preloaded actuator can take is 5 to 10% of the compressive load limit before depolarization occurs. To prevent the actuator from reaching these limits, preload conditions are usually applied. These conditions put the actuator in its compression state even at the maximum actuated state.

### **1.2.2 Servo Circuit Fuel Injectors**

The usual configuration that the fuel injector uses is the hydraulic servo circuit. The solenoid fuel injector (Figure 1) shown above is of this type. This is widely used because the actuator needed does not have to be a high force actuator. Actuation of the injector is dependent on the hydraulic pressure balance between the end of the needle and the control chamber. Without energizing the actuator, the valve seals the control chamber causing the control chamber to be pressurized. The pressurized control chamber pushes the needle downward because of the larger area at the plunger relative to the needle end. When the actuator is energized, the valve is lifted and depressurizes the control chamber causing the fuel under the needle shoulder to push the needle in the upward direction.

The speed of the needle is dependent on the rate of flow through the restrictor. The needle speed is generally faster with a higher rail pressure. Since the needle is controlled by fuel pressure, the needle opening fluctuates hence lowering the consistency of fuel sprayed. Because the needle is directly controlled by the hydraulic pressure balance within the circuit instead of

directly by the actuator, there is accumulation of needle actuation time. Not only is there a lag in response time from the actuator, but there is also a larger delay from pressurizing and depressurizing the control chamber before the needle starts to move. Although the needle actuation time can be shortened with the quick response of the piezoelectric actuator, the hydraulic servo system still contributes to the time accumulation.

### 1.2.3 Direct Acting Fuel Injectors

To overcome the lag time from the hydraulic servo circuit, another method for actuation is needed to replace the current configuration. However, in order to replace this system, an actuator producing large forces is required. The actuator that is suitable for this is the piezoelectric actuator. Because the actuation is directly driven by the actuator itself instead of the pressure balance, this type of injectors is categorized as direct acting fuel injectors.

One of the direct acting fuel injectors is developed by Delphi [3] as shown in Figure 3.

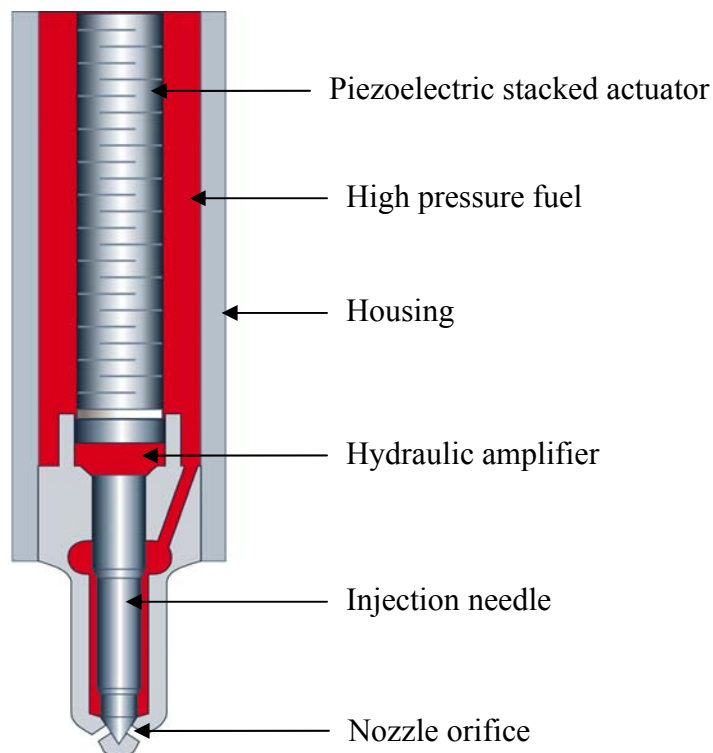


Figure 3 Delphi's direct acting fuel injector [3]

To overcome the need of large force generation, piezoelectric actuator is chosen over the solenoid actuator in the direct acting configuration. The hydraulic amplifier is used to amplify the stroke generated by the actuator. With this mechanism in place, the force at the needle end is reduced as a trade-off for larger displacement.

### **1.3 Existing Fuel Injectors**

With piezoelectric actuators more readily available, many companies are implementing this actuator in the fuel injector application. Out of all the injectors available, there are three that are more distinct in design and achievement. This section will summarize what these injectors can achieve. Through the achievements of these designs, the requirements and goals of the current design project are established.

#### **1.3.1 Denso**

The piezoelectric fuel injector from Denso is capable of achieving up to 5 injections per combustion cycle. This injector is part of the common-rail system functioning under pressure up to 180 MPa. This piezoelectric injector was evaluated in comparison with the solenoid counterpart. Both injectors used the hydraulic servo circuit configuration. The actuators controlled the pressure-balanced control valve to vary the pressure in the control chamber as shown in Figure 4.

By replacing the solenoid actuator with the piezoelectric actuator, the delay from the start of electronic activation to the start of mechanical response reduced from 0.4 ms to 0.1 ms.

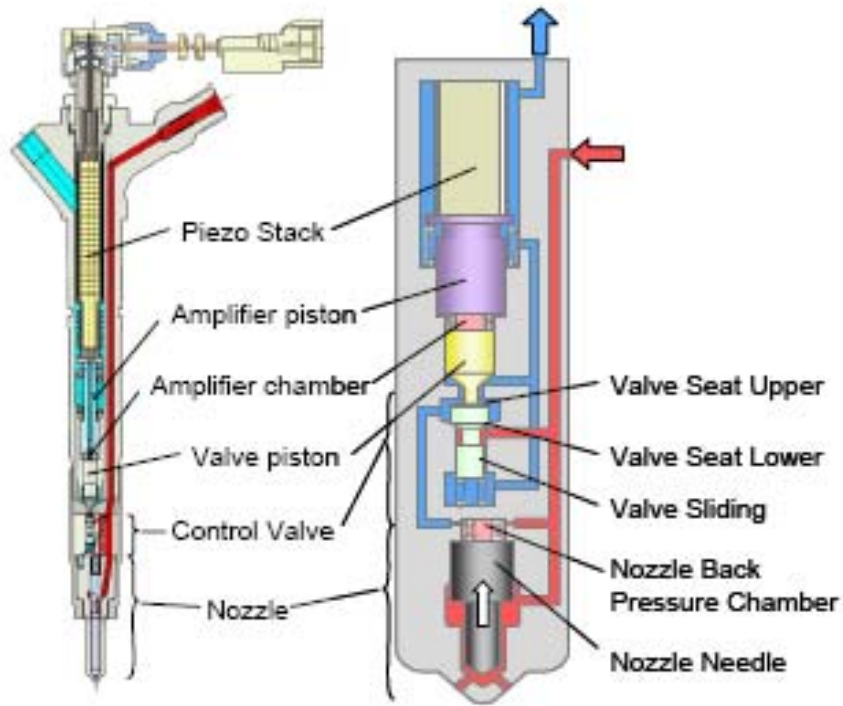


**Figure 4 Configuration of piezoelectric fuel injector from Denso [4]**

Because of this improvement, precise injection quantity, timing control, and finer spray atomization were achieved. Faster response time allowed more injections with smaller quantity and closer interval between each spray. Fast lifting of the nozzle promoted better spray penetration in the combustion chamber. This was due to the fast lift of the needle resulting nozzle choking duration to be minimal with a speed of 1.2 m/s. With these achievements from the piezoelectric fuel injector, the engine performance was improved in emission level and maximum power and torque output. Power increased from 110kW to 130 kW. Torque increased from 310 Nm to 400 Nm. Because of the smaller delay achieved by the piezoelectric injector, a larger number of multi-injections relative to the solenoid counterpart could be potentially achieved.

### 1.3.2 Midé

The piezoelectric fuel injector designed by Midé was made to be used with unit injector system instead of the common-rail system. However, this is worth noticing because of the design of the mechanical amplifier [7]. Figure 5 shows the schematic of the injector.

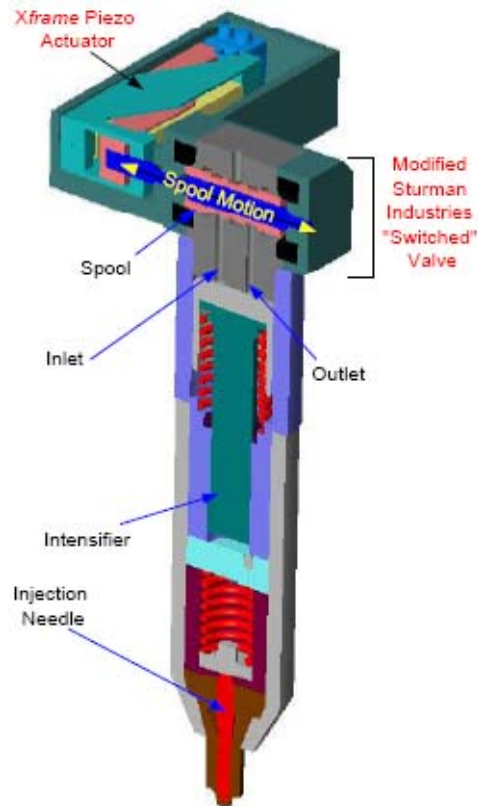


**Figure 5 Configuration of piezoelectric unit injector from Midé [8]**

The actuator controls the motion of a spool which terminates or activates oil in pushing the needle to sealed or opened position through an intensifier. The mechanical amplifier uses an X-frame to increase the stroke of 2 stacked actuators (5 x 5 x 50 mm each) as shown in Figure 6. One of the piezoelectric stacks is attached to the rigid housing and the flexure; the other piezoelectric stack is attached to the moving frame and the same flexure. The flexure is fixed as a cantilever at the rigid housing on the right-hand side. During actuation, both piezoelectric stacks extend longitudinally.

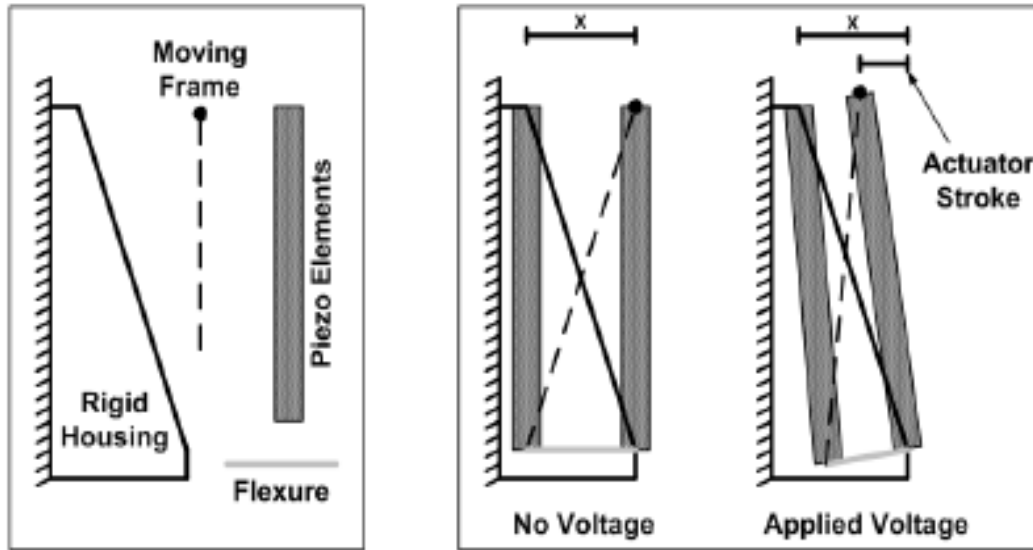


Figure 6 Mechanical amplified piezoelectric actuator from Midé [7]

The stack on the left causes the cantilevered flexure to rotate counter-clockwise causing the top of the stack on the right to move left. Since the stack on the right is energized also, the top of the stack on the right move further to the left with the elongation.

This mechanical amplifier was able to perform with an amplification factor of 5.3. The blocking force decreased to 66 N from 1000 N. The reduction of force was due to the way the actuator is mounted providing a rotational and bending force instead of a longitudinal linear force from the actuator. With this trade-off of force, the actuator was able to displacement 800  $\mu\text{m}$  of free displacement and 480  $\mu\text{m}$  against a component with a stiffness of 55 N/m. Potential improvement to this mechanical amplifier is to use the linear stroke for actuation. A mechanical amplifier with fewer components can potentially reduce the time delay between interactions between them thus increasing the responsiveness. Although not implemented into fuel injector, amplified piezoelectric actuator (APA) showed great potential for fuel injector application using mechanical amplifiers [9].

### 1.3.3 Delphi

A direct acting piezoelectric fuel injector (Figure 3) was developed by Delphi. This injector uses the piezoelectric actuator to drive the needle to sealed or opened position directly. A hydraulic amplifier is in place to increase the small stroke from the actuator by using the area difference from the input and output pistons. The output force generated is much less as a result of this trade-off.

This fuel injector was designed to be used as a part of the common-rail system showing that it is possible to use the force generated by the piezoelectric actuator to overcome the force from the high pressure fuel. This direct actuation would further enhance the response time of the injector. Using piezoelectric actuator over solenoid actuator shortens the delay of the actuator response to the electronic activation. Using direct actuation over servo circuit shortens the delay from the usual four steps (actuation of piezo, opening of servo valve, depressurizing control chamber through restricted outlet, and lifting of the needle) down to one single step (lifting of the needle by the mechanically amplified actuator). Along with the shortened delay, a high maximum needle speed of 3 m/s was achieved.

To utilize the actuator force to its full potential, Delphi's fuel injector used "de-energize to inject" configuration as suppose to "energize to inject". As the name suggests, "de-energize to inject" literally means that the fuel is injected as the actuator is de-energized. This implies that the piezoelectric actuator is energized 95% of the injector service life to seal the injector [10]. To seal the injector without leakage, relatively high voltages are applied to the actuator. By doing this, electrochemical migration of the electrodes in the actuator may short circuit with the moisture. In this configuration, piezoelectric actuator drains more power from the system to stay in the sealed state. However, in the "energize to inject" configuration, if piezoelectric actuator is

to maintain at a high negative voltage for a prolonged period of time, depolarization occurs. In order to use “de-energize to inject” configuration, Delphi developed an innovative way to control the actuator to minimize the voltage needed to maintain the injector at the sealed state helping the injector to maximize its lifetime [11].

## **1.4 Thesis objectives**

By gathering specifications and performance data from the fuel injectors developed by other companies, the current fuel injectors possess a few flaws. The servo circuit fuel injector design does not effectively use the high force generated by the piezoelectric actuator; thus, the response time of the actuator can still be improved. The direct acting fuel injector design improves the response time by directly controlling the needle with the actuator; however, it runs into the problem of reducing the lifetime of the actuator by charging the actuator 95% of the time. The objective for this project is to design a piezoelectric fuel injector that is capable of utilizing the high force generated by the piezoelectric actuator effectively to improve the response time and preserving the lifetime of the actuator. The fuel injector designed in this project is aimed to achieve the following requirements:

- Direct acting
- “Energize to inject” configuration
- 300  $\mu\text{m}$  maximum actuation stroke
- Operational fuel pressure in the range of 20 to 200 MPa
- 0.1 ms response time

A direct acting fuel injector eliminates the slow delay from the servo circuit configuration and greatly enhances the responsiveness of the injector. With a fast response time, the injector is

expected achieve a high number of injections per combustion cycle. The fast actuation speed of the allows more fuel to enter the combustion chamber in the same amount of lift time and also atomized fuel to penetrate into the combustion chamber better. As mentioned before in the Denso piezoelectric fuel injector servo circuit design, the achieved response time is 0.1 ms. Without the delay caused by the pressurization of the fuel reservoir, this response time is achievable with the direct acting design.

Because fuel injectors are in sealed state 95% of the injector service life as mentioned previously, it is advantageous to only energize the piezoelectric actuator during injection phase [10]. With the use of “energize to inject” configuration, the fuel injector is aimed to extend the lifetime of the piezoelectric actuator.

The current popular diesel injection system incorporates the common rail system featuring accumulation of fuel pressure from 20 to 200 MPa [2]. High fuel pressure also benefits the injection system by spraying fuel out of the nozzle quicker; thus, the maximum lift can be less.

Though the maximum actuation stroke can be decreased with the reasons given above, other literature suggests that the needle lift is around 300 to 400  $\mu\text{m}$  [12]-[14]. This is also congruent with the lifting displacement as shown by piezoelectric fuel injector developed by Denso. Therefore, the chosen needle lifting is 300  $\mu\text{m}$ . This poses a problem for piezoelectric actuator because of the limited displacement generated by this type of actuator.

# Chapter 2 Fuel Injector Designs

## 2.1 Generation 1 Concept

### 2.1.1 Objective

The idea of increasing the stroke of a piezoelectric actuator without using an amplifier was to use a cascaded configuration of two piezoelectric actuators. The cascaded design involved a larger ring stack actuator housing a smaller ring stack actuator with a coupler element in between them similar to a telescope [15]. This design aimed to achieve a prepressed condition through the use of a set of disc spring to extend the lifetime of the actuator.

### 2.1.2 Setup

Generation 1 injector, Figure 7, uses the telescopic design to increase the stroke of the actuator. This configuration was estimated to displace twice the amount of a single actuator. Steel was chosen to be the material used for the coupler to go against deformation initiated by the actuators. Disc springs were chosen due to the confined space. The interfacing plate acts as a connection component between the disc springs, inner actuator, and needle. Because of the requirement to design this injector with the configuration of “energize to inject”, the needle is situated inside the inner actuator. Because of the long length of the actuator, the needle is also very long. In order to prevent buckling, the upper portion of the needle is larger in diameter than that of the lower portion. High pressure fuel is filled in the nozzle housing and is kept from entering into the actuator area through the contact between the needle and the bottom end cap. An inlet, for feeding high pressure fuel, is made in the nozzle housing.

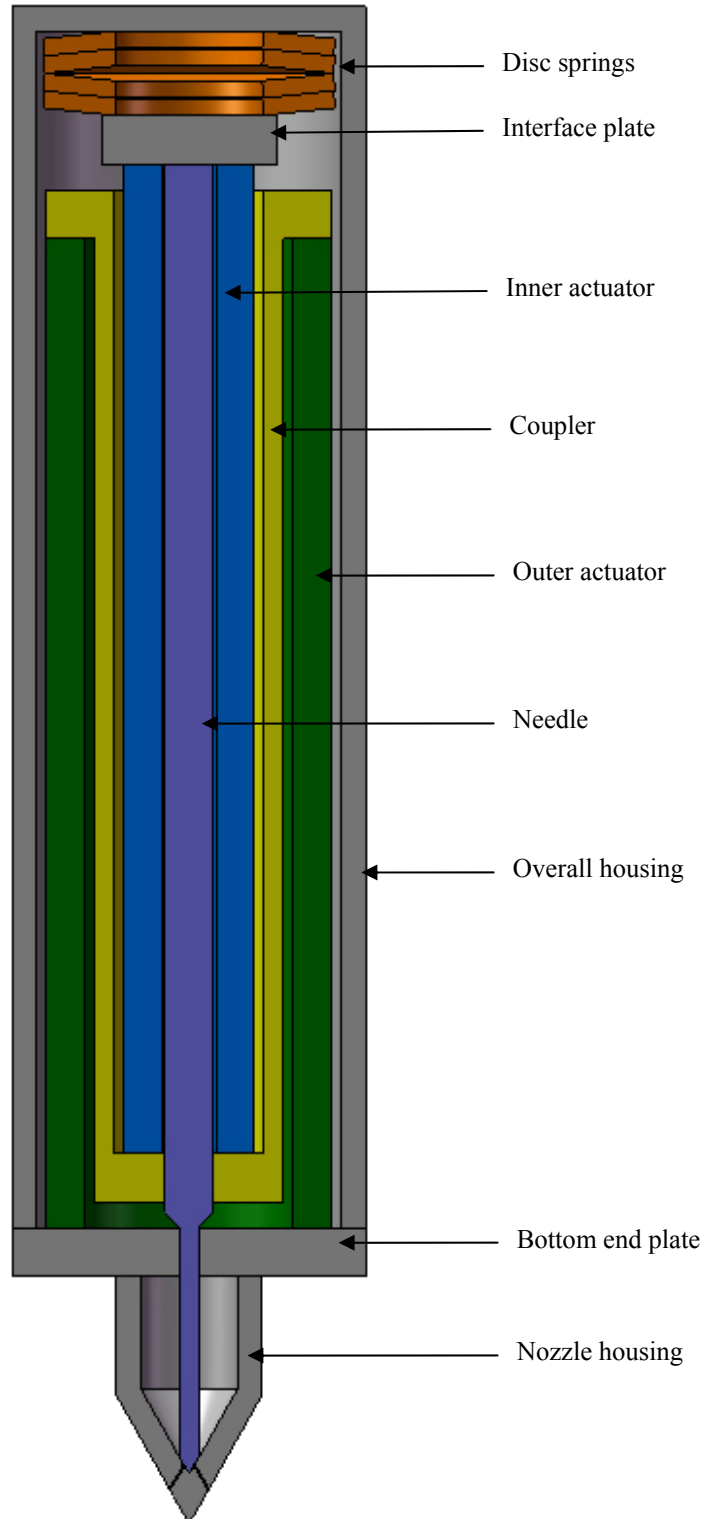


**Figure 7 Cross-sectional drawing of generation 1 injector**

In this version of injector, the fixed components are the overall housing, bottom plate, and nozzle housing. To initiate injection, the piezoelectric actuators are energized and the accumulated displacement is located at the interface plate. The actuator compresses the set of disc springs while lifting up the needle. Thus, fuel is injected into the combustion chamber. Operation terminates as the actuator is de-energized and is compressed back into the sealed state through the set of disc spring. The disc springs also push back the needle back to the sealed state.

### 2.1.3 Assembly Procedures

To clarify which components are connected together and which ones are stationed components, Figure 8 shows the connection between each component followed by the assembly sequence. Components that are in light blue are the stationary parts.

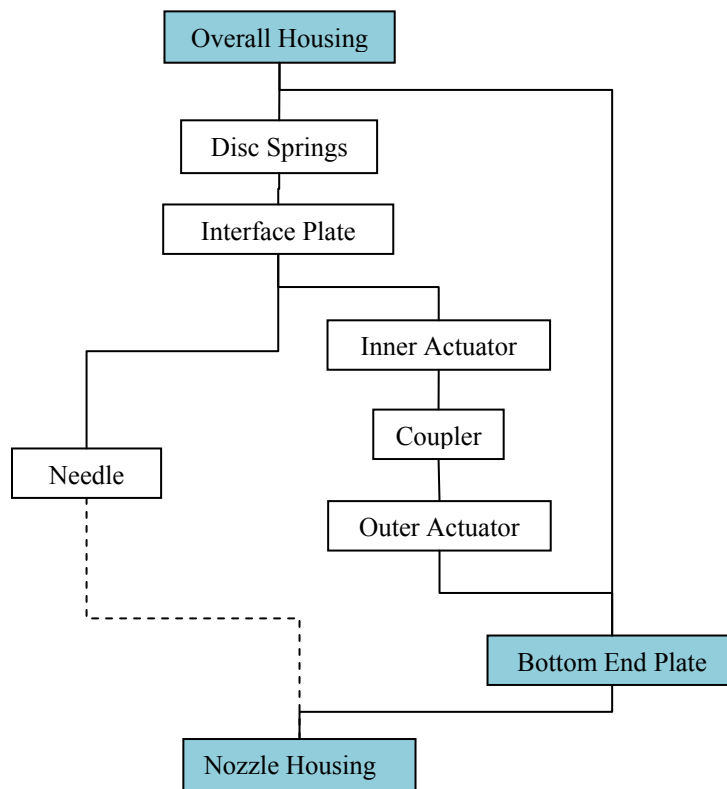


Figure 8 Generation 1 injector component connections diagram

1. Insert the coupler into the outer actuator.
2. Bond the outer actuator to the coupler through the ring that is protruding out of the lower end.
3. Insert the inner actuator into the coupler and bond at the underside.
4. Fix the outer actuator onto the bottom end plate.
5. Fix the needle to the center of the interface plate.
6. Fix the inner actuator onto the interface plate around the needle.
7. Install the set of disc springs on top of the interface plate.
8. Insert the module into the overall housing.
9. Adjust the amount of prepress using the threads between the overall housing and bottom end plate.
10. Attach the nozzle housing to the bottom end plate while adjusting the final prepress distance necessary to seal the nozzle shut.

#### **2.1.4 Limitations**

The size of this design is a concern. Electrical analysis was done on this injector and the result shows that the electrical equipments needed to drive the actuator are beyond the current technology. This is due to the amount of piezoelectric layers required by two piezoelectric actuators to produce the desired displacement. Not only is it demanding on the electrical equipment, but the cost of the piezoelectric actuator becomes exponential. This limitation shows that the telescopic design does not provide a viable solution to increase the actuator displacement.

## **2.2 Generation 2 Concept**

### **2.2.1 Objective**

This injector was designed to relieve the electrical requirements necessary to drive the piezoelectric actuators so the telescopic design is no longer part of this design. The idea to overcome the short stroke was to make use of a mechanical amplifier. The mechanical amplifier is to be made of a single piece of material to increase the response time. This is to eliminate time losses between components. Another goal was to minimize the dependency of the high fuel pressure effect on the needle during lifting and sealing phases. By minimizing the fuel pressure effect, the needle should be able to lift more freely thus increasing the maximum lifting stroke.

### **2.2.2 Setup**

To resolve the issue of the sophisticated electrical demand, generation 2 injector, Figure 9, uses a mechanical amplifier to increase the short stroke behavior that multi-stack piezoelectric actuator possesses. Another idea to lessen the load on the electrical part, a single actuator is used instead of the telescope design using two actuators. Also keeping the cost of the actuator in mind, the elimination of the cascaded idea in this design contributes to a cheaper cost due to the fact that some of the piezoelectric material for the outer ring is present due to manufacturing constraints. The usual amplifier used for piezoelectric injectors is the hydraulic type, however, a mechanical amplifier was chosen for this design in hope of achieving a faster response time.

The initial idea was to use three beams within a circular disc shown in Figure 10. Circular shape is used so that the top and the bottom part of the injector can clamp the outer ring in place. The beams are the elements used for amplifying the input displacement.

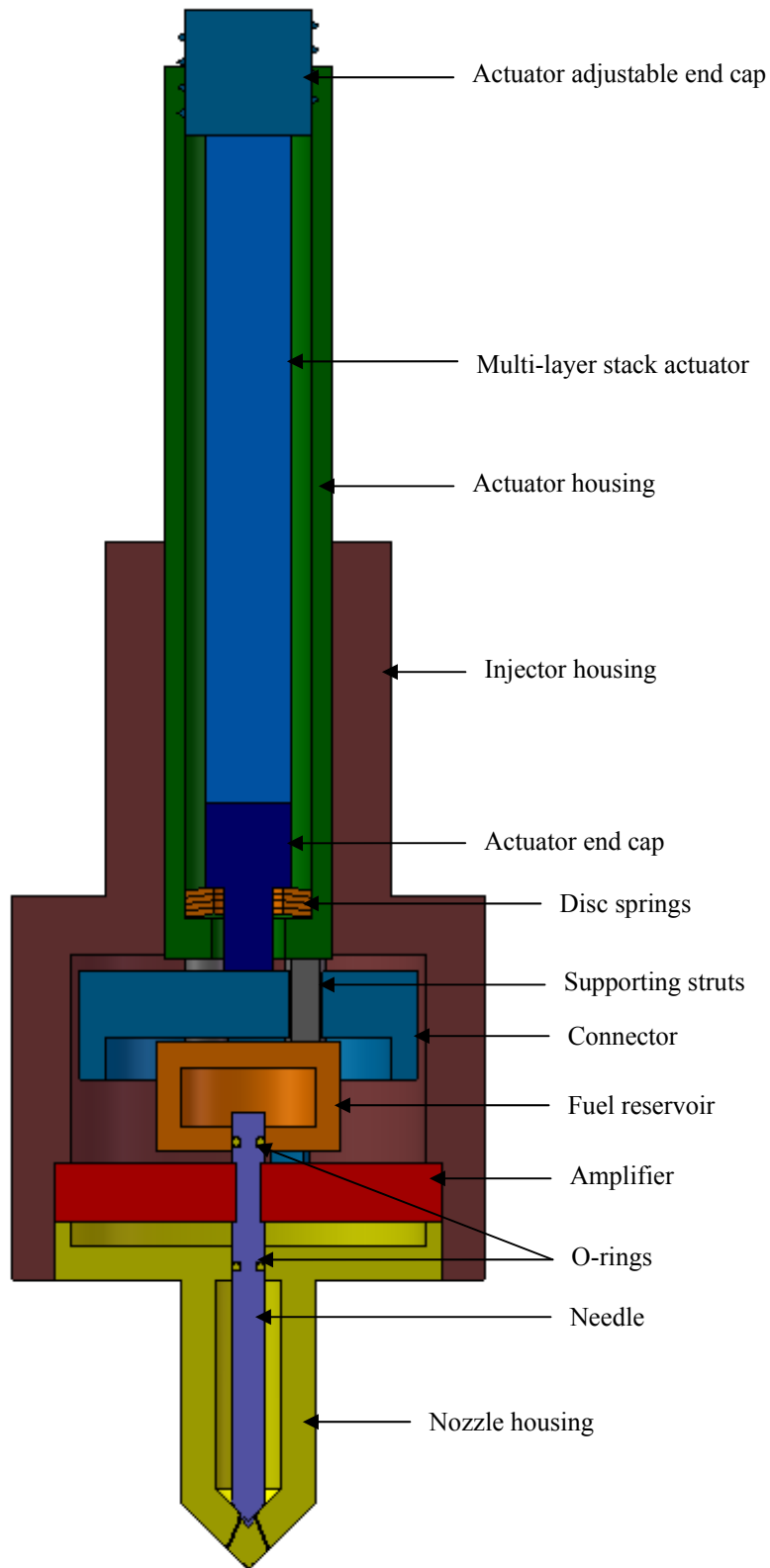


**Figure 9 Cross-sectional drawing of generation 2 injector**

The figure shows the input forces as  $F_i$  and output displacement as  $d_o$ . The output location is where the needle is connected to the amplifier. The output beam length of the beam is 3 times the length of the input beam length. The chosen material was copper to give the amplifier more flexibility.

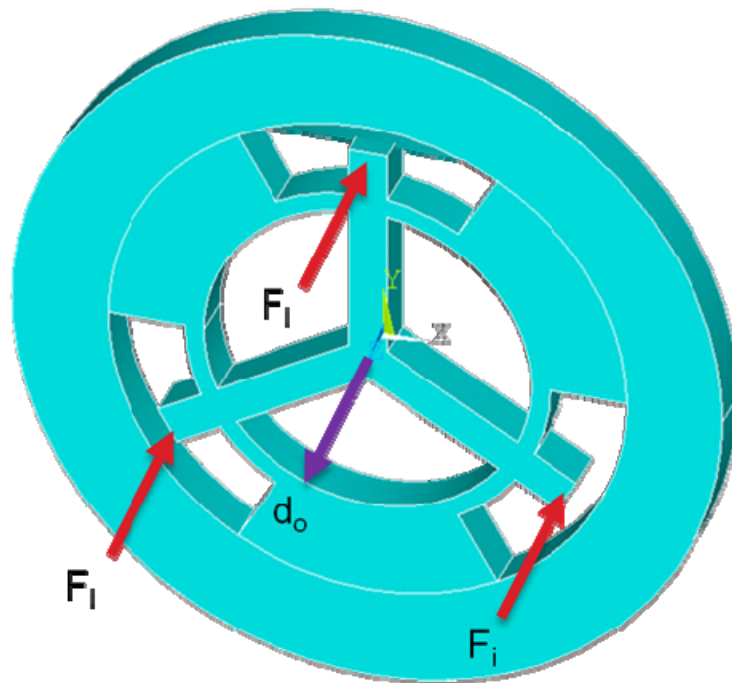


**Figure 10 Initial idea of mechanical amplifier indicating input forces and output displacement**

There are a few issues with this initial design. First issue is at the junction of the needle location and the beam; the junction is too rigid for bending motion to happen. Second problem occurs at the rotational part located at the beam pivoting point right. Rotational motion is prevented by the rigid connection. Third issue is due to unwanted deflection of the beam. The force has caused the whole beam to deflect downward. Resolving these factors aid the amplifier in increasing the output stroke.

The mechanical amplifier was modified as shown in Figure 11. The joint at the needle location and the beam was modified into serpentine spring design allowing more flexibility in

bending motion. The pivoting point was modified in the cross-sectional geometry. From a rectangular area to a square area lessened the rotational rigidity. To decrease the deflection amount of the beams, the rings had to be closed off as close to the beam as possible to act as a fixed end. The overall thickness of the amplifier was increased allowing the beams to resist as much bending deformation as possible.

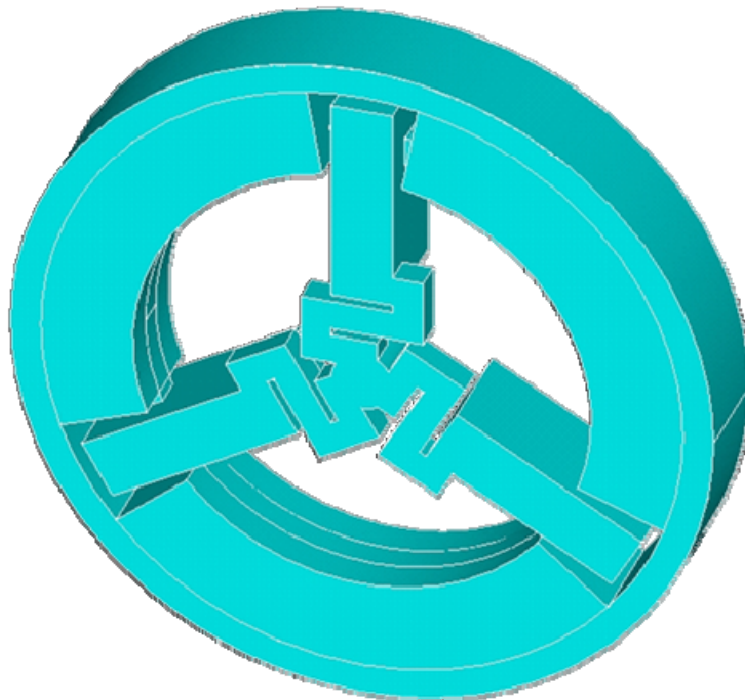


**Figure 11 Final modification of mechanical amplifier**

In terms of maximizing the needle lift, the idea was to lessen the fuel effect on the needle. The idea implemented in this design is to place a fuel reservoir on top of the needle. Since the nozzle housing only covers a small part of the effective area at the center of the needle, the fuel from the reservoir helped pressing the needle against the seat at sealed state. With this idea, the actuator still needed to overcome the extra sealing force in order to initiate lifting, however, once the needle is lifted, a balance of fuel pressure is reached at both top and bottom of the needle.

This balance eliminated the fuel pressure effect at the dynamic states allowing the injector to achieve maximum needle lift.

Needle lift is initiated as the piezoelectric actuator is energized pushing against the set of disc springs. The connector is attached to the actuator end cap thus as the actuator moves, the connector also moves in the same direction. The connector pushes on the mechanical amplifier and the amplifier will respond by lifting the needle in the direction opposite to the movement of the actuator and the connector. This motion is caused by the fact that the mechanical amplifier is also a motion inverter. More detail on the amplifier can be found in section 4.2.1. Fuel is within the fuel reservoir and also in the space between the needle and the nozzle housing. As the needle is lifted, fuel gets under the needle and into the nozzle channels in the nozzle housing into the combustion chamber. Injection is terminated when the actuator is de-energized and the disc springs will compress the actuator back to its pre-compressed state. The needle is also pushed back to the sealed position through this action.

### **2.2.3 Assembly Procedures**

The connection diagram for the injector concept is as follows:

1. Fix the multi-layer stack actuator onto the actuator adjustable end cap and the actuator end cap.
2. Insert the set of disc springs into the actuator housing.
3. Insert the assembled module into the actuator housing with the actuator end cap sitting on top of the disc springs.
4. Adjust the prepress force using the actuator adjustable end cap.
5. Fix the connector onto the actuator end cap.
6. Insert the supporting struts into the holes in the connector.

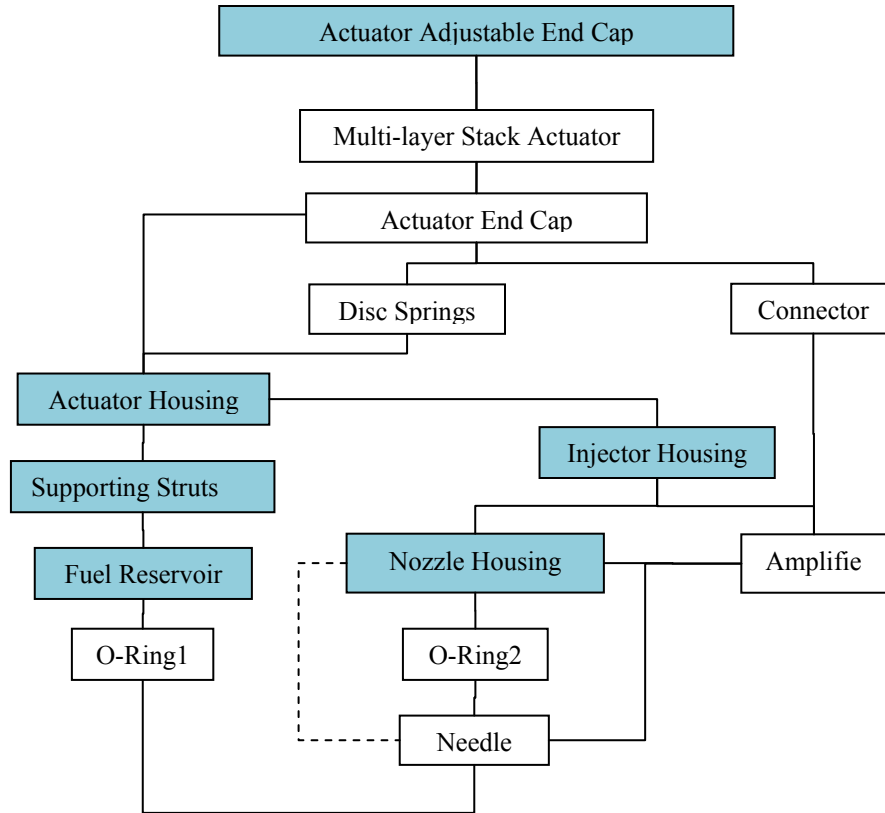


**Figure 12 Generation 2 injector component connections diagram**

7. Fix the fuel reservoir onto the supporting struts with the flat surface without hole.
8. Fit the needle into the amplifier using the temperature difference assembly process.
9. Fit o-ring1 and o-ring 2 around the needle at the crevices.
10. Attach the amplifier onto the connector while inserting the top part of the needle into the fuel reservoir.
11. Insert the injector housing around the actuator housing until the injector housing is contacting the amplifier at the outer ring.
12. Insert the nozzle housing around the needle until the nozzle housing is contacting the amplifier at the outer ring.

## **2.2.4 Limitations**

The success of this mechanical amplifier depended on how much force it can transmit to lift the needle. To achieve fast response time, the mechanical amplifier was to be made from a single piece of material. The challenge lied in making use of flexible joins because the amplifier had to be stiff enough to achieve a high natural frequency and to generate a high enough force to initiate needle lift. To help the mechanical amplifier in transmitting enough force to overcome the fuel pressure effect, the idea of achieving fuel pressure balance is applied to this design. Refer to section 3.5 for more detail.

## **2.3 Generation 3 Concept**

### **2.3.1 Objective**

Instead of making use of the mechanical amplifier, this design explored the hydraulic amplifier. Some hydraulic amplifiers were used as a reference in the process of designing [16][17]. Hydraulic amplifier is expected to be able to transmit more force than the mechanical amplifier; thus, it would be able to overcome the fuel pressure effect on the needle. Although hydraulic amplifier has been implemented in other fuel injectors as presented in section 1.3, this hydraulic amplifier was designed to be a motion inverter also. This allows the injector to be energized only at injection phase.

### **2.3.2 Setup**

Figure 13 is the schematic of the setup of generation 3 injector. The idea of this design remained very similar to that of the previous design. The largest modification to the design switched from mechanical amplifier to hydraulic amplifier.

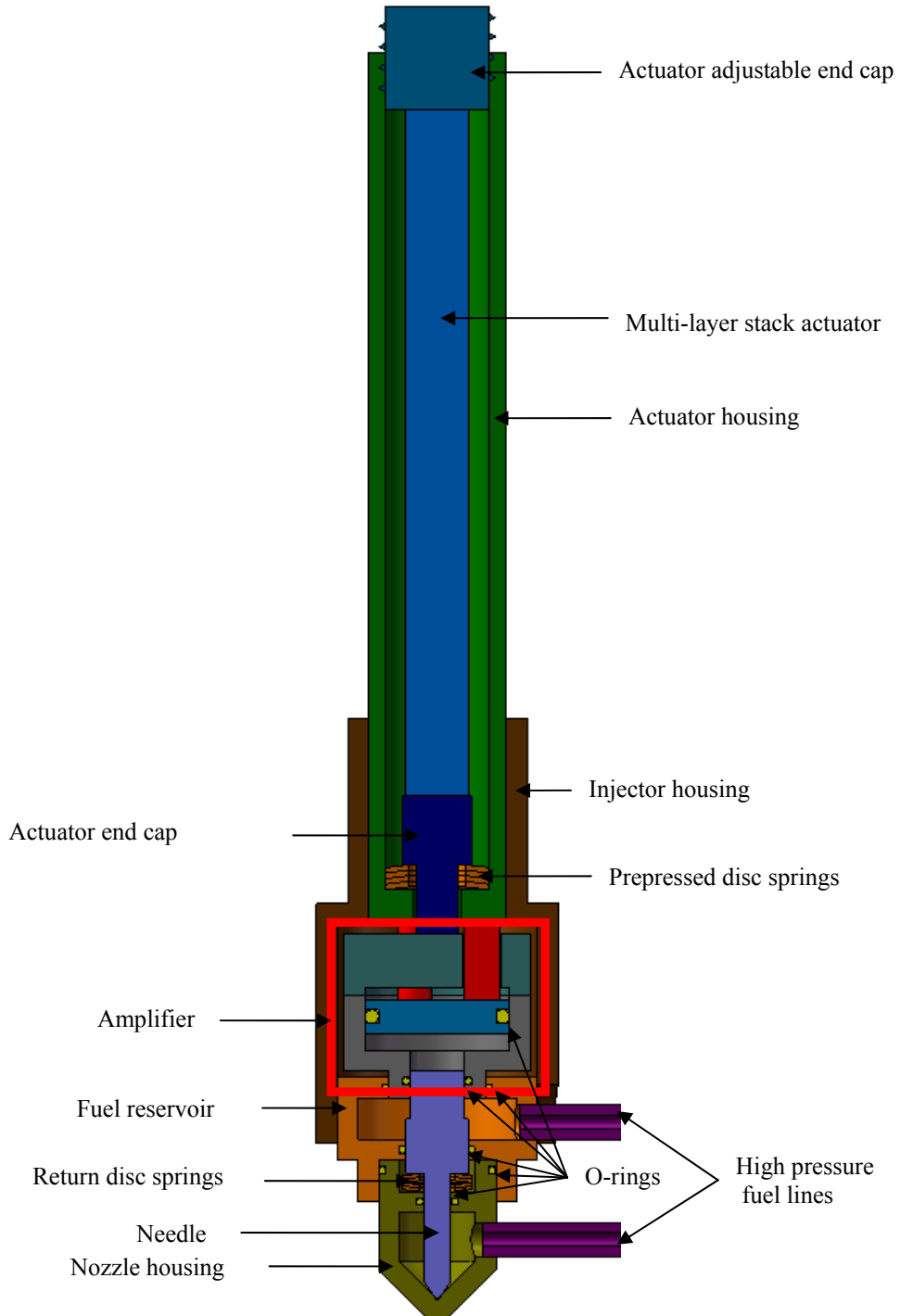


**Figure 13 Cross-sectional drawing of generation 3 injector**

Although the hydraulic amplifier enabled a stronger force transfer during the pushing phase, but during the retracting phase, cavitations were very likely to occur. To prevent cavitation from occurring, an additional set of disc spring was used to aid the needle piston to lift instead of relying solely on the power of suction. The idea of utilizing the high pressure fuel to achieve fuel balance at the lifting phase was kept in this design. The hydraulic amplifier used the end of the needle as the output piston so the fuel reservoir for balancing the fuel pressure was mounted around the needle instead of the end like the previous design. Like the previous design fuel pressure balance was achieved during the lifting phase.

In order to keep the injector to function under “energize to inject” configuration, a typical hydraulic amplifier was modified in the way it is mounted. An enlarged view of the hydraulic amplifier is presented in Figure 14.

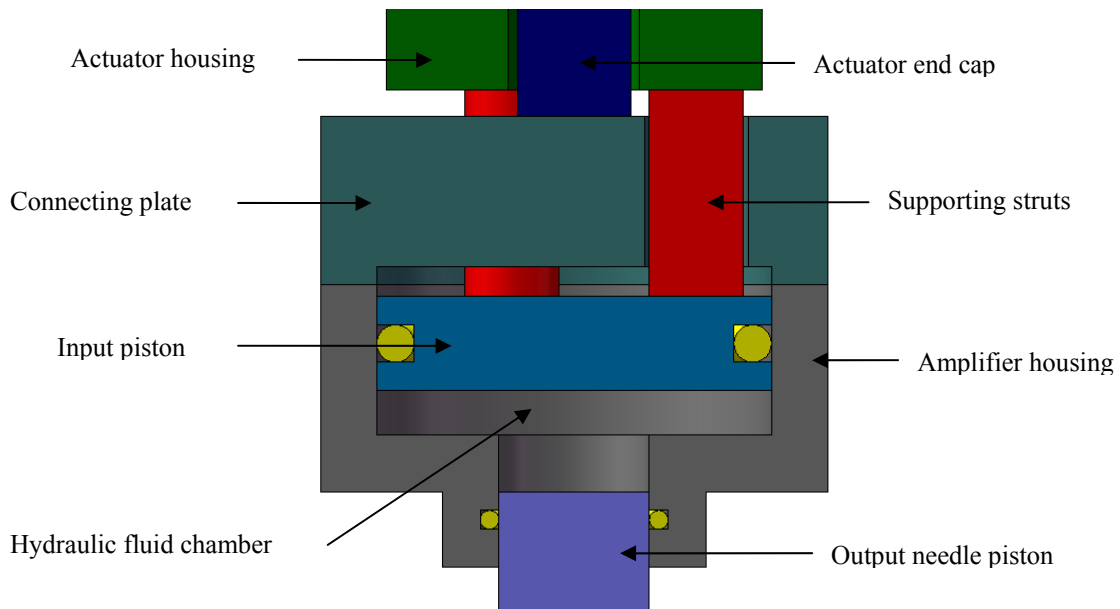


**Figure 14 Cross-sectional view of the hydraulic amplifier**

In a typical hydraulic amplifier, the input piston, connected to the actuator, pushes the hydraulic fluid increasing the pressure. To relieve the pressure, the output piston moves in the same direction. Movement is amplified due to the area difference of the output and input pistons.

The way this hydraulic amplifier works is that the actuator is connected to the connecting plate which is connected to the amplifier housing. The input piston is connected to the supporting struts which are connected to the actuator housing. The amplifier housing moves according to the actuator expansion and contraction. As the actuator energizes, the housing moves down to increase the volume of the hydraulic chamber reduces the pressure. The reduction in pressure creates a suction force on the output needle piston, causing the needle to lift keeping the volume of the chamber constant. This lifting motion is aided by a set of disc springs to help with the upward motion.

To send the needle back to the sealed position, the actuator is de-energized. With the input force reduced, the prepressed disc spring compresses the actuator and lifts the amplifier housing in the upward direction. This motion causes the hydraulic fluid to be compressed in the chamber. To remain in balance with the pushing force, the output needle piston is pushed into the closing direction.

### **2.3.3 Assembly Procedures**

Figure 15 shows the connections between all the components except for the o-rings.

1. Fix the multi-layer stack actuator onto the actuator adjustable end cap and the actuator end cap.
2. Attach the supporting struts onto input piston.
3. Put the supporting struts through the connecting plate and fix the connecting plate to the actuator end cap.
4. Attach the supporting struts to the actuator housing.
5. Insert the set of prepressed disc springs into the actuator housing.

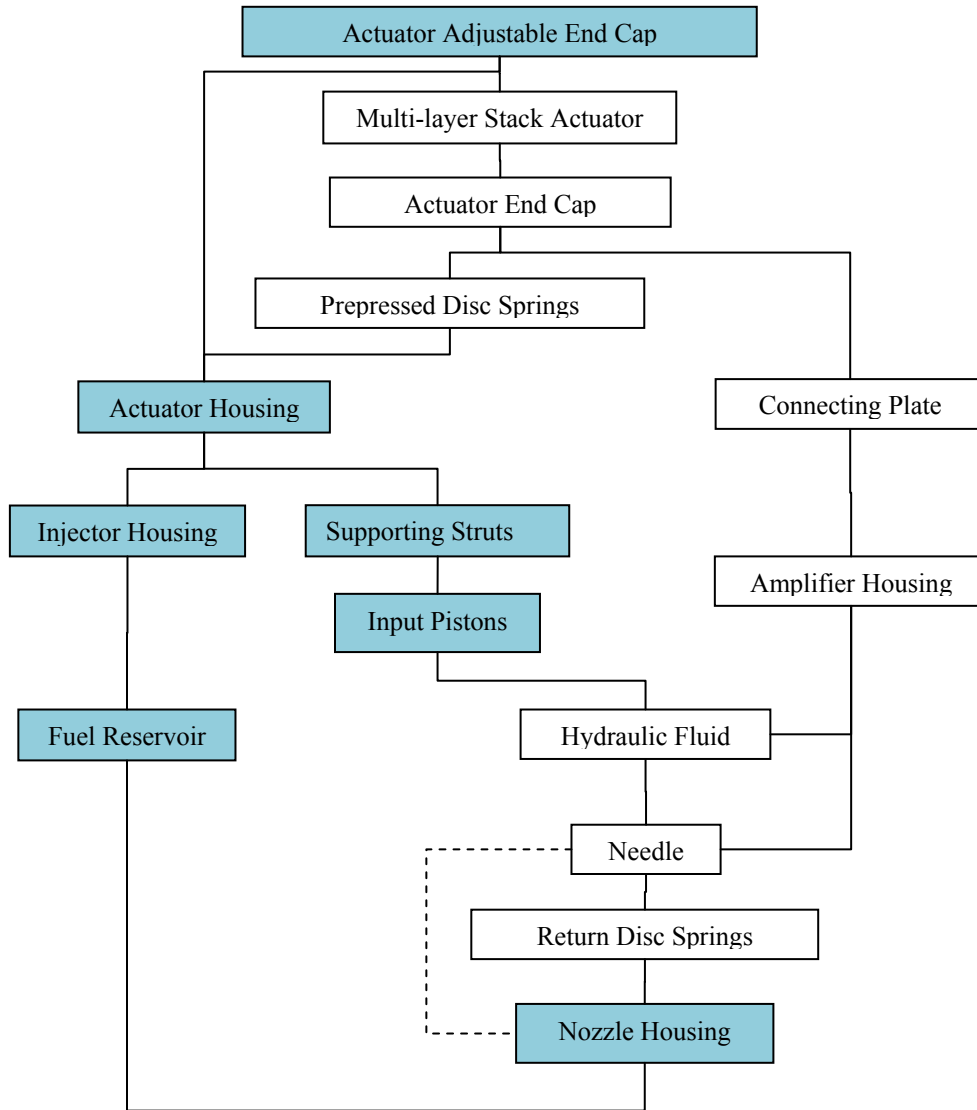


**Figure 15 Generation 3 injector component connections diagram**

6. Insert the assembled module into the actuator housing with the actuator end cap sitting on top of the disc springs.
7. Adjust the prepress force using the actuator adjustable end cap.
8. Connect the amplifier housing onto the connecting plate.
9. Insert the needle module into the amplifier housing.
10. Fill the chamber with hydraulic fluid.
11. Mount the injector housing around the actuator housing

12. Insert the fuel reservoir around the needle and fasten it onto the injector housing.
13. Insert the set of return disc springs around the needle.
14. Mount the nozzle housing onto the fuel reservoir and adjust the compression needed on the return disc springs.

### **2.3.4 Limitations**

One drawback with the hydraulic amplifier was the likelihood of cavitation occurring. Though a set of disc springs was placed to help with lifting the needle as to relying just on the suction force, it was still questionable whether cavitation could be prevented. Also, the inversion of having the input piston as a stationary component instead of the moving components added complexity to the design. Whether this could be fully realized physically was questionable. Many o-rings are needed to keep the fluid and fuel from leaking and these must be design accordingly.

## Chapter 3 Injector Components Design

In this chapter, each of the components used in designing all the injectors is discussed here. The advantages of each of these components are presented. Relevant mathematical models for estimating the performance of the components are presented to help understand how the overall analytical model estimates the needle lift for each design. Information in this chapter was taken from various sources as cited.

### 3.1 Piezoelectric Multi-layer Stacked Actuator

The two parameters that are often used to describe a multi-layer stacked actuator are the blocking force and the free displacement. The free displacement is the maximum displacement that the actuator can generate without any opposing force at the free end. It [6] can be evaluated using the following expression:

$$\Delta L = V d_{33} \frac{L_o}{t} \quad (1)$$

where  $V$  is the operational voltage in V,  $d_{33}$  is the piezoelectric charge constant in m/V,  $L_o$  is the overall length of the actuator in m, and  $t$  is the thickness of the piezoelectric layers in m. The blocking force is the maximum force generated by the actuator when no displacement is generated. Using the overall length of the actuator and the free displacement, the blocking force is estimated using this expression:

$$F_B = \frac{EA}{L_o} \Delta L \quad (2)$$

where  $E$  is the elastic modulus in N/m<sup>2</sup>,  $A$  is the cross-sectional area of the actuator in m<sup>2</sup>. With these two variables, a characteristic plot describing the force and displacement relationship of a piezoelectric stack actuator is shown in Figure 16.

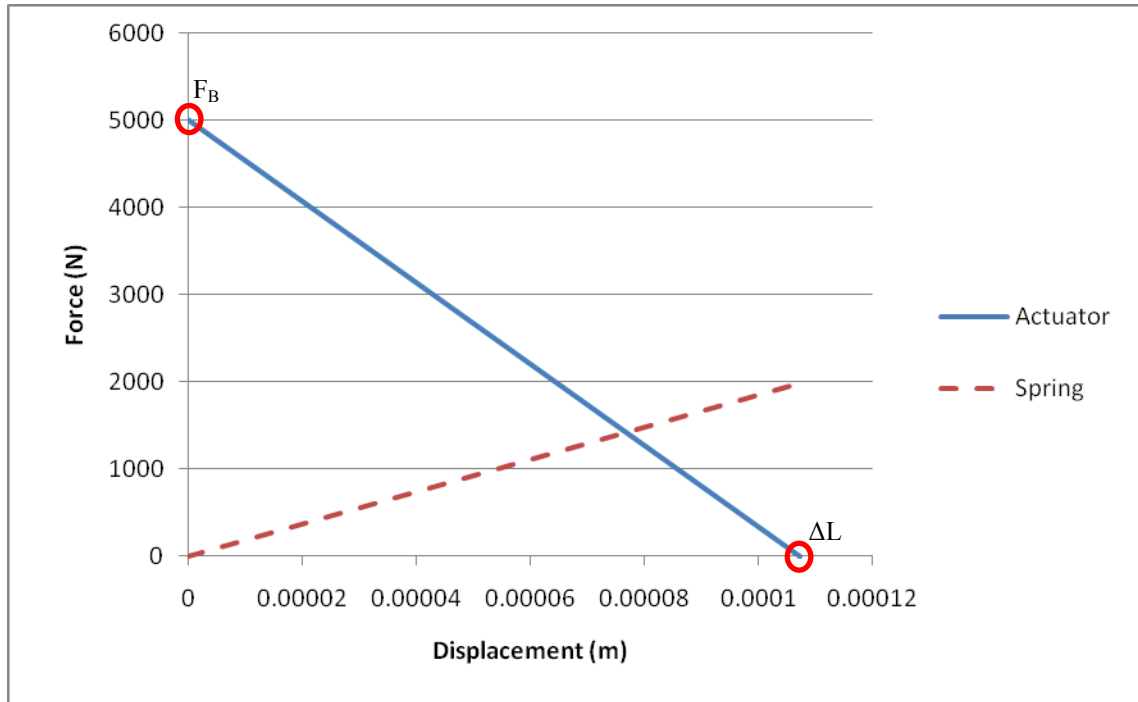


**Figure 16 Characteristic plot of piezoelectric actuator and spring**

The blocking force is the maximum force generated at the zero displacement point (y-intercept) and the free displacement occurs at the point where there is no external force (x-intercept) acting on it. A general expression describing this linear line can be expressed as:

$$F = F_B - \frac{F_B}{\Delta L} d \quad (3)$$

where  $F$  is a general force term generated in N and  $d$  is a general displacement term generated in m.

Piezoelectric material is much better at sustaining compressive load than tensile load, so a general rule in using the actuator is to keep the working range within compression. There are two ways to prepress the actuator so that it stays within the compression range. One typical way of compressing the actuator is by putting a spring at one end of the actuator. This method decreases the maximum displacement that the actuator exhibits. As shown in Figure 16, the dashed red line is a characteristic plot of a linear spring. The intersection of the actuator line and

the spring line is the maximum displacement that the actuator can produce with this specific spring pushing against it. The new displacement can now be evaluated through this expression:

$$\Delta L_S = \left( \frac{k_A}{k_A + k_S} \right) \Delta L \quad (4)$$

where  $k_A$  is the actuator stiffness in N/m,  $k_S$  is the spring stiffness in N/m, and  $\Delta L$  is the free displacement without the spring.

Another way of prepressing the actuator is by the placement of a constant force at the end. This method is advantageous than the previous because this does not have any adverse effect on the total displacement. This method simply offsets the starting point of the actuation. Even though the second method is preferred, it is difficult to implement a constant force against the actuator physically.

Because piezoelectric actuator is a smart material, the electrical aspect must be considered also. This is especially important in finding a suitable power supply in driving the actuator. It is necessary to find out the power requirement of the stack actuator used. First, the capacitance is developed based on the actuator properties. Then the current relationship is built. Lastly, the power relationship is presented.

$$C = \frac{L_A \epsilon_{33}^T \epsilon_0 A}{t_L^2} \quad (5)$$

$$I_{max} = 2\pi U_{max} C f \quad (6)$$

$$P_{max} = U_{max} I_{max} \quad (7)$$

where  $U_{max}$  is the maximum voltage in V and  $f$  is the frequency of operation in Hz.

## 3.2 Telescopic Stack Actuator

The first aspect in analyzing the behavior of the telescopic actuator is to find out the equivalent stiffness of the overall actuator including inner actuator, outer actuator, and coupler. Because piezoelectric stack must be operate under compression state at all times, prepressed load must be applied on the actuator. To gauge how much the overall actuator is compressed by the prepressed load, the equivalent stiffness of the actuator must be evaluated. Since the configuration of these three components is connected in series, the equivalent stiffness is as follows:

$$k_{AT} = \left( \frac{1}{k_I} + \frac{1}{k_C} + \frac{1}{k_O} \right)^{-1} \quad (8)$$

where  $k_I$  refers to the inner actuator stiffness in,  $k_C$  refers to the coupler stiffness, and  $k_O$  refers to the outer actuator stiffness expressed in N/m. Each of the individual stiffness of the inner actuator, coupler, and outer actuator is evaluated using the axial stiffness equation:

$$k_i = \frac{E_i A_i}{L_i} \quad (9)$$

where the subscript  $i$  refers to the specific material and parameters for that element.  $E$  is the elastic modulus in N/m<sup>2</sup>,  $A$  is the cross-sectional area in m<sup>2</sup>, and  $L$  is the length of the element in m. For the coupler, only the tubular part along the length is taken into evaluation and the ring plates along the radial direction is treated as rigid bodies in this analysis.

During the energizing phase, the total displacement of the telescopic actuator is the superimposed result of individual actuator displacements subtracted by the elongation of the coupler. The expression is as follow

$$\Delta L_T = \Delta L_I + \Delta L_O - \Delta L_C \quad (10)$$

With the total displacement and the overall stiffness of the actuators defined, the total blocking force can now be estimated using equation (2). A graph, similar to Figure 16, consists of the total displacement and the total blocking force can be plotted using the same method shown in section 3.1. A linear expression can be written to show how the blocking force changes depending on the displacement of the actuator.

$$F_A = F_B - \frac{F_B}{\Delta L_T} x \quad (11)$$

where  $x$  is the displacement in m.

### 3.3 Disc Spring

A disc spring, also known as a Belleville washer [18], has a number of advantageous properties that are useful in the injector designs. These properties include large loads can be supported within small space, unlimited combinations of individual disc springs to create a customized characteristic curve, and high service life under dynamic loading. Shown in Figure 17, disc spring is simply a conical shell that exhibits high resistance to axial force. When the disc springs are stacked in different configurations, the deflection and the maximum load that they can take changes giving designers the ability to optimize the best configuration for their designs.

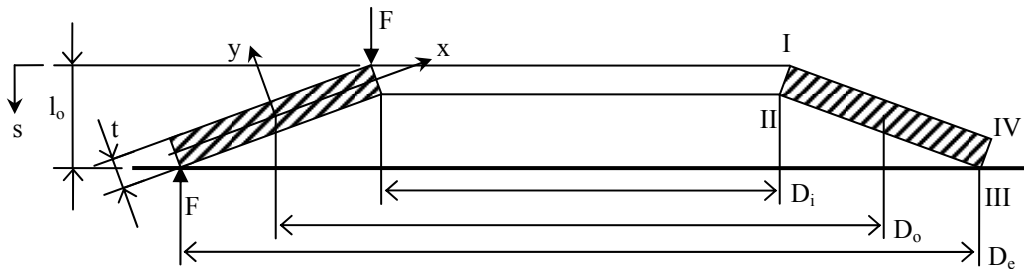


Figure 17 Cross sectional view of single disc spring with references

where  $D_e$  is the outside diameter,  $D_i$  is the inside diameter,  $D_o$  is the diameter of center of rotation,  $t$  is the thickness of a single spring,  $l_o$  is the height of an unloaded single spring,  $s$  is the deflection of a single spring, and  $F$  is the spring force of a single spring. All distance units are expressed in mm and force units are expressed in N.

To determine the diameter of the center of rotation, the design parameters, outside diameter and inside diameter, are used. Equations are from Schnorr Corporation catalog.

$$D_o = \frac{D_e - D_i}{\ln\left(\frac{D_e}{D_i}\right)} \quad (12)$$

The cone height of the disc spring is an important parameter defining the maximum deflection that the spring can have. It is expressed as:

$$h_o = l_o - t \quad (13)$$

Equations (14) to (20) present coefficients that will help simplify the equations of spring force and stresses that are presented later.

$$\delta = \frac{D_e}{D_i} \quad (14)$$

$$K_1 = \frac{1}{\pi} \cdot \frac{\left(\frac{\delta - 1}{\delta}\right)^2}{\frac{\delta + 1}{\delta - 1} - \frac{2}{\ln \delta}} \quad (15)$$

$$K_2 = \frac{6}{\pi} \cdot \frac{\frac{\delta - 1}{\ln \delta} - 1}{\ln \delta} \quad (16)$$

$$K_3 = \frac{3}{\pi} \cdot \frac{\delta - 1}{\ln \delta} \quad (17)$$

$$K_4 = \sqrt{-\frac{C_1}{2} + \sqrt{\left(\frac{C_1}{2}\right)^2 + C_2}} \quad (18)$$

$$C_1 = \frac{1}{\left(\frac{1}{4} \cdot \frac{l_o}{t} - \frac{1}{4}\right) \left(\frac{5}{8} \cdot \frac{l_o}{t} - \frac{5}{8}\right)} \quad (19)$$

$$C_2 = C_1 \left[ \frac{5}{32} \left(\frac{l_o}{t} - 1\right)^2 + 1 \right] \quad (20)$$

With these coefficients, the spring force can be estimated as follows:

$$F = \frac{4E}{1 - \mu^2} \cdot \frac{t^4}{K_1 \cdot D_e^2} \cdot K_4^2 \cdot \frac{s}{t} \left[ K_4^2 \cdot \left(\frac{h_o}{t} - \frac{s}{t}\right) \left(\frac{h_o}{t} - \frac{s}{2t}\right) + 1 \right] \quad (21)$$

where  $E$  is the elastic modulus in N/mm<sup>2</sup> and  $\mu$  is the Poisson's ratio of the disc spring material.

The stresses that are worth estimating are located at location II and III as pointed out in Figure 17. Dependent on the design parameters, the larger one of the two helps determining the fatigue life of the disc spring. Following equations estimate the stresses at the respective locations.

$$\sigma_{II} = \frac{4E}{1 - \mu^2} \cdot \frac{t^2}{K_1 \cdot D_e^2} \cdot K_4 \cdot \frac{s}{t} \left[ K_4 \cdot K_2 \left(\frac{h_o}{t} - \frac{s}{2t}\right) - K_3 \right] \quad (22)$$

$$\sigma_{III} = \frac{4E}{1 - \mu^2} \cdot \frac{t^2}{K_1 \cdot D_e^2} \cdot K_4 \cdot \frac{1}{\delta} \cdot \frac{s}{t} \left[ K_4 \cdot (K_2 - 2K_3) \left(\frac{h_o}{t} - \frac{s}{2t}\right) - K_3 \right] \quad (23)$$

Using the diagrams provided in pg. 33 and 34 from the catalogue, the maximum stress that the disc spring can withstand before reaching fatigue failure can be found by determining the minimum stress that the disc spring will experience.

With the disc spring stacked parallel to each other, the spring force increases proportionally. If stacked in series, the spring deflection is increased proportionally. These properties allow disc springs to be stacked in any configuration to suit a specific application.

### 3.4 Needle Design

The needle module that is commonly used in diesel fuel injection uses 2 components shown in Figure 18. The first module consists of a needle seat which is usually part of the

housing unit. The needle seat contains small nozzles going through the seat. These nozzles are where the fuel shoots out from the reservoir into the combustion chamber. The second component is the needle, used to seal the nozzle shut. Injection occurs when the needle is lifted away from the nozzle seat. Injection terminates when the needle and the nozzle seat are in contact.

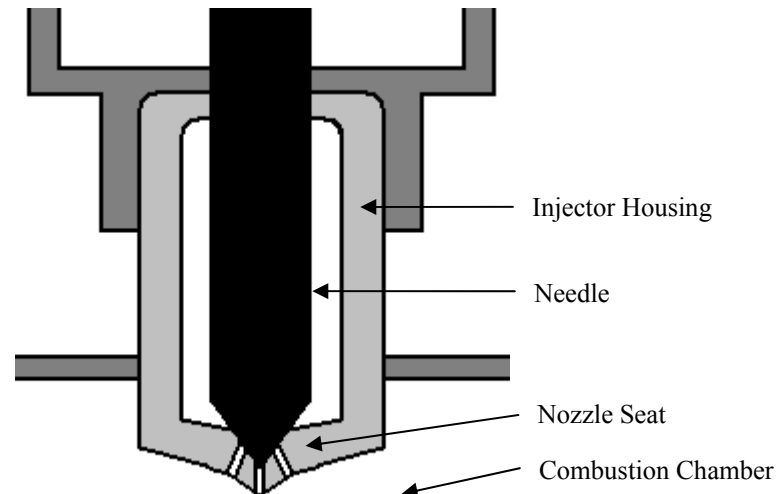


**Figure 18 Common diesel injector nozzle design**

Notice how the nozzle seat makes contact with a small effective area with the needle, this suggests that the fuel tends to push the needle up and a mechanism is required to push the needle shut by default. A compressive spring is usually used to push against the fuel pressure on the needle.

### **3.5 Fuel Pressure Balance**

The fuel pressure balance idea was developed in generation 2 fuel injector design and the idea was kept in generation 3 design. The purpose was to minimize the fuel pressure effect on the needle. This is critical on generation 2 design because to increase the response time, the mechanical amplifier is to design on one single piece of material including all the joints. This is

to prevent frictional losses and slow response occurring between components. Therefore, all the joints on the amplifier have to be kept flexible. However, having flexible joints weakens the overall stiffness of the actuator. Therefore, it is crucial to keep the fuel pressure effect on the needle on a minimal level.

As discussed in the previous section, the fuel pressure effect pushes the needle in the upward direction at sealed and opened state as shown in Figure 18. To lessen the fuel pressure force, a separate fuel reservoir is placed at the end of the needle as shown in Figure 19.

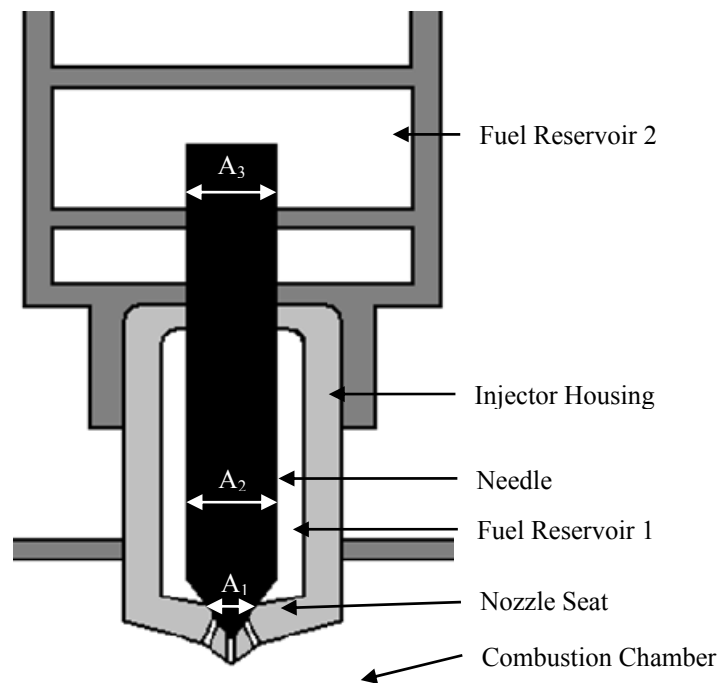


**Figure 19 Fuel pressure balance diagram**

With fuel reservoir 2 at the end of the needle and cross-sectional area  $A_2$  equals to cross-sectional area  $A_3$ , the fuel pressure now pushes the needle against the nozzle seat creating a sealing force at sealed state. The magnitude of that force is dependent on the size of  $A_1$  and the fuel pressure.

As the needle is lifted up, fuel gets under the needle tip. Because fuel is now at both ends of the needle, there exists a complete balance of fuel force. This allows the needle to be

controlled by the actuator without resistance force from the fuel. However, the balance can only be achieved at the opening state; at the sealed state, the actuator is required to overcome the sealing force to initiate needle lift.

The fuel pressure balance can be further adjusted by changing the cross-sectional area of  $A_3$  so that the less force is required at different phases. For example,  $A_3$  can be changed to be smaller than  $A_2$  but larger than the area difference of  $A_2$  and  $A_1$ . In this case, sealing force is still available at sealed state. Actuator is required to overcome sealing force to initiate lifting. At lifting state, the fuel pressure can help with the maximum lifting. Other combination of these cross-sectional areas can provide aid at different phases.

## Chapter 4 Analytical Models

All three designs were modeled analytically. Both design 1 and 3 were subjected under force analysis to estimate the maximum needle lift. For design 2, maximum needle lift was not estimated due to the lack of success achieved in the simulation. Only the serpentine spring was analyzed using the virtual work method.

### 4.1 Generation 1 Injector

There are two important aspects to consider in performing a static analysis on generation 1 injector. The first aspect is superimposing the strokes of the actuators together while keeping the overall length short. This is critical idea in extending the short stroke offered by a single stacked actuator. The second is the prepressed disc spring component. Other than keeping the actuator in the compressed state at all times, the disc spring offers crucial force in sealing the needle shut. The maximum stroke and the sealing force must be optimized in order to achieve both effectively.

#### 4.1.1 Precompression

Precompression in this design can be separated into two different steps. First, to ensure that the prepress force will not exceed the limit for damaging the stack actuators, the following equation determines the distance ( $d_{ap1}$ ) that the stack needs to be compressed by.

$$d_{ap1} = \frac{P_C A_A}{k_A} \quad (24)$$

where  $P_C$  is the limiting pressure before depolarization in Pa,  $A_A$  is the actuator area in  $\text{m}^2$ , and  $k_A$  is the stiffness of the actuator in N/m. If telescopic actuator is used,  $k_A$  is replaced with the

stiffness of the telescopic actuator,  $k_{AT}$ . The area taken for the telescopic actuator is the smaller one of the two to prevent depolarization.

The element that is used to compress the actuator is the disc spring and determining the distance required to compress this component is shown here. The same force is used because the two components are to reach equilibrium and is represent by  $F_{LS1}$ .

$$d_{sp1} = \frac{F_{LS1}}{k_{sp}} \quad (25)$$

where  $k_{sp}$  is the spring rate of the extension spring expressed in N/m.

As shown in Figure 20, the actuator is connected to the disc spring through an interfacing component which is treated as a rigid body. Because the two elements are connected in series, the two compressive distances are added together to estimate the distance,  $d_{LS1}$ , needed to generate the right amount of compressive force onto the actuator.  $L_1$  is the compressive distance with respect to  $x_1$  coordinate and  $L_2$  is taken with respect to  $x_1$  and  $x_2$ .

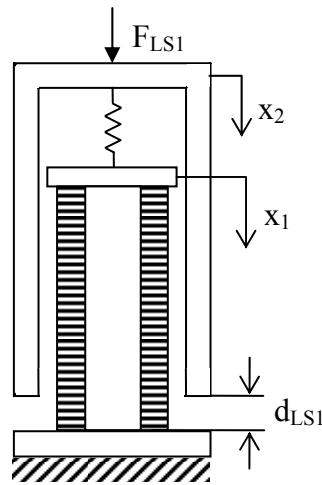


**Figure 20 Pre-compression of stack actuator**

After completing the compression of the actuator, the second step is applied. The disc springs must be offset further to ensure that the needle can be sealed shut. In the real application,

the high pressure fuel pushes the tip of the needle in the opening direction. This force is especially significant due to the integration of the common rail system. The system must be compressed further more to overcome this force. Figure 21 shows how the three components: disc spring, actuator, and needle are connected.

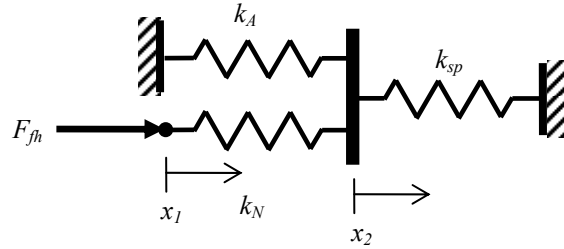


**Figure 21 Simplified schematic for estimating the extra prepress distance needed to overcome the fuel pressure for design 1**

The prepressed spring and the actuator are connected in parallel configuration, so the equivalent stiffness is the added stiffness of the two components. The needle is connected to these components in series configuration, so the overall is as follows:

$$k_{eq1} = k_A + k_{sp} \quad (26)$$

$$k_{eq2} = \frac{k_N k_{eq1}}{k_N + k_{eq1}} \quad (27)$$

For the needle to overcome the fuel pressure, the tip of the needle must be compressed by the distance as described.

$$d_s = \frac{F_f}{k_{eq1}} \quad (28)$$

where  $d_s$  is the displacement needed to overcome the fuel pressure force  $F_f$  in N. After the injector is pushed back at the needle tip by the displacement of  $d_s$ , the nozzle housing is fixed at that position and equilibrium is achieved with this design.

### 4.1.2 Needle Lift Estimation

Needle lift was first estimated through the static operation. The best place to start with this analysis is at the interface plate where most of the components of the injector are attached to. After analyzing the interface plate, the displacement of the needle was explored. Following the schematic in Figure 22, a net force equation could be written.

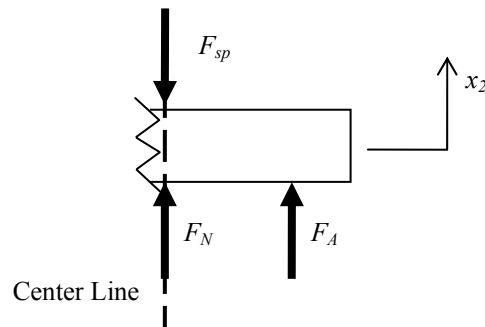


**Figure 22 Schematic of the interface plate indicating forces exerted by other components in the system**

During the initiation phase, the telescopic stacked actuator generates a force as described in section 3.2. This force must overcome the sealing force in order for the needle tip to lift off of the nozzle housing. The net force equation that describes this motion is shown in the following

$$F_B - \frac{F_B}{\Delta L_T} x_2 - k_{sp} x_2 - k_N x_2 = 0 \quad (29)$$

where the first two terms describe the force from the actuator, the third term represents the resistive force from the disc spring, and the last term is the resistive force from the needle. The last term shows that as the interface plate is being lifted in  $x_2$  direction, the needle is not as compressed thus reducing the resistive force.

Lifting phase requires two cases, high pressure fuel case and low pressure fuel case, to be considered. During the high pressure lifting phase, the only difference from the initiation is that

high pressure fuel force becomes a constant force thus eliminating the resistive needle term that reduces the actuation force as the interface plate moves in the positive  $x_2$  direction. There is no visible fuel force added due to the sealed condition achieved in the previous section where the fuel force is taken into consideration.

$$F_B - \frac{F_B}{\Delta L_T} x_2 - k_{sp} x_2 = 0 \quad (30)$$

In the low pressure fuel case, the force generated by the high pressure fuel is replaced by the low pressure fuel force as follows:

$$F_B - \frac{F_B}{\Delta L_T} x_2 - F_{fh} + F_{fl} - k_{sp} x_2 = 0 \quad (31)$$

By isolating the  $x_2$  term, the displacement of the interface plate can be estimated. To find the needle displacement ( $x_3$ ), further analysis is necessary. In the high pressure case, the needle displacement is the same as the interface plate displacement. Reason being that the high pressure fuel compresses the injector assembly the same amount as the nozzle housing compresses the injector assembly during the sealed phase. The equation representing the maximum needle stroke is as described in equation (32).

$$x_3 = \frac{F_B}{\frac{F_B}{\Delta L_T} + k_{sp}} \quad (32)$$

In the low pressure fuel case, the needle is compressed by a smaller force. The displacement of the needle must subtract the compression distance caused by the high pressure fuel and add the compression distance caused by the low pressure fuel.

$$x_3 = \frac{F_B - F_{fh} + F_{fl}}{\frac{F_B}{\Delta L_T} + k_{sp}} + \frac{F_{fl} - F_{fh}}{k_N} \quad (33)$$

The result should give a needle displacement less than that of the high pressure case.

Following table shows the dimensions (in meters) of the actuators, coupler, and needle used to estimate the needle lift of this design.

**Table 2 Dimensions of actuators, coupler, and needle for design 1**

$D_{Oo}$	$D_{OI}$	$D_{IO}$	$D_{II}$	$L_A$	$t_L$	$D_{CO}$	$D_{CI}$	$L_C$	$D_{nt}$	$D_{nb}$	$L_{nt}$	$L_{nb}$
0.059	0.043	0.027	0.011	0.2	0.0001	0.039	0.031	0.185	0.01	0.004	0.215	0.0465

The material properties used for calculation is in Table 3.

**Table 3 Material properties used in estimating needle lift for design 1**

$E_A$ (GPa)	$d_{33}$ (m/V)	$E_S$ (GPa)	$k_{sp}$ (N/m)
40	$680 \times 10^{-12}$	200	$14.2 \times 10^6$

Using the equations presented above, the results are as follows:

**Table 4 Estimated results using analytical model for design 1**

	<b>Initiation</b>	<b>Lifting during HP</b>	<b>Lifting during LP</b>
$x_2$ ( $\mu\text{m}$ )	279	419	383
$x_3$ ( $\mu\text{m}$ )	-	419	310

These results show that this design is able to lift and achieve more than 300 micron even during low fuel pressure phase. Even though this injector design meets the lifting requirement, it exceeded the electrical limitations on the piezoelectric actuator. With the use of the equations presented from section 3.1. The current required to drive this is over 300 A; thus, modification must be made to achieve the same requirement with less piezoelectric material.

## 4.2 Generation 2 Injector

Generation 2 injector uses a mechanical amplifier to increase the stroke of the piezoelectric stacked actuator. A similar method can be used to estimate the needle lift using the stiffness of each component. Regarding the mechanical amplifier, it is assumed that it will

behave like a spring, having a linear relationship with force and displacement. Analysis was done on the mechanical amplifier before the needle lift estimation.

#### 4.2.1 Mechanical Amplifier Analysis

This mechanical amplifier consists of three beams acting as levers to amplify the stroke from the actuator. Each of these beams consists of one pivoting point near the end where the force is applied and a bending mechanism near the needle end as illustrated in Figure 23. In order to increase the flexibility of the joints, copper is the material chosen of the amplifier. Analysis was done on the serpentine spring where most of the bending motion occurs at. Virtual work method was used for this analysis.

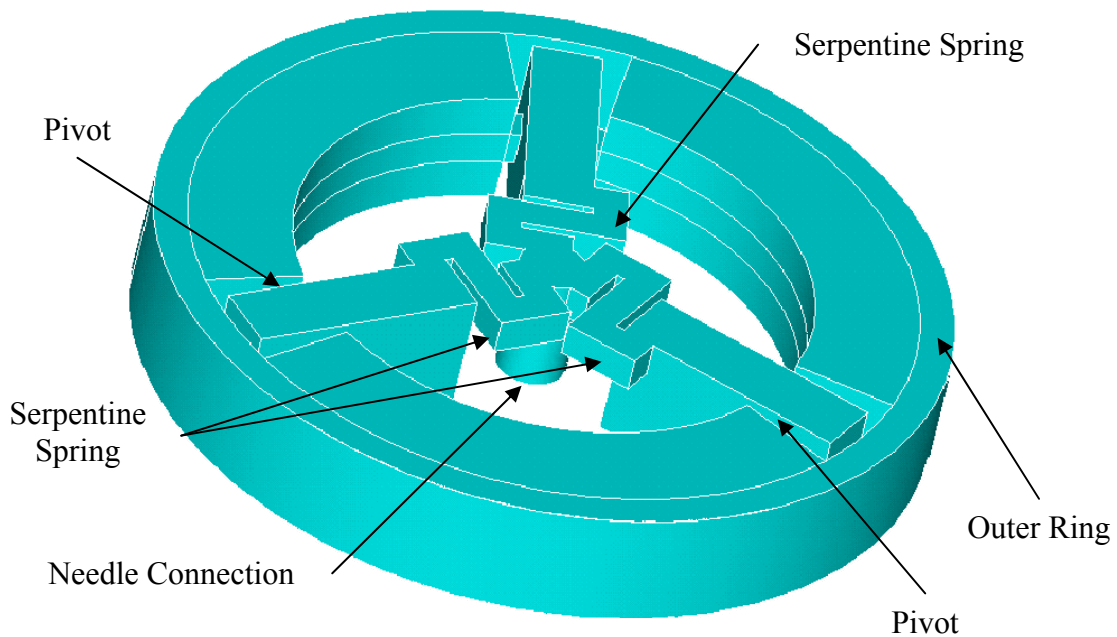


**Figure 23 Gen 2 injector serpentine spring diagram**

Taking the cross section of one of these beams along the length, a force is applied to the beam end causing the needle connection to lift as shown in Figure 24.

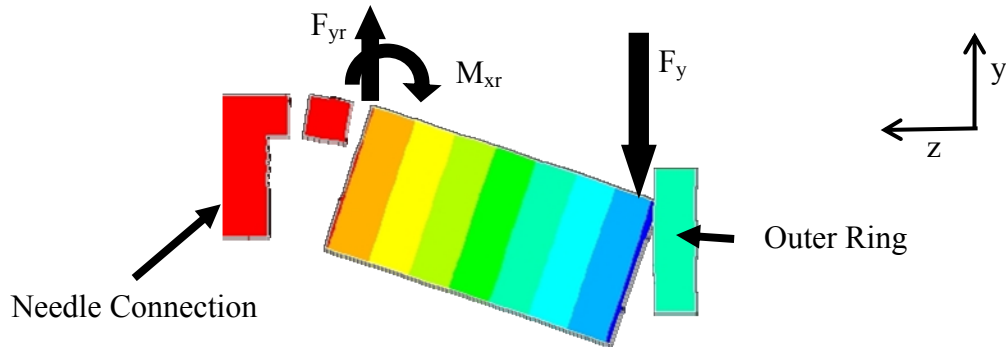


**Figure 24 Gen 2 injector input force and reaction forces shown on beam**

To analyze the serpentine spring, a cut has to be made between the beam and the spring. The outer ring of the mechanical amplifier is fixed in all direction through the clamping of the injector housing and nozzle housing. Located at the cut is an upward reaction force equivalent to the downward force exerted by the piezoelectric stacked actuator along with a moment generated by the same force is placed at the end of the serpentine spring. Before applying the virtual work method in analyzing the serpentine spring, the spring is illustrated with geometrical parameters as shown in Figure 25.

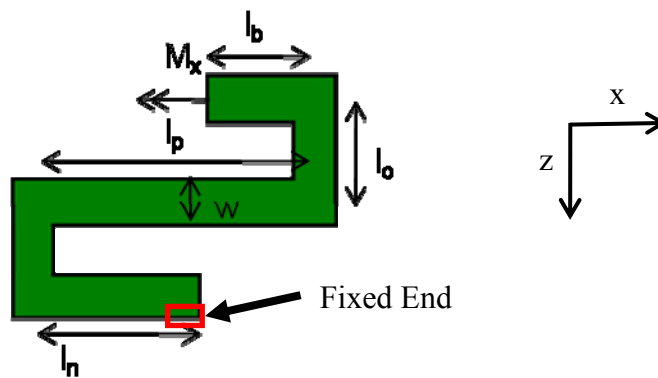


**Figure 25 Gen 2 injector serpentine spring geometry**

As shown in the figure, the beams that are along the x direction are subjected under a twisting force from  $M_x$  where as the beams that are along the z direction are subjected under a bending force from  $M_x$ . With a procedure presented by Barillaro [19] in analyzing the serpentine spring,

the following equation can be formed. The most flexible part is the serpentine spring. The main beam is considered to be rigid. The losses at the pivoting point are not considered. If the bending angle is found, the deflection can be estimated.

$$\theta = \sum \left( \int \frac{T_L T_U}{GJ} dx + \int \frac{M_L M_U}{EI_x} dz \right) \quad (34)$$

By applying this equation to the serpentine spring, 5 integrals can be obtained. Further simplification is obtained by applying the unit loads [20]. Integrate these terms using the parameters shown in Figure 25, the following equation is formed.

$$\theta = M_x \left[ \frac{2l_o}{EI_x} + \frac{l_n + l_p + l_b}{GJ} \right] \quad (35)$$

The dimensions of the serpentine spring are tabulated in the following table listed in millimeters.

**Table 5 Dimensions of the serpentine spring for design 2**

t	w	l <sub>o</sub>	l <sub>b</sub>	l <sub>p</sub>	l <sub>n</sub>
2	1.8	2.3	1.1	6.2	4.1

The moment of inertia from the bending motion and the polar moment of inertia are calculated to be  $1.2 \times 10^{-12} \text{ m}^4$  and  $2.172 \times 10^{-12} \text{ m}^4$  respectively. The Young's modulus used is 110 GPa and the shear modulus used is 41 GPa. The moments applied to test this model out are 0.0018 Nm, 0.009 Nm, and 0.018 Nm. With these parameters, the following results were obtained.

**Table 6 Results of the serpentine spring analytical model for design 2**

Moment (Nm)	Angle (degrees)
0.0018	0.17
0.009	0.84
0.018	1.68

Due to the inability of this displacement amplification provided by this amplifier, further development in the analytical model was not pursued.

### 4.3 Generation 3 Injector

Generation 3 injector uses hydraulic amplifier instead of mechanical amplifier. For this design, only analytical model was built. Simulation in ANSYS was not done due to the integration of the fluidic portion consumes a substantial amount of time. An analytical model was built to estimate whether the needle lift is sufficient. The prepressed analysis from generation 1 design was employed here to subject the actuator under compression. A quick overview of the hydraulic amplifier is presented followed by the needle lift estimation through force analysis.

#### 4.3.1 Hydraulic Amplifier

One of the advantages of using hydraulic amplifier over the mechanical amplifier is the higher stiffness. This increases the force transfer from the input to the output. In this analysis, fluid is considered to be incompressible. Volume of the fluid remains unchanged. With this, the relationship between the input distance, output distance, and the amplification ratio is as follows.

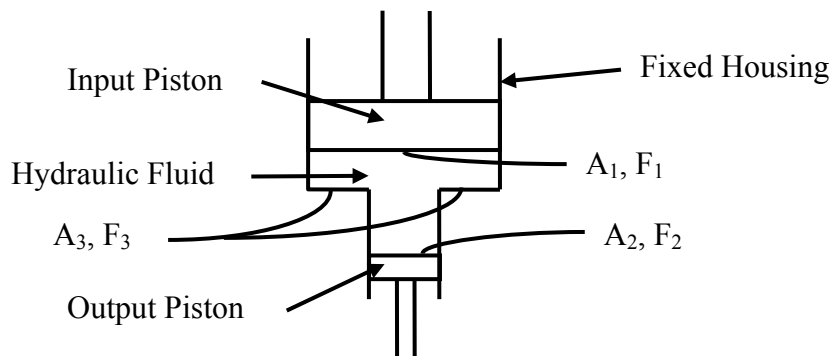


Figure 26 General hydraulic amplifier diagram

As input piston moves in the downward direction by a distance of  $d_1$ , the output piston moves in the same direction by a distance of  $d_2$  to keep the volume of the hydraulic fluid unchanged. This can be represented by the following expression.

$$d_2 = AF \times d_1 \quad (36)$$

where  $AF$  is always defined as a factor larger than 1. The quantity of  $AF$  is the ratio of the cross-sectional areas of pistons 1 and 2.

After analyzing the distance relationship, the force relationship is explored. The assumption employed here is that the pressure between the two pistons remains unchanged. The following expresses the force output with respect to the input force and the amplification ratio. These expressions hold true when losses are not considered.

$$F_2 = \frac{F_1}{AF} \quad (37)$$

The difference between the hydraulic amplifier used in this design and the general hydraulic amplifier described above is the inverted relationship between input piston and the fixed housing. The inverted hydraulic amplifier fixes the input piston and the actuator controls the motion of the housing. As the housing moves downward, pressure drop is created causing the needle to move upward. With this change, the equations above still apply with the change from  $F_1$  and  $d_1$  to  $F_3$  and  $d_3$ .

### **4.3.2 Precompression**

To estimate the maximum needle lift, precompression must be done first to keep the actuator in compression. The analysis for precompression used in section 4.1.1 and equations (24), (25), and (26) can be used in this section. The analysis in section 4.1.1 is relevant up to the first step. The ends of the prepressed spring and the actuator are fixed after compressing the actuator

The second step in this design is to attach the hydraulic amplifier (AMP) and the return disc spring to the actuator group as shown in the following diagram. This is to help the needle to lift during the energizing phase.

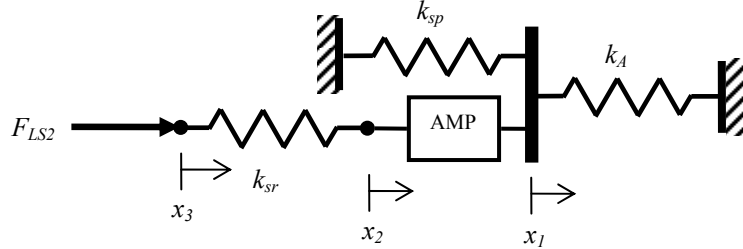


**Figure 27 Simplified schematic for compressing the return disc spring at load step 2 for design 3**

The AMP is attached to the actuator end cap in order to extract the displacement from the actuator. At the other end of the amplifier, the return spring ( $k_{sr}$ ) is connected to aid the needle in lifting in the opening direction. The expression representing the equivalent stiffness of the actuator and prepressed spring in parallel configuration is represented as equation (26). This expression only is only valid at the input side of the amplifier. At the output end of the amplifier, the stiffness must be expressed differently as shown:

$$k_{eq1n} = \frac{k_{eq1}}{AF^2} \quad (38)$$

With this expression at the output end, another equivalent stiffness representing the return spring and equivalent stiffness 1 connected in series configuration can be expressed as:

$$k_{eq2} = \left( \frac{1}{k_{sr}} + \frac{1}{k_{eq1n}} \right)^{-1} \quad (39)$$

In series configuration, the displacements generated by the applied force are expressed as:

$$x_2 = \frac{F_{LS2}}{k_{eq1n}} \quad (40)$$

$$x_3 = \frac{F_{LS2}}{k_{eq2}} \quad (41)$$

$$d_{sr2} = x_3 - x_2 \quad (42)$$

$$d_{sp2} = x_1 \quad (43)$$

These parameters give estimation on how much the actuator is being compressed providing crucial information on how much voltage can be applied while keeping the actuator in compression limits.  $F_{LS2}$  is an adjustable force that compresses the return disc spring. Larger  $F_{LS2}$  compresses the return disc spring more. This gives the needle a higher lifting force. This must be optimized so that the precompression on the actuator still remains.  $d_{sr2}$  represents the distance the return spring is compressed and  $d_{sp2}$  represents the distance the prepressed spring is stretched by.

The third step requires the nozzle housing to compress the injector from the needle end. This is to ensure that the injector can overcome the high pressure fuel at the closing phase. Following figure helps further the analysis.

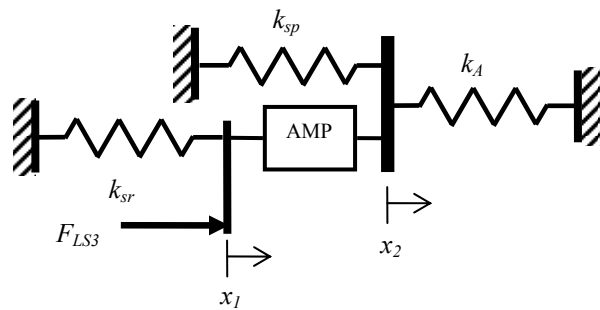


**Figure 28 Simplified schematic for generating sealing force at load step 3 for design 3**

Compare with the physical model, the component that is missing from this figure is the needle. This is ignored due to the fact that the needle is much stiffer than the other component thus it does not affect the result significantly. For simplification, the needle is ignored.

When observed with care, all three spring components are connected in parallel configuration and can be expressed as follows.

$$k_{eq3} = k_{eq1} + k_{sr} \quad (44)$$

The displacements of the return disc spring, prepressed disc spring, and actuator can be obtained using the following equation:

$$x_1 = d_{sr3} = \frac{F_{LS3}}{k_{eq3}} \quad (45)$$

$$d_{sp3} = x_2 \quad (46)$$

With all these load steps, the actuator, prepressed disc spring, and return disc spring are compressed and stretched by a combination of displacements. The total compressed distance of the actuator is as follows:

$$d_{aT} = d_{ap1} - d_{sp2} - d_{sp3} \quad (47)$$

The total compressed distance of the prepressed disc spring and the return disc spring are shown respectively:

$$d_{spT} = d_{sp1} + d_{sp2} + d_{sp3} \quad (48)$$

$$d_{srT} = d_{sr2} - d_{sr3} \quad (49)$$

To realize some physical quantity of these displacements, the properties of these components must be listed first. The actuator chosen for this design has a stiffness of 40 N/ $\mu$ m and a cross-sectional area of 0.0001 m<sup>2</sup>. The stiffness of the prepressed disc spring is 7.19 N/ $\mu$ m and the return disc spring is 0.591 N/ $\mu$ m. The theoretical amplification ratio of the hydraulic amplifier is 4.6. Following table list out all the equivalent stiffness calculated from the component stiffness, the forces applied at different load steps, and the compressed amount of all the components with high pressure fuel.

**Table 7 Quantities used to estimate precompression for design 3 at HP**

$F_{LS1}$	$d_{ap1}$	$d_{sp1}$	$k_{eq1}$	$k_{eq1n}$	$k_{eq2}$	$F_{LS2}$	$d_{sr2}$	$d_{sp2}$	$k_{eq3}$	$F_{LS3}$	$d_{sr3}$	$d_{sp3}$
4500	113	625	47.2	2.23	0.467	200	338	19.5	2.82	350	124	27

These quantities are obtained using the equations presented above. For the above table, the unit for force quantities is in N. For displacements,  $\mu\text{m}$  is used. As for stiffness,  $\text{N}/\mu\text{m}$  is used.  $F_{LS1}$  is fixed due to the maximum compressible amount.  $F_{LS3}$  is fixed to the maximum force generated by the high pressure fuel.  $F_{LS2}$  is the only force parameter that can be optimized to meet the lifting requirement. With these quantities specified, the overall displacements of the actuator, prepressed disc spring, and return disc spring were tabulated.

**Table 8 Overall compression of the actuator, prepressed disc spring, and return disc spring at HP**

$d_{aT}$	$d_{spT}$	$d_{srT}$
66	672	214

The most important parameter from this precompression analysis is the overall compression distance of the actuator. The actuator was originally compressed with a distance of  $113 \mu\text{m}$  but had been reduced to  $66 \mu\text{m}$  due to compression of other components. The estimation of needle lift takes this value into consideration to prolong the life time of the actuator.

At the low pressure fuel state,  $F_{LS3}$  is a reduced by a magnitude of 10 and the following results are obtained.

**Table 9 Quantities and overall compression of various components at LP**

$F_{LS3}$	$d_{sr3}$	$d_{sp3}$	$d_{aT}$	$d_{spT}$	$d_{srT}$
35	12.5	272	90	648	326

In this state, the actuator is compressed more so the actuator can have a larger deformation. This is very advantageous due to the lack of needle lift at LP in the conventional servo-circuit injector

design. Because of the varying load exerted on the needle, the injector system requires voltage to be varied as the common-rail pressure changes.

### 4.3.3 Needle Lift Estimation

With precompression done on injector components, an analysis on how these components interact with each other to generate needle lift was examined. Because the hydraulic amplifier is also a motion inverter, the force analysis was focused on the amplifier. Figure 29 shows the hydraulic amplifier with forces applied on the input end and the output end.

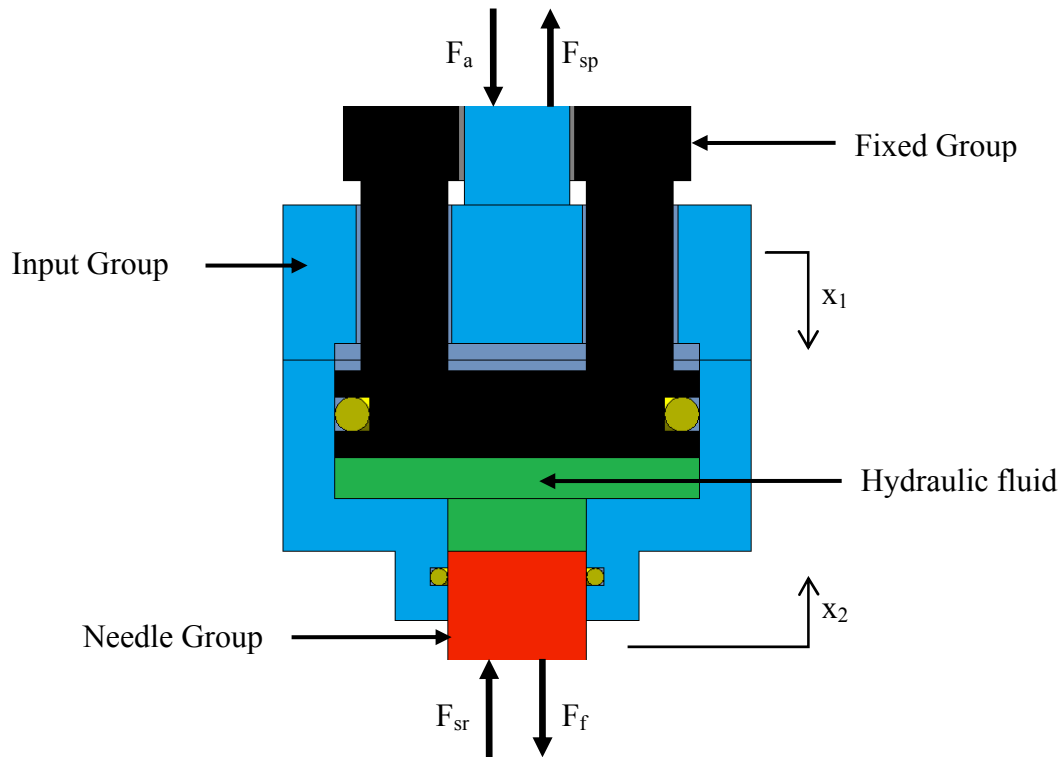


Figure 29 Forces acting on hydraulic amplifier of design 3

All the components in this diagram are specified with a certain color to denote the function of that particular group of parts. The input group is directly controlled by the actuator ( $F_a$ ) and prepressed spring ( $F_{sp}$ ). All parts in this group move as a whole. The main function of this group is to exert force and displacement into the hydraulic system. The fixed group is attached

to the housing that is stationary at all times. This group is to be treated as a fixed piston. The needle group is the output of the whole system. It is connected to return disc spring ( $F_{sr}$ ) and is surrounded by high pressure fuel ( $F_f$ ).

During initiation phase, by taking all the forces on the input side at  $x_1$ , the following net force equation is realized as actuator is energized.

$$F_B - \frac{F_B}{\Delta L_T} x_1 - k_{sp} x_1 - k_{sr} A F^2 x_1 = 0 \quad (50)$$

The first two terms with the variable  $F_B$  describe the force generated by the actuator. As the actuator expands in the  $x_1$  direction, the prepressed spring is compress and generates a force in the opposing direction. The return spring expands in the  $x_2$  direction as actuator is energized thus reducing the resistive return spring force. The  $AF$  factor is used to put the return spring force on the input side. Fuel pressure has no effect at this stage because it is assumed that fuel has not gotten to the bottom of the needle.

After the needle is lifted off the seat, fuel is all around the needle, thus aiding the actuator in lifting the needle in the open direction. The following expression is observed:

$$F_B - \frac{F_B}{\Delta L_T} x_1 - k_{sp} x_1 - k_{sr} A F^2 x_1 + F_f A F = 0 \quad (51)$$

This is very similar to equation (50) with the addition of the fuel pressure term at the end. Because the summation of forces is at the input end, the amplification factor is present to ensure the correct forces are taken.

By isolating these two equations with respect to  $x_1$ , the maximum expansion of the actuator can be tracked. In terms of location the position of the needle, the simple relationship of the input and output of a hydraulic amplifier is used. Refer to equation (36) for more details on

how to relate the input to the output displacement. The prismatic stack actuator (square cross-sectional area) chosen for this design has the following characteristics listed in Table 10.

**Table 10 Dimensions and properties of the stack actuator in design 3**

<b>d<sub>s</sub> (mm)</b>	<b>L (mm)</b>	<b>t (μm)</b>	<b>d<sub>33</sub> (m/V)</b>	<b>E<sub>a</sub> (GPa)</b>
10	100	250	680 x 10 <sup>-12</sup>	40

With this specific actuator, prepressed disc spring, return disc spring, and the load steps, the injector is estimated to have the following performance in terms of lifting.

**Table 11 Estimated results using analytical model for design 3**

	<b>Initiation</b>	<b>Lifting at HP</b>	<b>Voltage at HP</b>	<b>Lifting at LP</b>	<b>Voltage at LP</b>
x <sub>1</sub> (μm)	38.3	65.5	210 V	90.2	480 V
x <sub>2</sub> (μm)	176	301		415	

As shown in Table 11, a minimum of 300 micron lifting was achieved in both LP and HP cases. A more desirable condition was achieved with this design is the larger lifting distance achieved at LP. This was due to the larger compression on the actuator allowing the actuator to expand more while staying in the compression region. Simulation was not done on this design due to the difficulty in incorporating the fluid portion with the solid aspect of the design. This design requires the use of multi-physics portion of ANSYS. Due to time constraint, a prototype is the next step for this design.

## **Chapter 5 Simulations**

The first two injector designs were simulated in ANSYS. The main objective here is to verify the analytical models shown in the last chapter. The simulation helped identify whether the designs can meet the requirements of this project.

### **5.1 Generation 1 Injector**

The static simulation done on this design was based on the displacement. Results obtained from this are compared with the results from the analytical analysis. Modal analysis was done for the dynamic simulation to ensure that the design could be subjected under high frequency of operation.

#### **5.1.1 Static Simulation**

The piezoelectric actuator must be in compression at all times and thus requires an application of a prepressed load. To apply this load accurately, 2 load steps are required. The first step is to apply the load at the free end. The second step is to fix the free end where the load was applied on. This prepressed load is crucial in this design simulation because it is needed to validate the behavior of the piezoelectric actuator under prepressed load. To do this preload condition in one load step requires an innovative way to apply the prepressed load on the actuator. A cross-section showing all the components used in the simulation is shown in Figure 30.

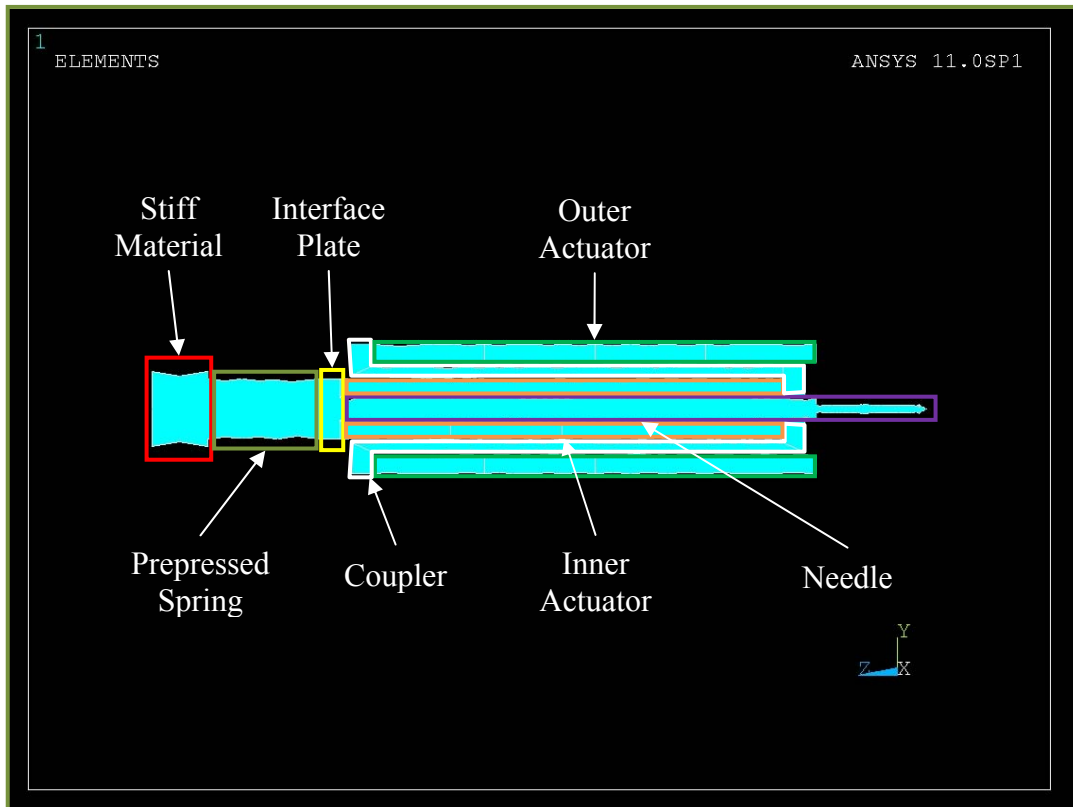


**Figure 30 Gen 1 injector component diagram in ANSYS**

The end of the outer actuator is fixed. At the point where the load is applied, a virtual material with a very high stiffness (stiff material) is modeled at that location. The circumferential area of that material is fixed. A high load is applied at the end of the stiff material to induce deformation. This deformation causes the prepressed spring to deflect. Because the material is very stiff, as the piezoelectric actuators are energized, the force it exerts onto the stiff material is not able to deform it thus simulating a fixed end boundary condition. In this simulation, the elastic modulus used is  $10 \times 10^4$  GPa and the force applied is  $45 \times 10^9$  N. To make sure that the right amount of load is applied on the injector, the deflection of the stiff material must be verified before and after the application of voltage onto the actuators.

Because of the long length of piezoelectric stacked actuators required in this design, a large number of layers are required for each actuator. This number can go up to thousands for

one single actuator. Applying voltage onto layers becomes a very difficult task with increasing number of layers. With thinner layers, the elements limited by the thickness are finer but the number of elements increases at the same time. This pushes the limits of the maximum number of elements provided by ANSYS educational version. To avoid this issue, a method was developed to overcome this. It is known that  $d_{33}$  is the property that determines the deformation of piezoelectric stacked actuators. This parameter is changed proportionally to keep the deformation the same while lowering the number of layers. In this design, the number of layers for one actuator is 2000. With the use of equation (1), the new piezoelectric strain constant can be defined. Keeping the voltage the same, following equation can be used to determine the new piezoelectric strain constant.

$$d_{33\_new} = \frac{n_{old}}{n_{new}} d_{33\_old} \quad (52)$$

The new piezoelectric strain constant calculated is  $3.4 \times 10^{-7}$  m/V.

In the actual design, the outer actuator has a larger cross-sectional area than the inner actuator. This is done to prevent the rings thickness from being too thin. The actuator with a larger cross-sectional area generates a higher blocking force. In the analysis from section 4.1, the blocking force used is the smaller of the two. Therefore, in order to compare the simulation result with the analytical result, the outer actuator must be modeled with the same cross-sectional area relative to the inner actuator.

To find out the needle lift, 2 separate simulations must be done. Reason behind this is because of the additional load applied at the needle tip to make sure that the injector can overcome the high pressure fuel force and seal the nozzle. The first simulation models the sealed position where voltage of 0 V is applied to all electrodes and a pressure of 200 MPa is applied at the needle tip as shown in Figure 31.

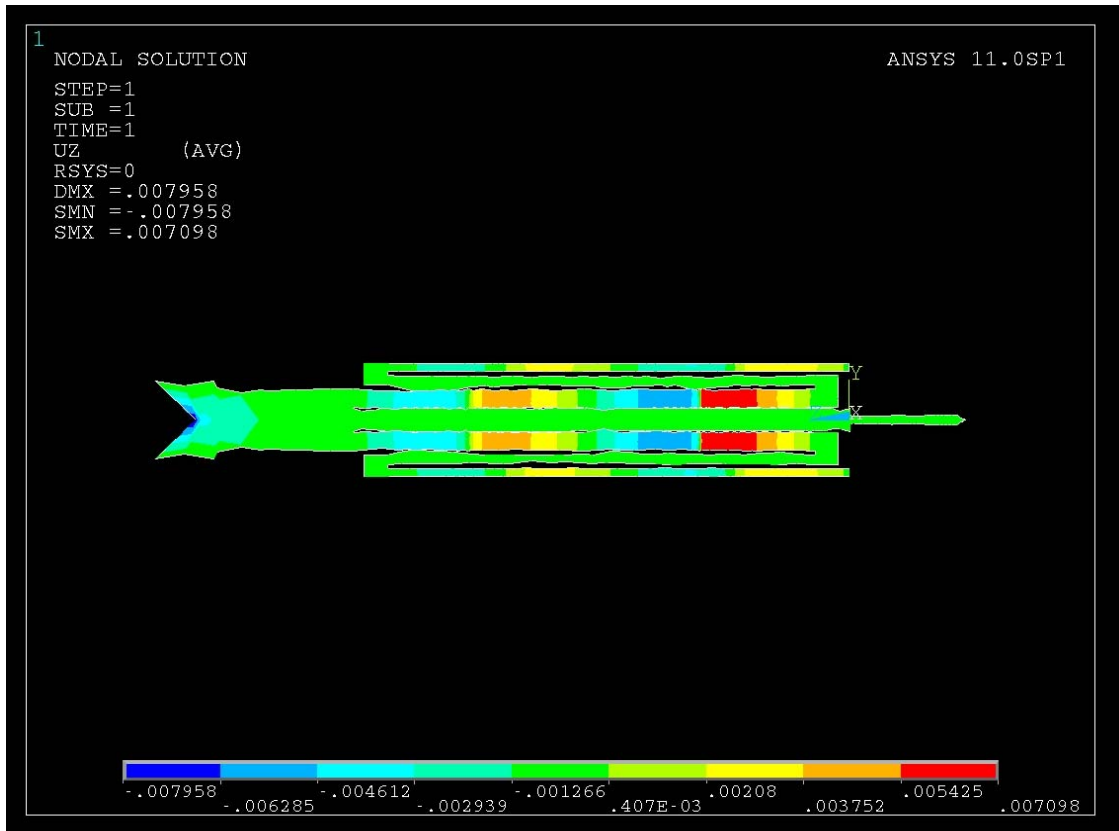
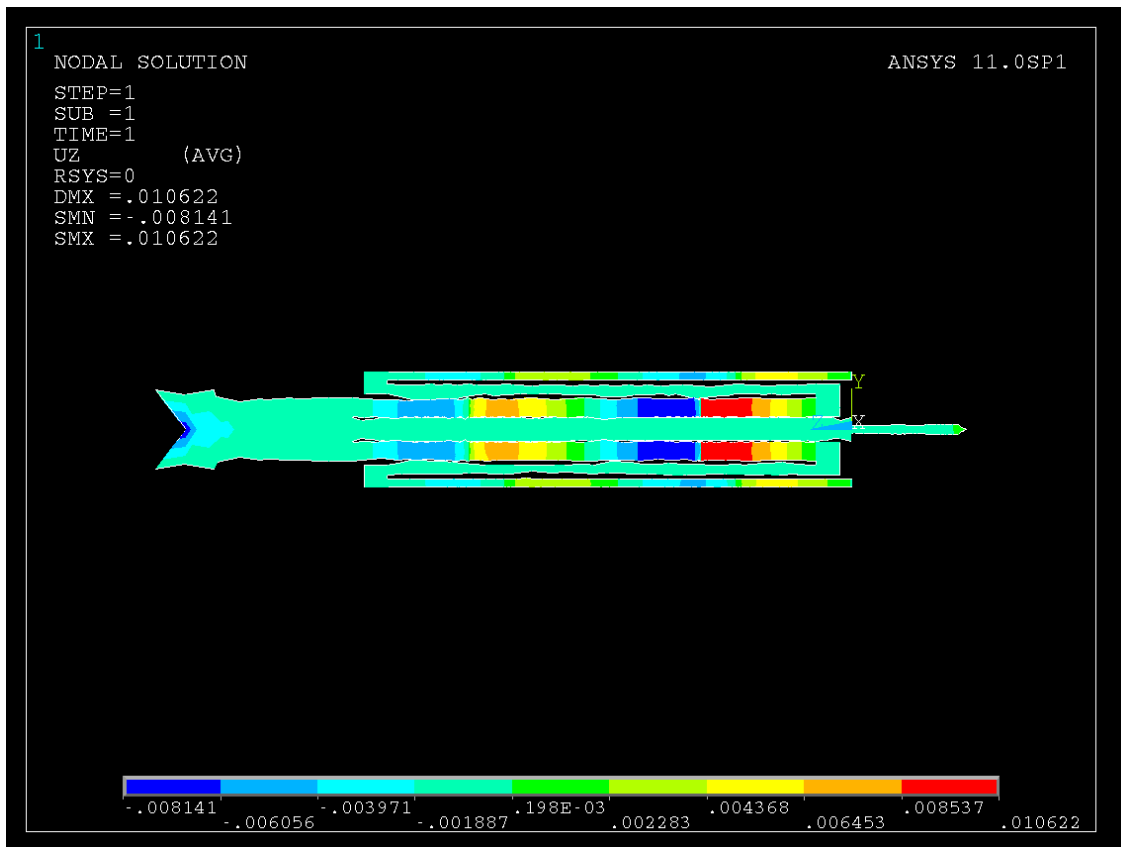


Figure 31 Gen 1 injector under sealed state simulated in ANSYS

There are a few displacements results that are important to look at. The first one is the stiff material displacement. A displacement of -2.2724 mm was taken from the center on the left side where the force is applied. The actual deformation from this prepressed displacement should be -2.07 mm. However, with the non-uniform deflection due to the constraint at the circumferential area of the stiff material, a value larger than -2.07 mm is more realistic due to the decrease in deflection with increase radial direction. The second displacement of interest is the needle location. The tip of the needle was found to be at -202.19  $\mu\text{m}$ .

The second simulation represents the lifting phase and is split into 2 separate simulations because of the high and low pressure fuel cases. During high pressure fuel case, voltage of 200 V is applied to every other electrodes and 200 MPa is applied at the needle tip as illustrated in Figure 32.



**Figure 32 Gen 1 injector under lifting state at high pressure case simulated in ANSYS**

By extracting the displacement results from the simulation, the deflection of the stiff material remained the same at -2.2724 mm as suspected. The tip of the needle was located at 210.26  $\mu\text{m}$ . For the low pressure fuel case, voltage of 200 V is applied to every other electrodes and 20 MPa is applied at the needle tip. This is seen in Figure 33.

The results from this simulation showed that the stiff material remained at the same position and the tip of the needle was at 96.86  $\mu\text{m}$ . The total needle lift is the addition of the needle position of the two phases as tabulated in Table 12. These results are very close to the analytical result presented in Table 4. The difference between the results calculated using analytical method and simulation was calculated to be 4 % for both HP and LP cases. This showed that that analytical model on the Precompression was done correctly.

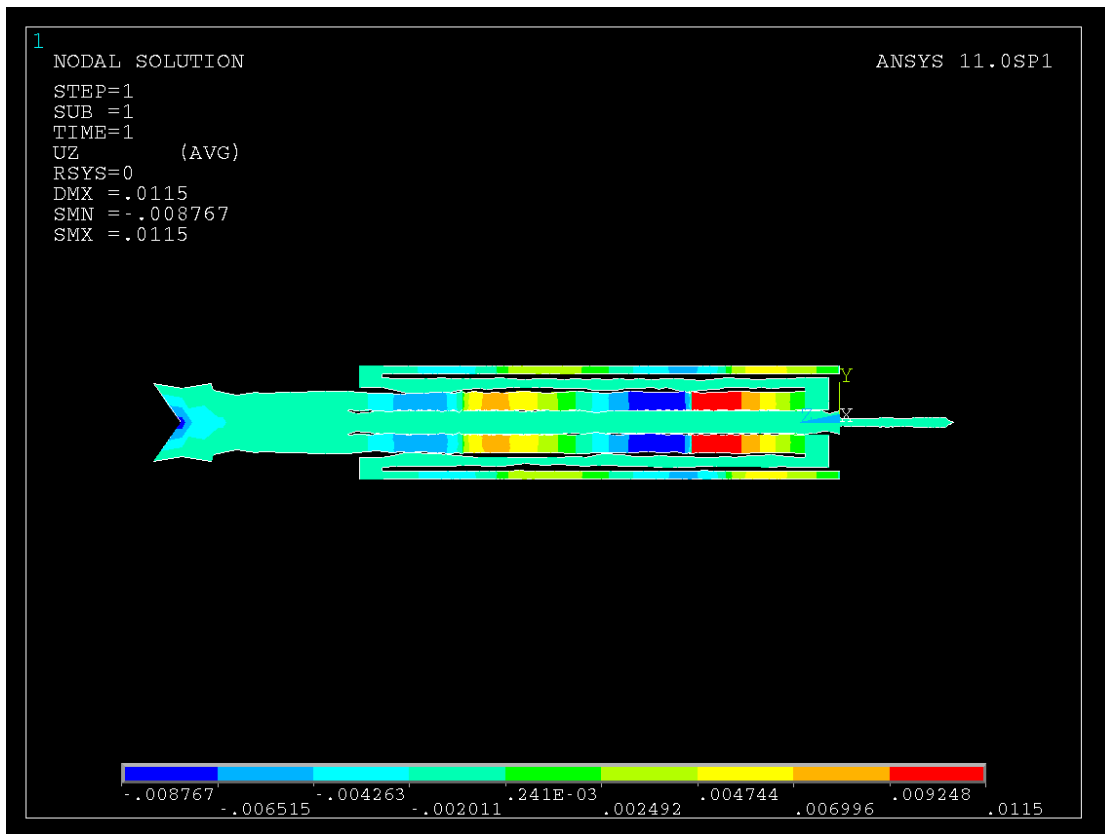


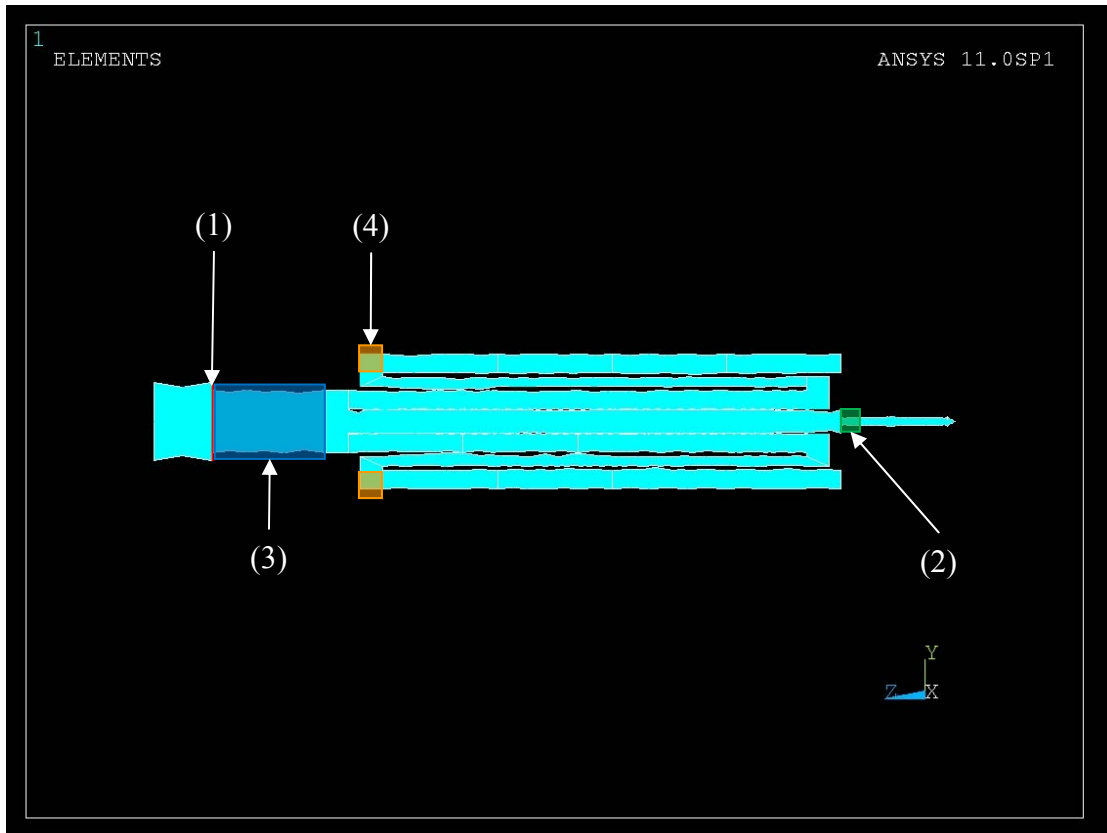
Figure 33 Gen 1 injector under lifting state at low pressure case simulated in ANSYS

Table 12 Simulated results using ANSYS

$x_3$ ( $\mu\text{m}$ )	At HP	At LP
Sealed	-202.19	-202.19
Lifting	201.26	96.86
Total	403.45	299.05

### 5.1.2 Dynamic Simulation

For the dynamic simulation done in ANSYS, the same geometric model is used as shown in Figure 34.



**Figure 34 Gen 1 injector modal analysis fixed locations**

The difference is the location of the fixed end. In modal analysis, loads are not taken into part of the simulation, thus it is not necessary to apply the prepressed force onto the injector. Because of this, the stiff material is not included in the analysis. The fixed end is located at the cross-sectional area between the stiff material and the prepressed spring as shown by indicator (1). With this restraint in all direction, the first mode occurred at 130 Hz, implying that this injector could not achieve the desired frequency of 1000 Hz. This could be improved by adding additional constraints to the system. A new constraint was added at (2) on the circumferential area of the needle acting as a roller support. The support allowed the needle to have motion in the z direction only. This increased the first mode to 277 Hz. Another constraint was placed on the prepressed spring as shown by indicator (3) acting as a guide for the spring. This allowed only motion in the z direction. An improvement up to 398 Hz was achieved. Lastly, the coupler

wall thickness was increased from 4 mm to 5 mm. An additional restraint was placed at (4) as a roller support allowing only motion in the z direction. A frequency of 733 Hz was achieved.

If this design were to be pursued, restraints using bearings or other supports must be positioned at (1) to (4) along with the wall thickness of the coupler to increase the natural frequency of the injector. This can be difficult to apply in reality.

## **5.2 Generation 2 Injector**

In the static simulation, simulation on the serpentine spring is presented first to compare with the results obtained from the analytical model. After that, the two aspects of the mechanical amplifier that must be verified through ANSYS are presented. The first one is the linear relationship between the force input and the displacement output. The second one is the maximum lifting against the fuel high pressure fuel. Modal analysis was performed again to ensure the natural frequency is higher than 1000 Hz.

### **5.2.1 Static Simulation**

To verify the analytical model built in section 4.2.1, a simple ANSYS model was built to check how accurate the analysis was. A geometrical model was built in ANSYS with a fixed end and a coupled moment. The material chosen was copper. Simulation was carried out 3 times varying in the moment applied at the input end. The following results were obtained as a comparison to those shown in Table 6.

Because results obtained are linear, the three sets of results show that there is around 35% error. A large part contributing to this error can be the length of the beam. The beams are very short, so the assumption of treating them as beams under bending moment might not be a good idea.

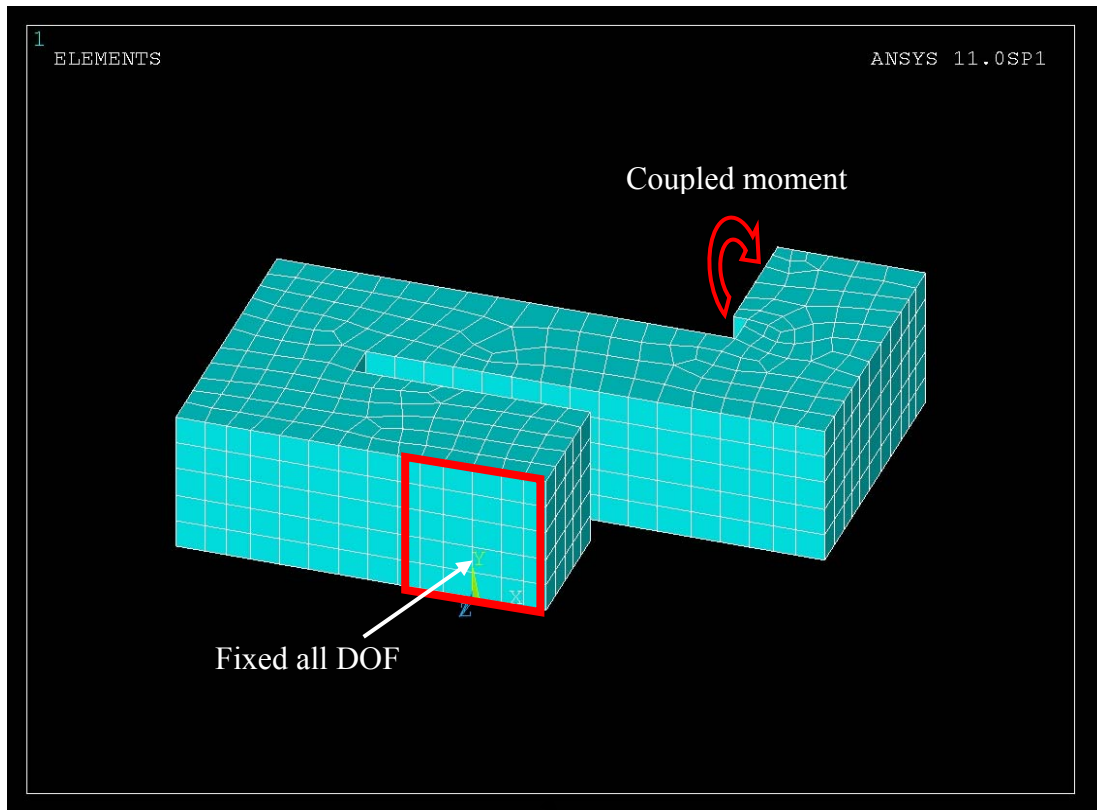


Figure 35 Geometrical model of the serpentine spring built in ANSYS

Table 13 Simulated results of serpentine spring

Moment (Nm)	Angle (degrees)
0.0018	0.11
0.009	0.58
0.018	1.05

After simulating only the serpentine spring, a geometrical model of the mechanical amplifier was built along with the needle attached at the end as shown in Figure 36. The actuator was not modeled in this simulation due to the difficulty in mounting the contacting surface to the end of the beam. Instead, actuator force was directly applied onto the end of the beam. To verify the relationship between force input and displacement output, 3 separate loads were applied to the model and results were tabulated as follows.

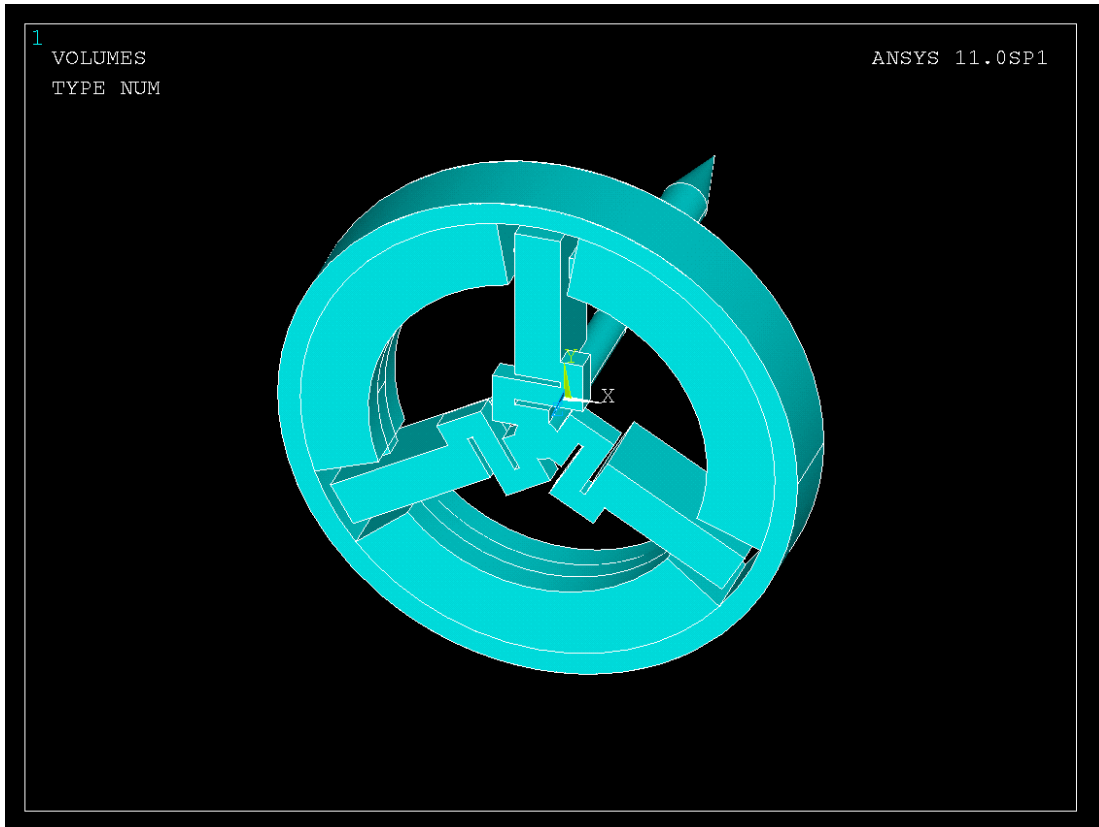


Figure 36 Gen 2 injector geometrical model done in ANSYS

Table 14 Gen 2 injector tabulated static simulation results from ANSYS

<b>Force (N)</b>	2000 N	500 N	20 N
<b>Input displ. (<math>\mu\text{m}</math>)</b>	108	27	0.977
<b>Output displ. (<math>\mu\text{m}</math>)</b>	188	46.9	1.69
<b>Ratio</b>	1.74	1.737	1.73
<b>Stiffness (N/<math>\mu\text{m}</math>)</b>	10.638	10.661	11.834

With the different loads applied onto the amplifier, the amplification ratio and the stiffness stayed fairly consistent except at the lower end of the force range. Therefore, a linear relationship between the force and output displacement relationship could be assumed. These simulations were done without the consideration of the fuel pressure. Once the fuel pressure is incorporated into the system, the amplification ratio is expected to be less.

Instead of simulating the needle lift conditions right away, the initiation phase was simulated first separating into high pressure fuel case and low pressure fuel case. In this design,

the fuel pressure helps by pushing the needle against the nozzle seat contributing to the sealing force. The force applied to simulate the actuator force is 2000 N because once the actuator starts to expand, the blocking force decreases generating less force. In the low pressure fuel case, the input displacement of 93.58  $\mu\text{m}$  was measured at the beam end and the output displacement of 126.39  $\mu\text{m}$  was measured at the needle tip as shown in Figure 37. This revealed that the amplification ratio dropped to 1.35.

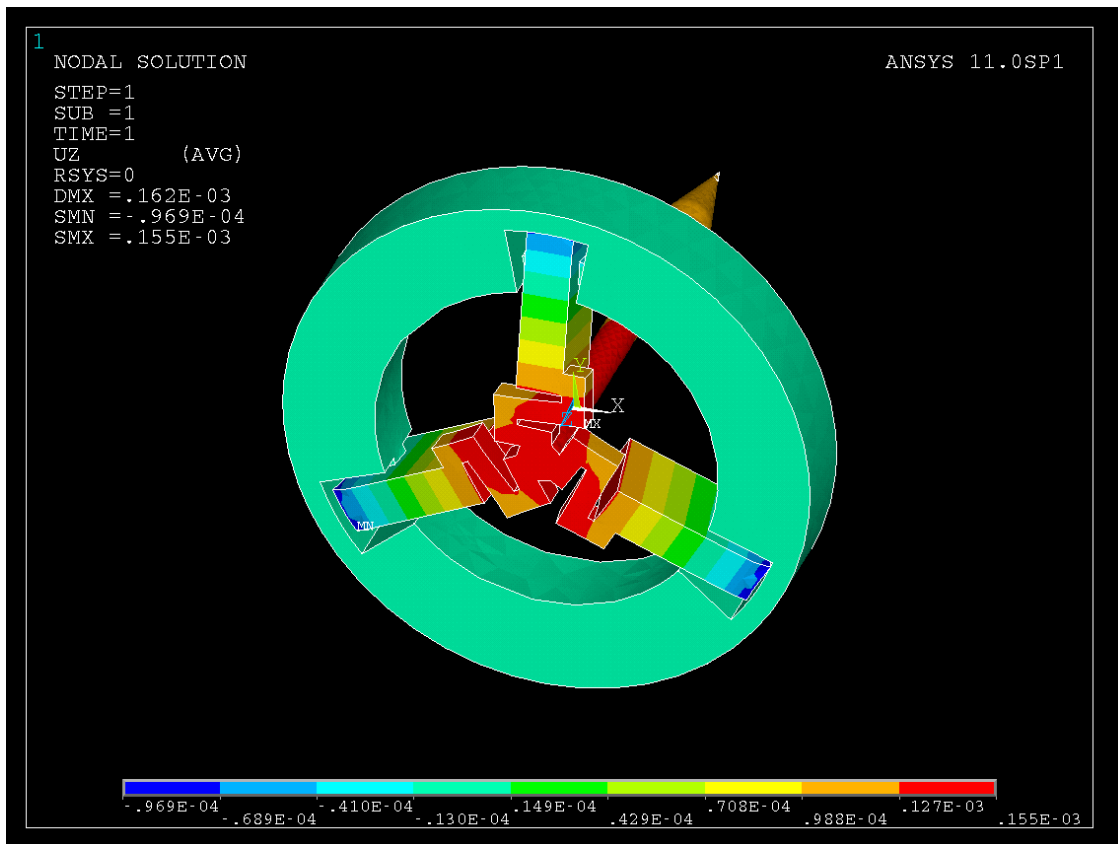


**Figure 37 Gen 2 injector static analysis with low pressure fuel in ANSYS**

Under the high pressure fuel case, the input displacement measured was 2.64  $\mu\text{m}$  and the output displacement was -388.9  $\mu\text{m}$  as shown in Figure 38. In this case, the mechanical amplifier could not overcome the fuel pressure to lift the needle off the nozzle seat. It could be argued that a higher force should be applied to simulate the blocking force.

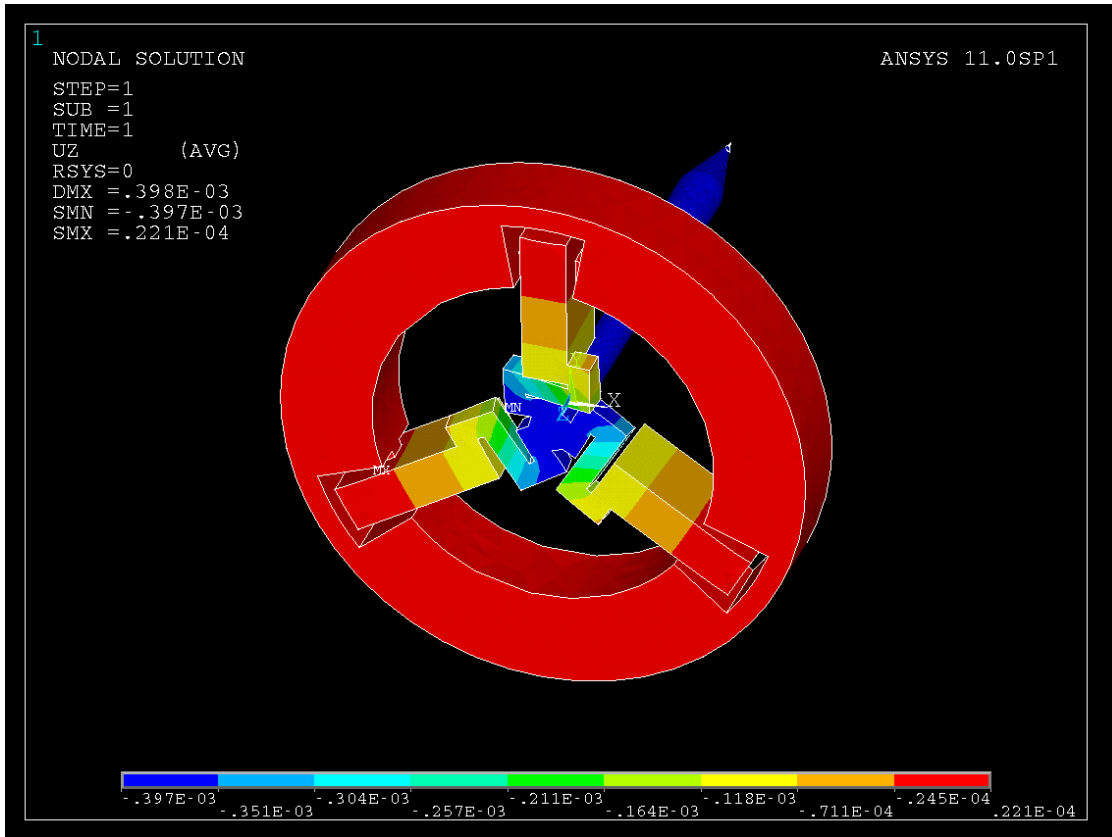


**Figure 38 Gen 2 injector static analysis with high pressure fuel in ANSYS**

Even if the blocking force were applied, the needle will still be shut at the nozzle seat because a lot of force is required to overcome a displacement of  $-388.9 \mu\text{m}$ . The only way to increase the blocking force is to increase the cross-sectional area of the actuator; however, this will once again put a heavy strain on the electrical requirement and is not feasible to apply. If the serpentine were to be strengthened to stiffen up the beam at the joint to minimize twisting motion, the bending motion will be affected thus dampening the amplification ratio. Considering the results from this simulation, it was decided that this design will not be further developed. Because of this, analytical needle estimation was not done on this design; thus, the third fuel injector design is to overcome this problem.

## **Chapter 6 Design of Experiments**

The first two designs were not promising for further development; therefore, only the third design was developed for further testing and experimentation. Before designing the experiments, both the test rig and injector prototype were built. The combination of the two simulated the real conditions of the actual injector as close as possible. Because the third design consists of a hydraulic amplifier, experiments were split into testing just the actuator, the hydraulic amplifier, and the whole assembly together.

### **6.1 Prototype and Fixture Design**

The prototype was designed to simulate the design 3 built in SolidWorks. The test rig was designed to hold the prototype in the upright position and to provide a fixed rigid support. It is required to secure sensors to measure the input and output displacement. This section shows the most general configuration of whole setup.

#### **6.1.1 Design**

By modifying Figure 13, most of the parts remained in the prototype. The connections between components appeared differently. The prototype with the fixture is shown in Figure 39. CS1 refers to a hole made for capacitive sensor in sensing the input displacement. A set screw hole is made to secure the capacitive sensor in the desired location. LC refers to the screw holes made for the locating load sensor securely. In this prototype, incorporation of the high pressure fuel is neglected due to the lack of facility to properly simulate the common-rail system; therefore, the fuel reservoirs are not included in the prototype.

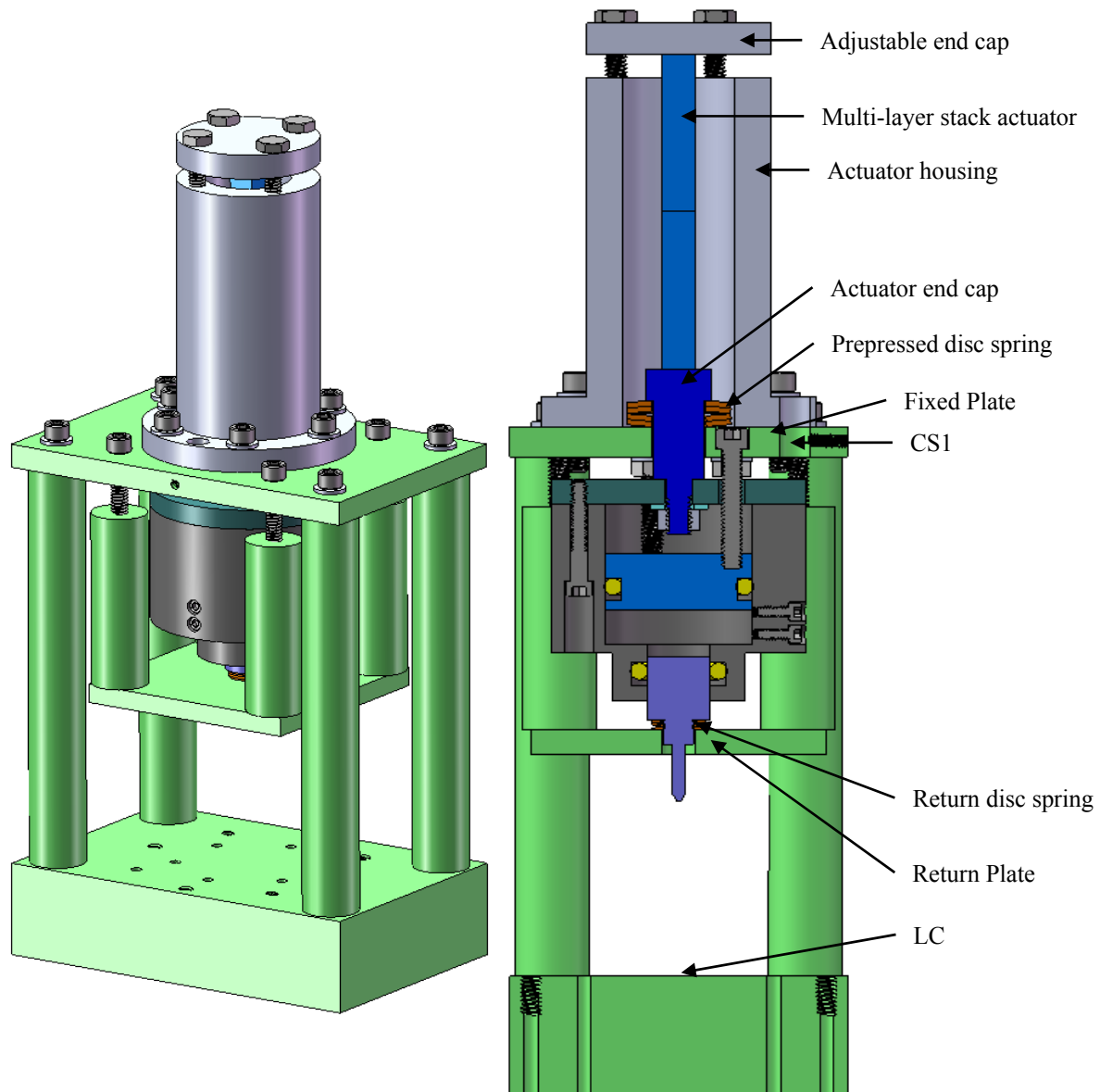


**Figure 39 Isometric and cross-sectional drawing of prototype with test rig**

With the fuel pressure neglected, the confirmation whether the needle can initiate lifting in the presence of high pressure fuel cannot be verified. However, the maximum needle lifting can still be verified through this prototype. The breakdown of all the components for the hydraulic amplifier is shown in Figure 40.



**Figure 40** Diagram showing all the components in the fuel injector prototype

## **6.1.2 Assembly**

For this prototype, the assembly procedure is different from the proposed one from section 2.3.3. One main reason is because the hydraulic amplifier cannot be assembled with just the injection of the fluid through the inlet. By injecting through the inlet, a lot of air is still trapped within the fluid chamber. Because of this, an innovative way of assembling the hydraulic amplifier by submerging the whole structure under the fluid is implemented. The procedure for assembling the hydraulic amplifier is presented first before assembling all the other components. Technical drawings of all the components can be found in Appendix A.

### **Hydraulic amplifier**

Some of the parts of the hydraulic amplifier were machined out of raw steel (cold-rolled 1018). Other parts were purchased from McMaster-Carr [21] with a part number specified.

Before the procedures, a bill of material is shown in Table 15 to list out all the parts needed in this section and a diagram showing the breakdown of all the parts is shown in Figure 41. An assembled view of the hydraulic amplifier is shown in Figure 42.

**Table 15 Bill of material for hydraulic amplifier**

No.	Part Name	Part #	Quantity	Description
1	Fixed Plate	Machined	1	Provides fixed support for injector.
2	Actuator end cap	Machined	1	Transfers the spring force on the actuator and connects to the amplifier housing.
3	Connecting plate	Machined	1	Connects the end cap with the amplifier housing.
4	Input piston	Machined	1	Provides fixed end for the hydraulic amplifier.
5	Needle	Machined	1	Connects to the return disc spring and provides output displacement.
6	Amplifier housing	Machined	1	Holds the hydraulic fluid inside the fluid chamber.
7	Supporting struts	9125A546	3	Connects the input piston to the fixed plate 1.
8	Spring washer	9110A229	3	Rigidly fixes the upward and downward movement of the input piston with the nut.
9	Nut	90480A029	3	Rigidly fixes the upward and downward movement of the input piston with the spring washer.
10	Washer	98019A385	1	Fixes the actuator end cap with the connecting plate with the locknut.
11	Locknut	93591A200	1	Fixes the actuator end cap with the connecting plate with the washer.
12	Connecting screws	93705A249	3	Attaches the connecting plate to the amplifier housing
13	O-ring 1	8333T347	1	Keeps hydraulic fluid from leaking from the input piston.
14	O-ring 2	8333T337	1	Keeps hydraulic fluid from leaking from the needle.
15	Prepressed disc spring	96445K289	4	Prepresses the actuator and keeps the injector in the sealed position when not energized.
16	Sealing screws	95198A415	2	Seals the inlet and outlet holes on the amplifier housing.
17	DTE25	2158K12	-	Hydraulic fluid.

There are a few important features to note here. The first one is regarding the supporting struts. Each of these struts requires a set of spring washer and nut to tightly secure it in both upward and downward directions. This is crucial in locking the input piston in a specific location as the amplifier housing pushes against or pulls away from it.



**Figure 41 Diagram showing all the components of the hydraulic amplifier**

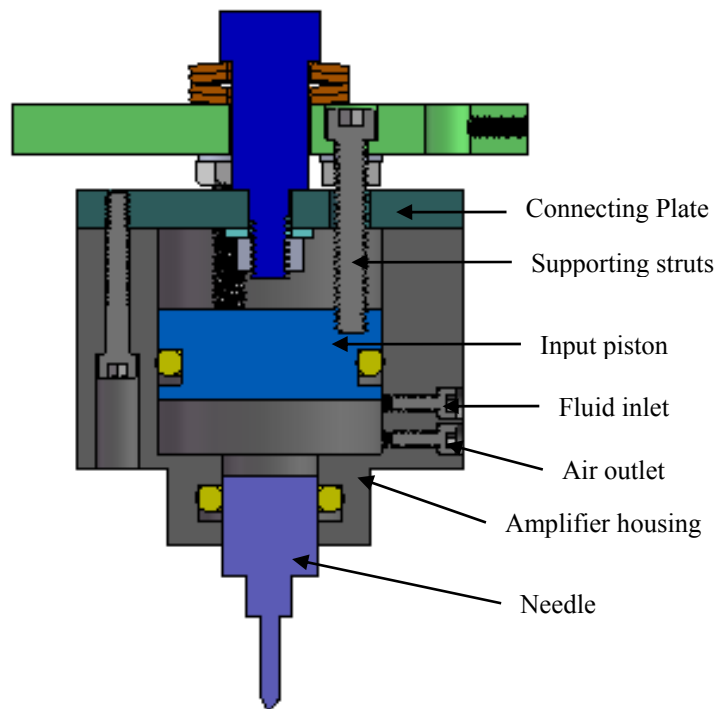


**Figure 42 Cross-sectional drawing of the hydraulic amplifier**

The second feature is the two holes on the amplifier housing. At the assembly stage where fluid is injected into the fluid chamber through the inlet, and air is extracted from the outlet. This is

no longer implemented because the amplifier is assembled under the hydraulic fluid. The two holes are each sealed with screw with an o-ring at the end of the socket head. This helps to keep the fluid from leaking out of the amplifier.

### **Assembly Procedures:**

1. Assemble the prepressed disc spring in the proper configuration and slide them through the actuator end cap. The disc spring configuration requires four disc springs in total. Each set contains two disc springs in parallel. The sets are connected in series.
2. Put the three supporting struts through fixed plate 1.
3. Slide the fixed plate 1 into the actuator end cap so the assembled disc spring is between the actuator end cap and the fixed plate 1.
4. Slide the spring washer and nut through the supporting struts until the spring washer is contacting the fixed plate 1 but not tightened.
5. Slide the connecting plate, washer, and locknut onto the threaded portion of the actuator end cap. Align the holes on the connecting plate with the fixed plate 1. Fix the assembly tightly with a wrench and pliers.
6. Put o-ring 1 around input piston. Screw the supporting struts onto the input piston with Allen wrench.
7. Tighten up the nuts and spring washers around the supporting struts.
8. Fit the o-ring 2 inside the amplifier housing.
9. Put the amplifier housing, connecting screws, sealing screws, and needle inside a large container with DTE25. All parts must be completely submerged. Submerge the entire input piston component of assembly into the liquid. Wait 30 minutes until all the air

bubbles have escaped. Check by rotating parts inside the liquid to make sure all air have escaped.

10. Slide the amplifier housing through the input piston so it contacts the connecting plate. Fasten the connecting screws to the amplifier housing tightly. The input piston must remain submerged through the whole process.
11. Slide the needle into the amplifier housing and make sure the o-ring 2 is contacting the needle.
12. Tighten the sealing screws to completely shut the reservoir.
13. Leave the assembly to dry by hanging or with paper towel.

## Fixture

The fixture is the part that holds the joins other parts of the injector together. The fixture could be assembled in different configurations for different experiments. The basic injector configuration is shown in Figure 39.

**Table 16 Bill of material of all the components for the fixture**

No.	Part Name	Part #	Quantity	Description
1	Bottom plate	Machined	1	Provides a rigid support for the injector and sensors.
2	Fixed pillar	Machined	4	Tightly fixes the position of the injector with respect to the bottom plate.
3	Return plate	Machined	1	Provides strong support for the return disc spring.
4	Return pillar	Machined	4	Connects the return plate to the fixed plate.
5	Actuator housing	Machined	1	Provides a rigid support for the adjustable end cap to compress the actuator.
6	Adjustable end cap	Machined	1	Provides compressive load with strong cap.
7	Bolts	95362A105	4	Holds the adjustable end cap to the actuator housing.
8	Spring washer	9110A229	18	Prevents screws from loosening.
9	Fixing screw 1	91251A542	18	Fixes different components together.
10	Fixing screw 2	91251A544	4	Fixes the fixed plate to the return pillars.
11	Return disc spring	96475K233	3	Additional force helps with lifting the needle.

### **Assembly Procedures:**

1. Attach the fixed pillars to the bottom plate with the use of spring washers and fixing screw 1.
2. Carefully install the hydraulic amplifier on the other end of the fixed pillars using spring washers and fixing screw 1.
3. Position the actuator housing by aligning the CS1 holes to the fixed plate. Fix the position using spring washer and fixing screw 1.
4. Fasten the return pillars to the return plate with spring washer and fixing screw 1.
5. Assemble the return disc spring and insert it around the needle. Fixes the return disc spring by compressing it with the return plate. Attach the return pillar to the fixed plate loosely with fixing screw 2.
6. Adjustable plate end cap can be attached at the end of the actuator housing using the bolts after the actuator has been inserted.

### **Sensors Mounting**

There are several locations to mount the capacitive sensor to measure the input and output displacement. As shown in Figure 39, the location to mount the capacitive sensor to measure the input displacement is label by CS1. At this location, the capacitive sensor is inserted into the hole and the location is secured by a set screw with nylon tip. Nylon tip is used to protect the capacitive sensor casing from warping. In order to make sure that the measurement is accurate, a copper plate is fixed onto the flat surface of the connecting plate. Copper is chosen due to its high conductivity. A wire is soldered onto the copper plate and grounded by fixing the other end of the wire to the casing of the capacitive sensor. This ensures the copper plate is properly grounded. A detailed diagram is shown in Figure 43.

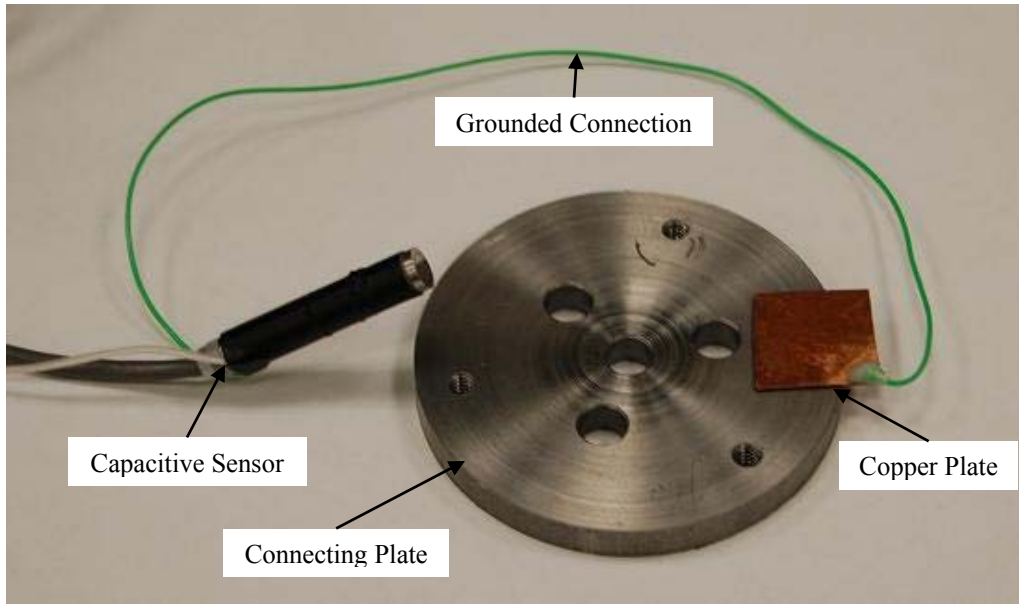


**Figure 43 Capacitive sensor mounting diagram for location 1**

The second location for mounting the capacitive sensor is at the output end, which is at the needle. This requires two additional components to properly measure the displacement at the output end. An aluminum plate (C.S. Clamp) designed to secure the capacitive sensor and another aluminum plate (Measure Plate) designed to fix itself onto the body of the needle were fabricated. The C.S. clamp is mounted on the adjustable mechanical stage allowing the height of the capacitive sensor to be adjusted easily. A copper plate is fixed onto the end of the measure plate to ensure the displacement is measured with minimal error. A wire is also soldered on this copper plate and attached to the casing of the capacitive sensor for proper grounded connection. A detail diagram showing all the parts is shown in Figure 44. Refer to Appendix A for technical drawings of the two aluminum plates.

For the load cell, the sensing location is at the center of the sensor. A bolt of size 3/8-24 is used as the interface component between the load cell and the location for load application or sensing so that the load application or sensing location is evenly distributed at the center. The bottom fixed plate has six threaded holes for securing the position of the load cell.

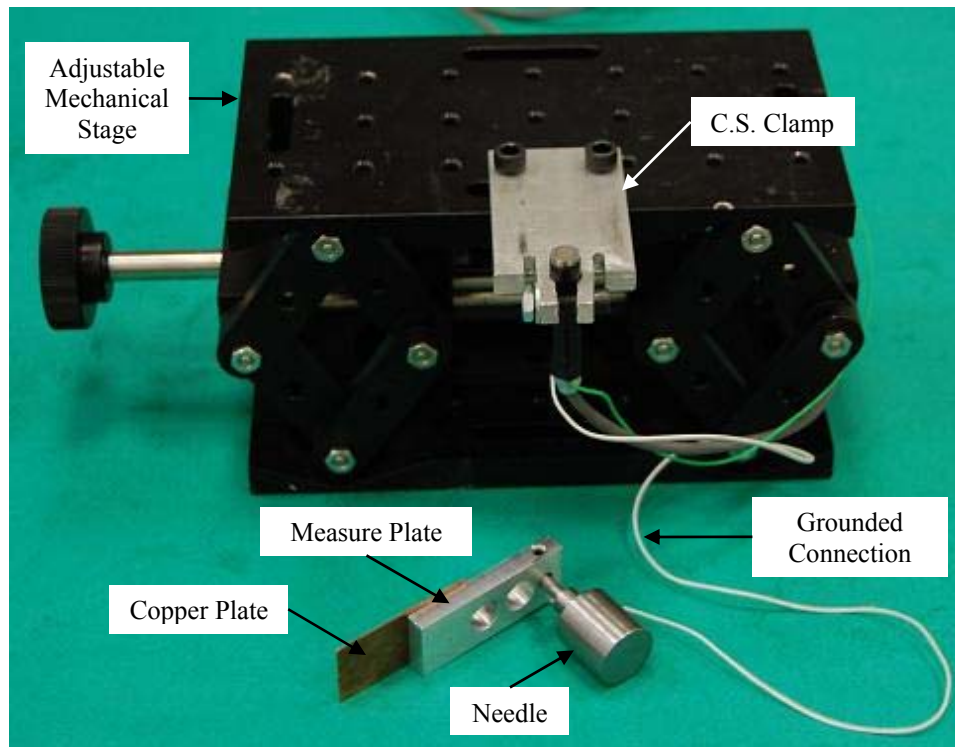


Figure 44 Capacitive sensor mounting diagram for location 2

## 6.2 Prepressed Piezoelectric Actuator Performance Test

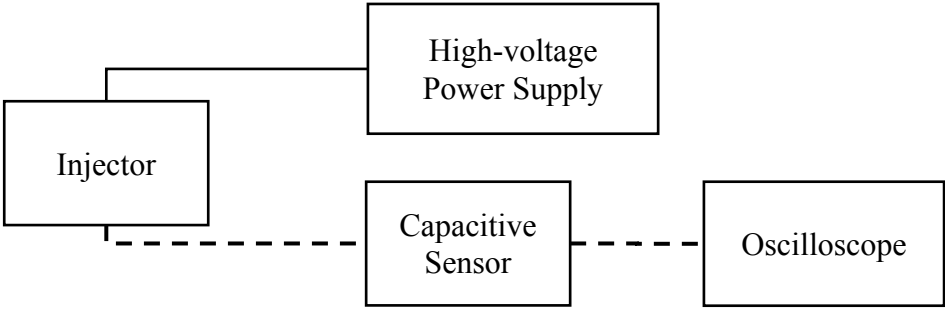
The available piezoelectric stack actuator was purchased from SensorTech. The actuator is to be subjected under a preload force from the prepressed disc spring. Since the stiffness of the prepressed disc spring is known, preload force is measured by the total distance moved with the use of a capacitive sensor. The parts that are necessary to set this test up are shown in Table 17.

Table 17 List of componenets required for actuator performance test

No.	Part Name	Part #	Quantity	Description
1	Fixed Plate	Machined	1	Provides fixed support for injector.
2	Actuator end cap	Machined	1	Transfers the spring force on the actuator and connects to the amplifier housing.
3	Connecting plate	Machined	1	Connects the end cap with the amplifier housing.
4	Bottom plate	Machined	1	Provides a rigid support for the injector and sensors.
5	Fixed pillar	Machined	4	Tightly fixes the position of the injector with respect to the bottom plate.

6	Prepressed disc spring	96445K289	4	Prepresses the actuator and keeps the injector in the sealed position when not energized.
7	Washer	98019A385	1	Fixes the actuator end cap with the connecting plate with the locknut.
8	Locknut	93591A200	1	Fixes the actuator end cap with the connecting plate with the washer.
9	Actuator housing	Machined	1	Provides a rigid support for the adjustable end cap to compress the actuator.
10	Adjustable end cap	Machined	1	Provides compressive load with strong cap.
11	Bolts	95362A105	4	Holds the adjustable end cap to the actuator housing.

The equipments needed in this part of experiment are capacitive sensor, oscilloscope, and high-voltage power supply. Equipments are connected as shown in Figure 45.



**Figure 45 Presentation of how equipments are connected for actuator performance test**

The solid line represents the high-voltage connection between the injector and the power supply. The dash line represents information flow. Capacitive sensor captures the physical information provided by the injector and converts into analog data. Since the capacitive sensor only has an analog dial for data output, an oscilloscope is connected to read the digital signal for more data analysis. The test equipments and the prototype arrangement are shown in Figure 46.

**Testing Procedures:**

1. Insert the actuator into the actuator housing and secure using bolts.



**Figure 46 Physical arrangement of the prototype and test equipments for actuator test**

2. Position the capacitive sensor probe so that it is in sensing range with the connecting plate.
3. Tighten the bolts to increase the preload to desired amount.
4. Energize the actuator to find out the maximum displacement at that specific voltage level. Increase voltage by steps before reaching depolarization limit.
5. Repeat steps 3 and 4 by adjusting the preload up to 4000 N.

### **6.3 Actuator with Hydraulic Amplifier Test**

The hydraulic amplifier was tested together with the stack actuator. This test was designed to see how the input displacement is affected with the hydraulic amplifier attached. Also it showed the performance of the hydraulic amplifier with the use of piezoelectric actuator as the input mechanism.

All components were required for this portion of testing except for the return disc spring, return pillars, and return plate. The return plate was not tightened so the return disc spring was not engaged with the needle. The equipments and connections of this test were the same as the

previous test with the exception that a new sensing location was added at the needle location for the output displacement. Following figure shows the physical arrangement of all the equipment and prototype used for this test.



**Figure 47 Physical arrangement of the prototype and test equipments for hydraulic amplifier test with actuator**

### **Testing Procedures:**

1. Insert the actuator into the actuator housing and secure using bolts.
2. Position the capacitive sensor probe so that the connecting plate is in range.
3. Tighten the bolts to increase the preload to desired amount.
4. Energize the actuator to find out the maximum input displacement at that specific voltage level. Increase voltage by steps before reaching depolarization limit.
5. Remount the capacitive sensor so that it is at the output location (needle).
6. Energize the actuator using the same voltage as step 4 to find out the maximum output displacement at that specific voltage level. Increase voltage before reaching depolarization limit.
7. Repeat steps 2 and 6 by adjusting the preload up to 4000 N.

## 6.4 Hydraulic Amplifier Performance Test

Due to the lack of a proper piezoelectric actuator, an innovative way of actuating the hydraulic amplifier was used to carry out this experiment. An adjustable mechanical stage and a load cell were used to replace the actuation of the piezoelectric actuator. The performance of the hydraulic amplifier could be tested better without stroke limitation. Figure 48 shows how the injector and fixture is configured for this test.

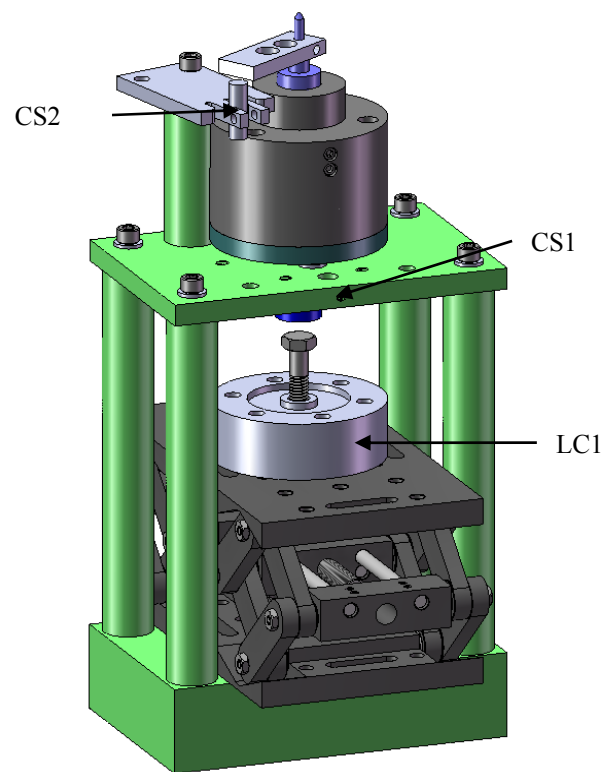


**Figure 48 Hydraulic amplifier performance test configuration**

For this part of experiment, capacitive sensor, oscilloscope, mechanical stage, and load cell are utilized. Following figure shows how each of these equipments are connected.

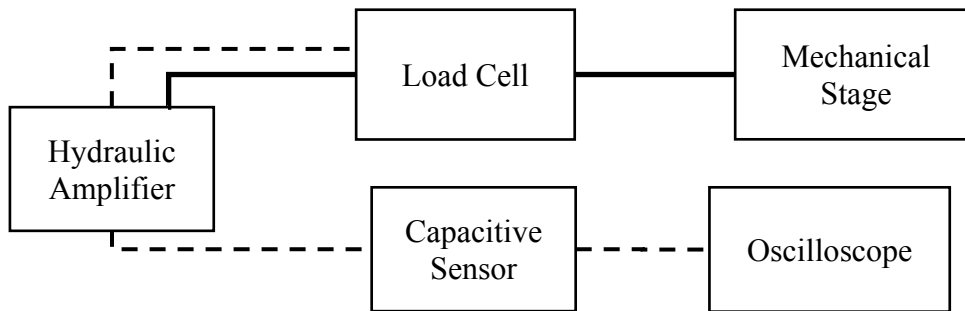


**Figure 49 Presentation of how equipments are connected for hydraulic amplifier performance test**

In this test, a known load was placed at the input end and both the input and output distances were measured to find out the amplification ratio of the hydraulic amplifier. In an ideal situation, one load cell and two sets of capacitive sensors are required to conduct this test. However, with limited equipment, the capacitive sensor was placed at CS1 and load cell at LC1 to find out the relationship between the input force and the input distance. After a consistent relationship was obtained, the capacitive sensor was moved to CS2 to find out the output distance. The input end was controlled only by the load cell at this point. Because the load cell was physically connected to the needle and was also used as a sensing device for monitoring the load, it is shown to have both physical and informational connection. Figure 50 shows the physical arrangement of the hydraulic amplifier and fixture.

### **Testing Procedures:**

1. Position the load cell and the capacitive sensor at the input location (LC1 and CS1).
2. Apply desired load by adjusting the mechanical stage and record the resulting input displacement.
3. Repeat step 2 by increasing the input load by steps until 334 N (75 lb).

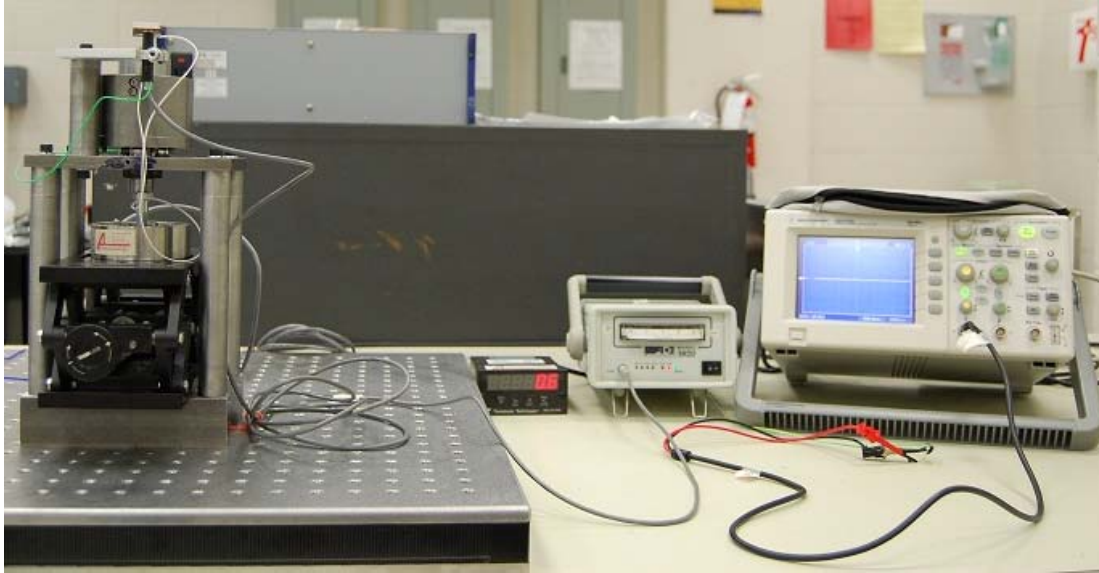


**Figure 50 Physical arrangement of the prototype and test equipments for hydraulic amplifier performance test**

4. After the relationship between the input load and displacement is established, remount the capacitive sensor at the output end (CS2).
5. Apply desired load used in step 2 by adjusting the mechanical stage and record the resulting output displacement.

## **6.5 Piezoelectric Injector Static Test**

In this section of experiment, all the parts were assembled together to simulate the injector working in real condition. This test determined how much stroke can be generated by this prototype. Figure 51 shows how the prototype and fixture is configured for this test. Unlike the hydraulic amplifier test with the actuator, the screws above the return pillars were tightened so that the return disc spring is engaged with the needle. The load cell at the bottom acts as the nozzle housing which provides proper sealing force on the injector. The capacitive sensor was mounted at CS1 for input displacement and at CS2 for output displacement. For quick and accurate adjustment, capacitive sensor was mounted on a mechanical stage.

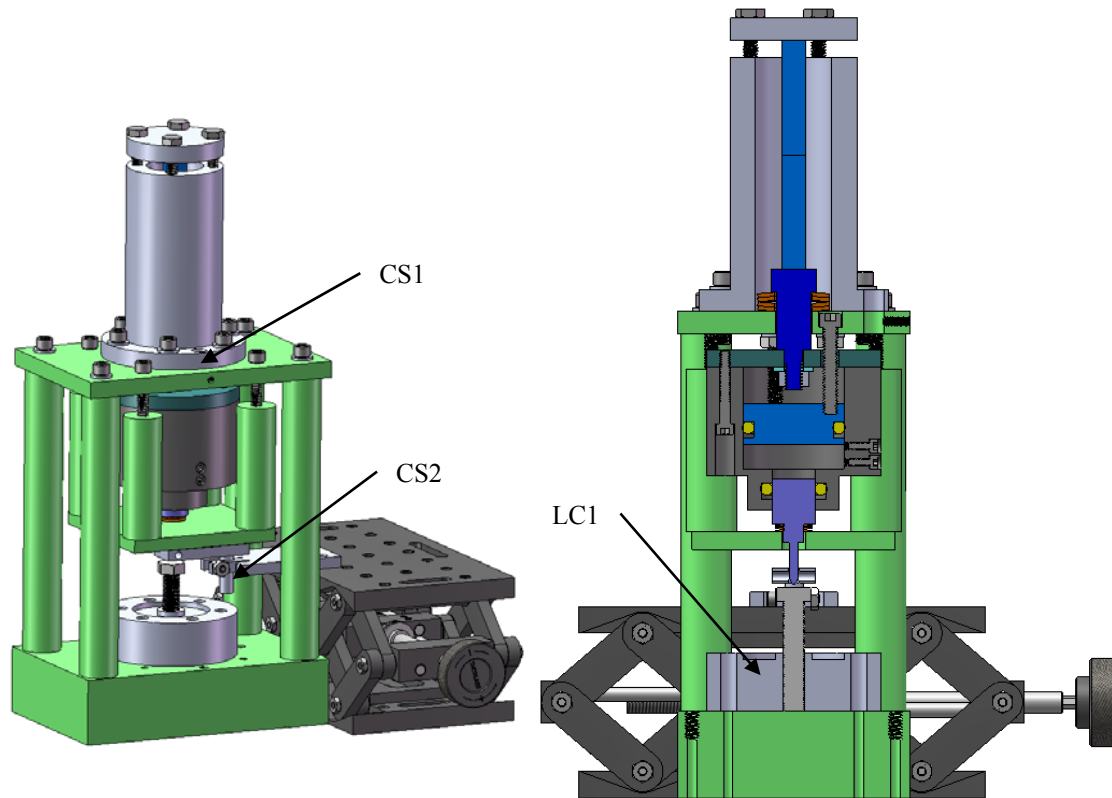


**Figure 51 Injector static test configuration**

The equipments used were capacitive sensor, oscilloscope, high-voltage power supply, mechanical stage, and load cell. Connection of equipments is shown in Figure 52.

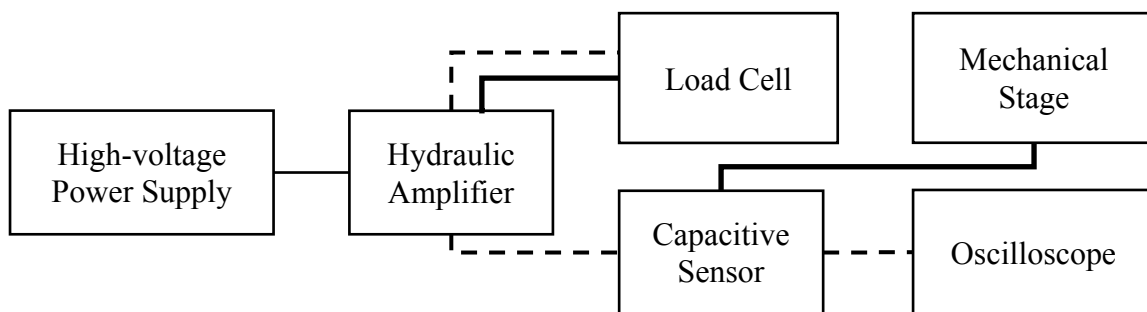


**Figure 52 Presentation of how equipments are connected for injector static test**

### Testing Procedures:

1. Insert the actuator into the actuator housing and secure using bolts.
2. Tighten the bolts to increase the preload to desired amount.

3. Tighten the screws on top of the return pillars to engage the return disc spring to desired amount.
4. Engage the bolt on the load cell to the needle to desired sealing force.
5. Position the capacitive sensor probe so that the connecting plate is in range.
6. Energize the actuator to find out the maximum input displacement at that specific voltage level. Increase voltage by steps before reaching depolarization limit.
7. Remount the capacitive sensor so that it is at CS2.
8. Energize the actuator using the same voltage as step 6 to find out the maximum output displacement at that specific voltage level. Increase voltage by steps before reaching depolarization limit.
9. Repeat steps 2 and 8 by adjusting the preload up to 4000 N.

# Chapter 7 Experimental Results

## 7.1 Prepressed Piezoelectric Actuator Performance Result

The actuator that was tested was obtained from SensorTech. The actuator is 10 X 10 mm with a length of 20 mm. Under a voltage of 200 V, the actuator is to displace around 10  $\mu\text{m}$  according to specifications. It possesses properties given in Table 18:

**Table 18 Piezoelectric actuator properties [5]**

Layer thickness ( $\mu\text{m}$ )	Relative Dielectric Constant	Charge Constant ( $10^{-12} \text{ m/V}$ )	Compliance ( $10^{-12} \text{ m}^2/\text{N}$ )
250	3250	590	20

Following the test procedures given in section 6.2, a set of input displacement measurements was taken. The results are tabulated in Table 19 and plotted in Figure 53.

**Table 19 Piezoelectric actuator performance test results under various preloads**

PL = 1000 N		PL = 2000 N		PL = 3000 N		PL = 4000 N	
Volt (V)	IP ( $\mu\text{m}$ )						
50	0.8	50	0.72	50	0.64	50	0.56
85	1.44	100	1.6	100	1.68	100	1.44
-	-	150	2.72	150	2.72	150	2.48
-	-	170	3.28	200	4.00	200	3.52
-	-	-	-	250	5.36	250	4.96
-	-	-	-	-	-	300	6.24
-	-	-	-	-	-	345	7.60

At a smaller preload, the stack actuator was compressed less thus it cannot be energized over the compression limit. This was to prevent depolarization of the stack. Figure 53 showed that as the preload increases, there was a slight reduction in displacement; however, this difference was less than 1 micron.

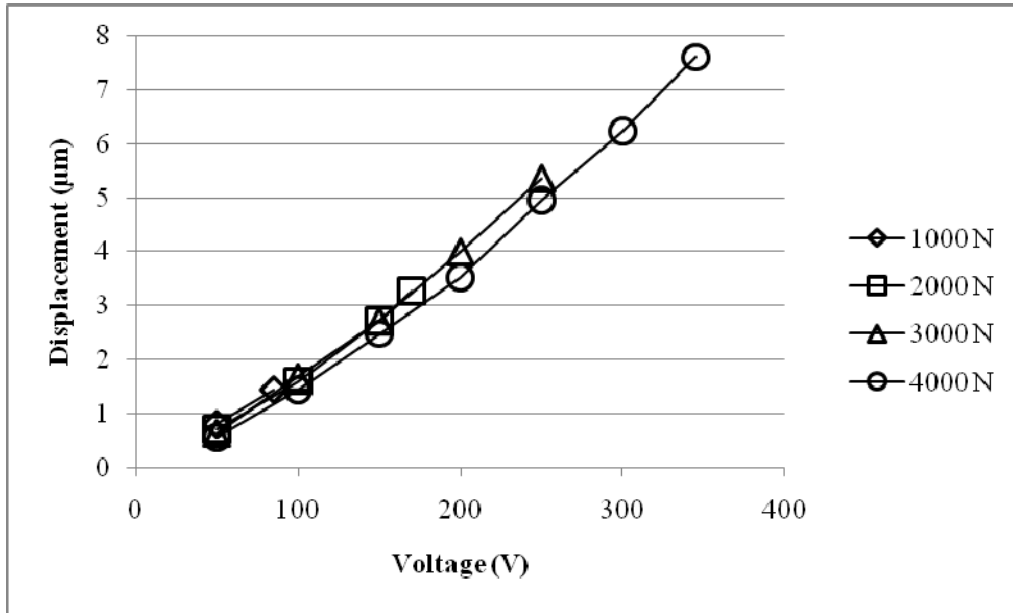


Figure 53 Graphical test result of actuator performance

This slight reduction in displacement is likely to be the result of measurement error. The general trend of the voltage and displacement relationship is fairly linear as described by many literatures [5][6]. There exists a large difference between the test data and the specifications provided by the company. The error can be in the equipment used due to the sensing surface having minor scratches. Also, the unit has not been calibrated regularly.

## 7.2 Actuator with Hydraulic Amplifier Result

Table 20 and Table 21 show the test results of the piezoelectric actuator integrated with the hydraulic amplifier.

Table 20 Actuator with hydraulic amplifier test result under preloads of 1000 N and 2000 N

PL = 1000 N				PL = 2000 N			
Volt (V)	IP (µm)	OP (µm)	AF	Volt (V)	IP (µm)	OP (µm)	AF
50	0.50	0	0	50	0.56	0	0
85	0.96	0	0	100	1.20	0.72	0.6
-	-	-	-	150	2.00	1.12	0.56
-	-	-	-	170	2.24	1.7	0.76

**Table 21 Actuator with hydraulic amplifier test result under preloads of 3000 N and 4000 N**

PL = 3000 N				PL = 4000 N			
Volt (V)	IP ( $\mu\text{m}$ )	OP ( $\mu\text{m}$ )	AF	Volt (V)	IP ( $\mu\text{m}$ )	OP ( $\mu\text{m}$ )	AF
50	0.56	0.40	0.71	50	0.56	0.96	1.71
100	1.36	1.44	1.06	100	1.44	2.24	1.56
150	2.16	3.52	1.63	150	2.24	3.68	1.64
200	3.28	4.64	1.41	200	3.28	4.80	1.46
250	4.40	7.76	1.76	250	4.40	7.52	1.71
-	-	-	-	300	5.60	11.0	1.96
-	-	-	-	345	6.64	15.0	2.26

Two plots were extracted from these data. Figure 54 showed the input and output displacements on the same graph. Figure 55 showed the amplification factor against the input voltage.

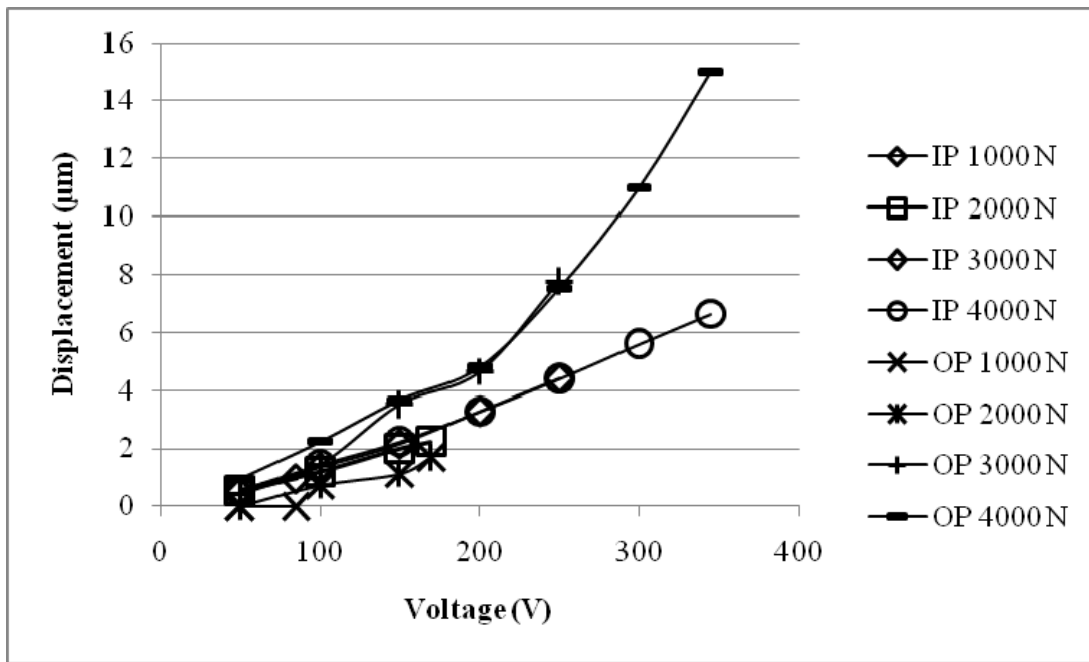


**Figure 54 Graphical test result of actuator with hydraulic amplifier showing the input and output displacement**

In Figure 54, input displacements generated by the piezoelectric actuator under the four different preloads were very consistent. In this test, the maximum output displacement obtained is 15 $\mu\text{m}$  with an input displacement of 6.64  $\mu\text{m}$  at a preload of 4000 N.

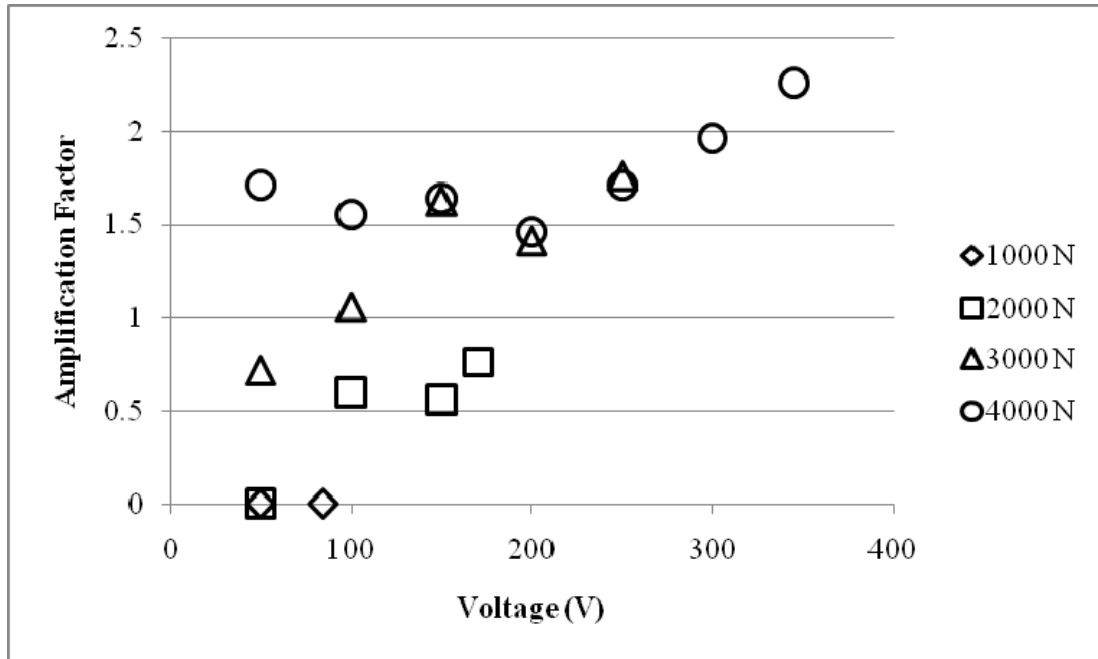


**Figure 55 Graphical test result of actuator with hydraulic amplifier showing the amplification factor**

As shown in the graph, all the input measurements from preloads of 1000 N to 3000 N laid very close to the same line that is made up of input measurements taken at the preload of 4000 N. The trend is linear showing behavior like the previous test. This is not the same with the output reading. At low preload and voltage, there is no displacement reading. This could be a result of the components not properly engaged. Without enough preload, there might be gaps between different components. As the actuator is energized, the input displacement is lost due to these gaps. Also, because the input displacement is small, without enough movement, displacements could easily be lost to friction force between the o-ring and the cylinder wall.

Because of these factors, another important note was that the amplification factor was below 1 at low preload and voltage. This can be seen more clearly in Figure 55, as preload rises above 3000 N, the amplification factor slowly rose above 1. At 4000 N preload, the amplification factor was always above 1, however, the amplification factor fluctuated instead showing consistent result. One factor contributing to this fluctuation could be a result of

experimental error. Other than this error, the hydraulic amplifier had not been able to show performance comparable to the theoretical value (4.6). To find out what is causing these inconsistencies, it was necessary to test out the hydraulic amplifier itself more extensively to investigate if the poor performance was contributed by the hydraulic amplifier or other components.

### 7.3 Hydraulic Amplifier Performance Result

With the set up as describe in section 6.2, 5 sets of input data were taken first with the capacitive sensor at the CS1 location. Another 5 sets of output data were recorded after with the capacitive sensor mounted at CS2 location. The data are recorded in Table 22.

**Table 22 Five sets of results of the hydraulic amplifier test**

Load (lb, N)	IP 1	IP 2	IP 3	IP 4	IP 5	OP 1	OP 2	OP 3	OP 4	OP 5
10, 44.5	10.8	11	10.8	10.4	9.8	28	29.2	30.4	34.8	30
15, 66.7	17.4	17	17	-	-	43.2	45.6	45.6	-	-
20, 89	22.6	24.2	23.6	23	21.2	56.4	58.4	58	61.2	55.6
25, 111.2	30.2	29.8	29.8	-	-	69.4	68.8	69.6	-	-
30, 133.4	33.8	35	36	34.4	31.4	79.34	81.2	81.2	84	78.4
35, 155.7	38.8	39	41.2	-	-	91.14	92.8	94	-	-
40, 177.9	43	44.2	45.6	43.6	40.2	101.74	102.4	104.8	106.5	99.2
45, 200.2	47.2	47.4	50	-	-	111.74	112.4	115.2	-	-
50, 222.4	51.6	51.2	54	53	49	123.34	124	124.4	127.6	120
55, 244.7	55.2	54.6	58	-	-	134.54	133.6	130	-	-
60, 266.9	58.4	58	61.8	61	56.2	143.14	143.2	142	145.2	137.6
65, 289.1	62.4	62	65.2	-	-	152.94	153.2	151.2	-	-
70, 311.4	66.2	64.8	68.6	68.4	63.4	161.34	163.2	161.2	165.14	155.6
75, 333.6	69.6	68	72	71.8	67.2	168.94	172.8	172	172	162.8

All IP and OP values were listed in  $\mu\text{m}$ . Because the values shown in Table 22 showed only small deviations between each set of data, the averages of these data were calculated as shown in Table 23.

**Table 23 Average of input distance, output distances, and amplification ratio of amplifier test**

Load (lb, N)	IP Avg ( $\mu\text{m}$ )	OP Avg ( $\mu\text{m}$ )	AF
10, 44.5	10.56	30.48	2.89
15, 66.7	17.13	44.8	2.61
20, 89	22.92	57.92	2.53
25, 111.2	29.93	69.27	2.31
30, 133.4	34.12	80.83	2.37
35, 155.7	39.67	92.65	2.34
40, 177.9	43.32	102.93	2.38
45, 200.2	48.20	113.11	2.35
50, 222.4	51.76	123.87	2.39
55, 244.7	55.93	132.71	2.37
60, 266.9	59.08	142.23	2.41
65, 289.1	63.20	152.45	2.41
70, 311.4	66.28	161.30	2.43
75, 333.6	69.72	169.71	2.43

The average input and output displacements are plotted in a graphical format for trend observations as shown in Figure 56. The plot has shown a consistent rise both in input and output displacements. Sudden drops or rises are not observed on this graph. Therefore, this input load and displacement relationship was used to aid determining the amplification ratio of the hydraulic amplifier to see how well the hydraulic amplifier performed. The average values of the input distances and output distances were calculated as shown in Table 23. The amplification factor was plotted in Figure 57. This experiment showed a consistent amplification factor of 2.5 which is much smaller than the one calculated theoretically (4.6).

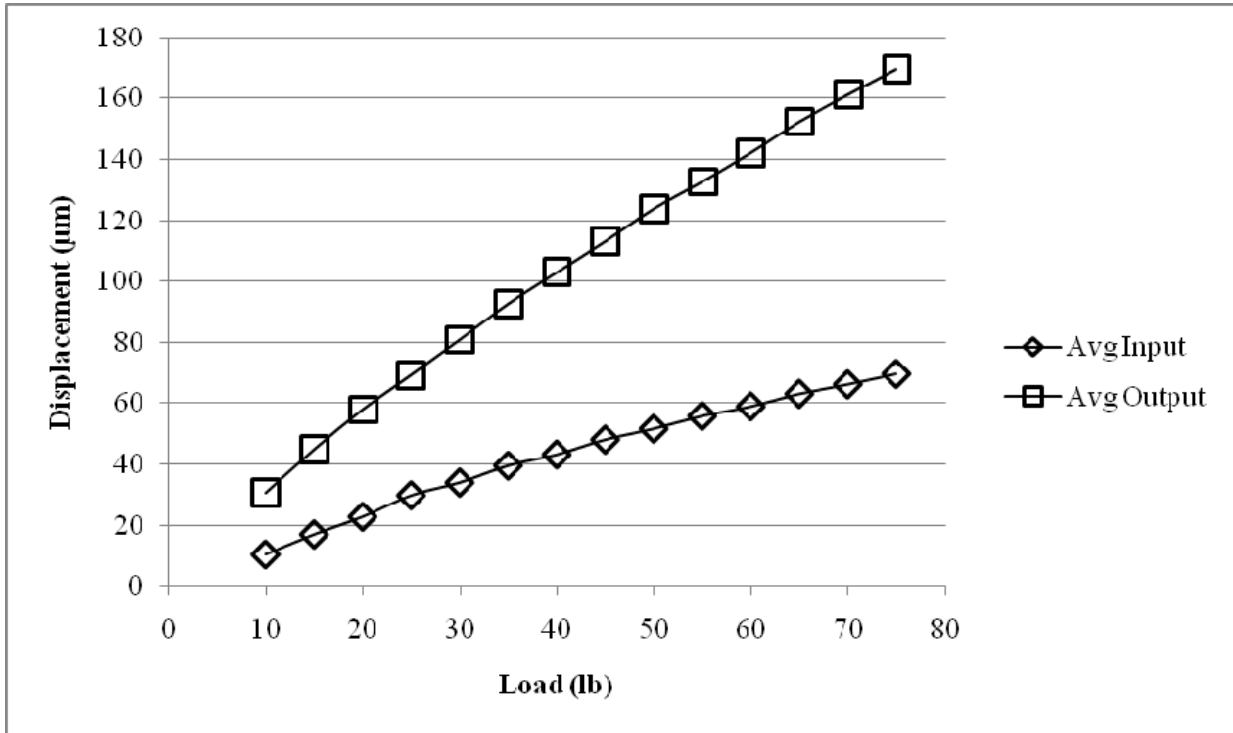


Figure 56 Graphical test result of average input and output displacement of hydraulic amplifier

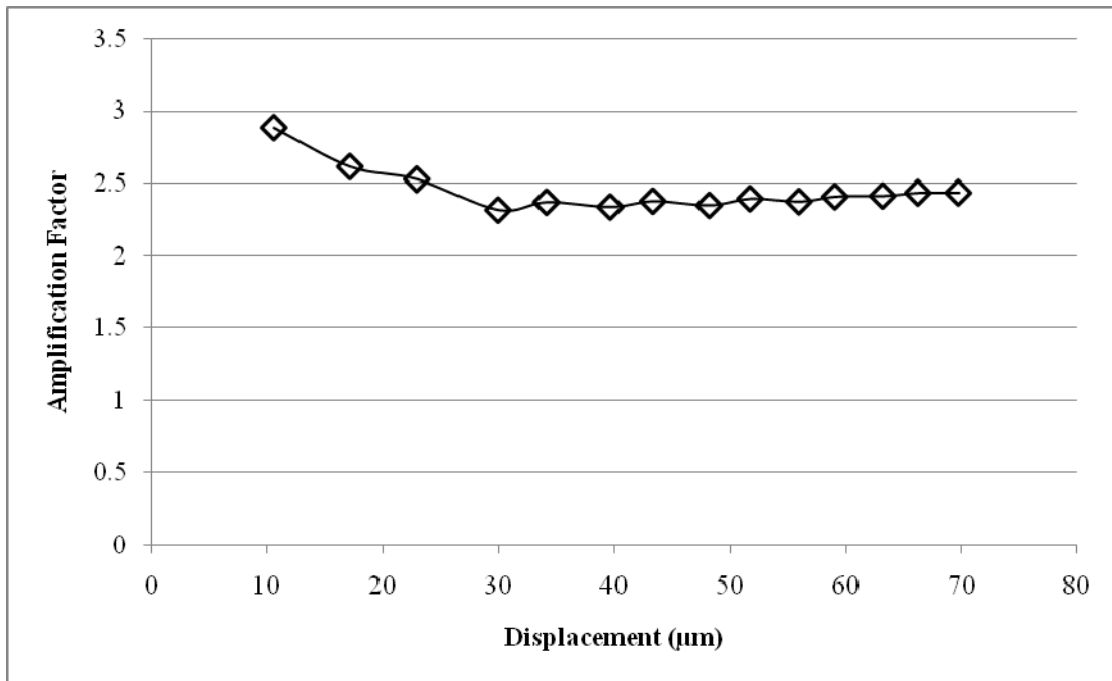


Figure 57 Graphical test result of hydraulic amplifier showing the amplification factor

Compared with the hydraulic amplifier from the literature, this amplifier designed in this project achieved 53% of the theoretical value. The amplifier designed and tested by Yoon was only able to achieve 40% of the theoretical value [17]. Although the amplifier in this project seems to have achieved a better result, the amplifier designed by Yoon was aiming to achieve an amplification factor of 79.6.

One major factor contributing to this loss of output displacement was the friction between the o-rings to the cylinder wall as pointed out also in the previous test. The components between the amplifier and the actuator also contributed to this loss due to the lack of stiffness. This test showed fairly consistent reading of around 2.5 as the input displacement exceeds 30  $\mu\text{m}$ . With a displacement less than 30  $\mu\text{m}$ , the amplification factor dropped consistently from 2.89. This test had shown that, without a proper piezoelectric actuator generating enough displacement, the hydraulic amplifier was unable to produce proper result.

## **7.4 Piezoelectric Injector Static Result**

As shown in the setup in section 6.5, the prototype was subjected to a static performance test. However, the prototype was not able to perform with consistent results. As the actuator was energized, the needle remained in the closed position or moved in the closing direction. Gradual increase of preload and voltage did not aid the injector to perform as it should.

There are several speculations into this occurrence. The injector was designed to work with a piezoelectric actuator with a length of 100 mm and a free displacement of 50  $\mu\text{m}$  at 200 V. As observed by previous experiments, the stack actuator used in the experiment produced a maximum of 4.0  $\mu\text{m}$  at 200 V. With the lack of input displacement and an additional force placed at the output end with the return disc spring, it is possible that the hydraulic amplifier

depleted the input displacement through frictional loss between the o-ring and the cylinder wall. The additional force from the return disc spring can cause the hydraulic fluid to be pressurized which induces leakage to occur. If leakage occurs, displacement will decrease. Also, the mechanism for adjusting the return spring force is through the use of four parallel bolts. If any one of them is adjusted at a different height, it would exert an unbalanced force onto the needle, causing error to occur. Another reason contributing to this problem could be the design of the fixed input piston. For the needle to move in the closing direction, the implication is that the input piston is also moving in the closing direction. This suggests that the mechanism holding the input piston in place is not rigid enough, thus allowing it to move. If the input piston moves with the hydraulic amplifier housing, then the needle will move in the closing direction as observed.

## Chapter 8 Conclusions and Recommendations for Future Work

To further improve the existing fuel injectors, the piezoelectric fuel injector developed in this project utilizes the high force generated by the piezoelectric actuator effectively to improve the response time and preserve the lifetime of the piezoelectric actuator. It utilizes direct acting to overcome the large delay from pressurizing and depressurizing the fuel chamber of the servo-circuit fuel injectors. By using the “energize to inject” configuration, the lifetime of the piezoelectric actuator is preserved. Analytical work has proven that the injector is capable of achieving a needle lift of more than 300  $\mu\text{m}$  under the fuel pressure from the common-rail system. Through the process of improving the designs, various achievements were obtained through the design iterations and these contributed to the final design.

In the generation 1 design, the disc spring is implemented to precompress the piezoelectric actuator to keep it within the compression region. This helps to extend the lifetime of the actuator by preventing it from reaching the tensile region. To make sure the modeling of the piezoelectric actuator can be done analytically, the whole injector was modeled in ANSYS to compare the results.

- According to the analytical results from Table 4 and the simulated results from Table 12, the results deviates from the other by 4% in both HP and LP cases. This suggests that the analytical model of the piezoelectric actuator under precompression is correct.
- The idea of using telescopic actuator is implemented in the generation 1 design. Through ANSYS simulation, it was verified that this idea is theoretically possible.

However, because of the large electric power output demand due to the use of large quantity of piezoelectric material, this design cannot be realized physically.

To overcome the large power output required to drive the telescopic actuator design, the generation 2 design makes use of a mechanical amplifier to increase the limited displacement generated by the piezoelectric actuator.

- The mechanical amplifier was design to be fabricated using one single piece of material to improve the response time.

However, the mechanical amplifier is proven to be too weak through ANSYS simulation, thus, the actuator cannot overcome the fuel pressure acting on the needle.

- The fuel pressure balance idea was generated in the process of lessening the fuel pressure effect on the needle.

Although the force on the needle is lessened, it did not alter the inability of overcoming the fuel pressure effect of the mechanical amplifier.

Because the mechanical amplifier design is proven to be too weak to overcome the fuel pressure on the needle, the generation 3 design makes use of the high force transfer capability of the hydraulic amplifier to increase the input displacement generated by the piezoelectric actuator.

- To keep this generation of fuel injector design to be in “energize to inject” configuration, modification is done to the amplifier so that it also acts as a motion inverter.
- Through analytical estimation on needle lifting, the design concept is capable of meeting the output stroke requirement.

Although simulation was not done on this design due to time constrain, a prototype was fabricated to verify how this injector will perform.

A prototype was fabricated according to the generation 3 design. Although the prototype cannot be used in a real engine, it was designed to make sure the design concept is possible.

Separate tests were done on the actuator and the hydraulic amplifier to find out the performance of each. The piezoelectric actuator performed as stated in many literatures [5][6].

- As input displacement increases beyond 30  $\mu\text{m}$ , AF increases to 2.5.
- For the hydraulic amplifier, although the amplification factor taken from the experimental data is only 53% of the theoretical value, it performed better than the hydraulic amplifier designed by Yoon which only achieved 40% of the theoretical value [17].

The piezoelectric actuator and the hydraulic amplifier were integrated together to see how the performance of each part affect the other. The fabricated hydraulic amplifier successfully amplified the input displacement.

- In this test, the highest output displacement of 15  $\mu\text{m}$  is achieved with an input displacement of 6.64  $\mu\text{m}$  at a preload of 4000 N.

Lastly, all the parts were integrated together to simulate a prototype with all the force conditions considered except for the fuel pressure effect.

With all the parts assembled together and preloads set on the injector, the prototype failed to perform the static test successfully.

- It was speculated that the problem lies in the lack of a proper piezoelectric actuator. The small displacement generated by this short actuator can easily be reduced by the friction between the o-ring and cylinder wall.
- With limited facility, the hydraulic amplifier did not meet the tolerances specified. This potentially led to leakages in the mechanism; thus, further reducing the displacement output.

The inability to properly seal the hydraulic fluid within the chamber could cause the injector to perform poorly.

- The fixture design can also affect the result. This can be seen most clearly at the return disc spring where the spring force is adjusted by 4 bolts. If any of the bolts are not adjusted to the same level to the others, tilting is very likely to occur, causing an uneven distribution of force on the fuel injector.

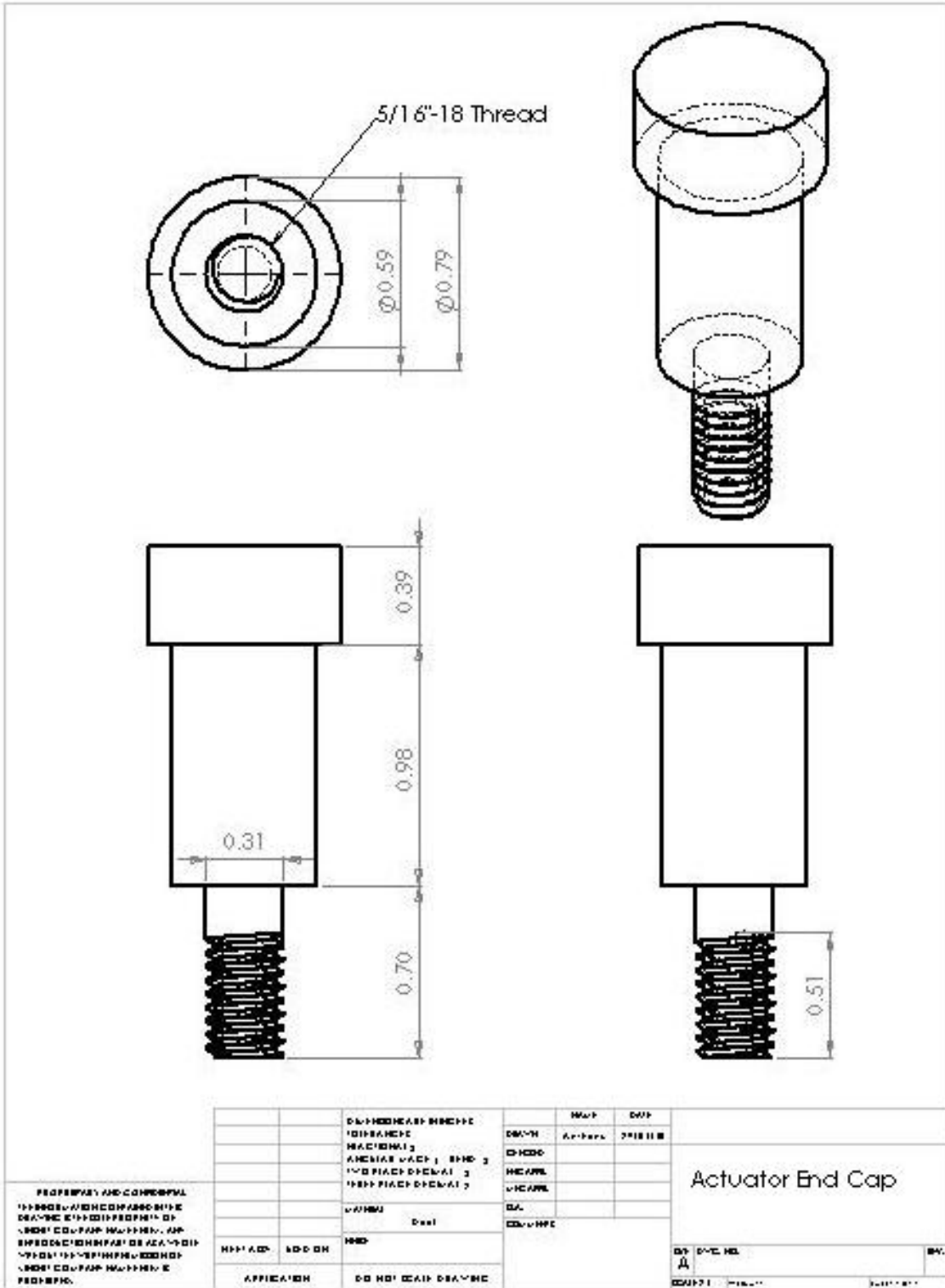
Even though the injector static test failed to perform as it should, the test results show that with a proper piezoelectric actuator, the needle lift can be achieved.

- With a piezoelectric actuator having a length of 150 mm, a piezoelectric constant of  $590 \times 10^{-12}$  m/V, and a layer thickness of 250  $\mu\text{m}$ , at 345 V, a displacement of 122  $\mu\text{m}$  is expected. Since the hydraulic amplifier performance test showed that as input displacement exceeds 30  $\mu\text{m}$ , amplification factor of 2.5 is expected. A needle lift of 305  $\mu\text{m}$  is expected.

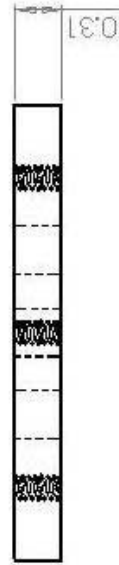
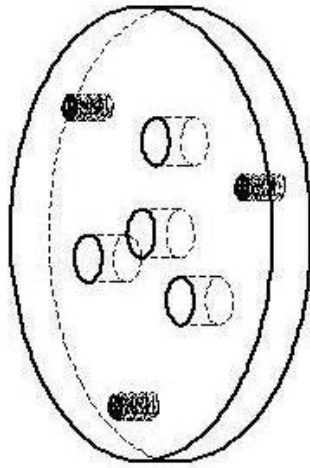
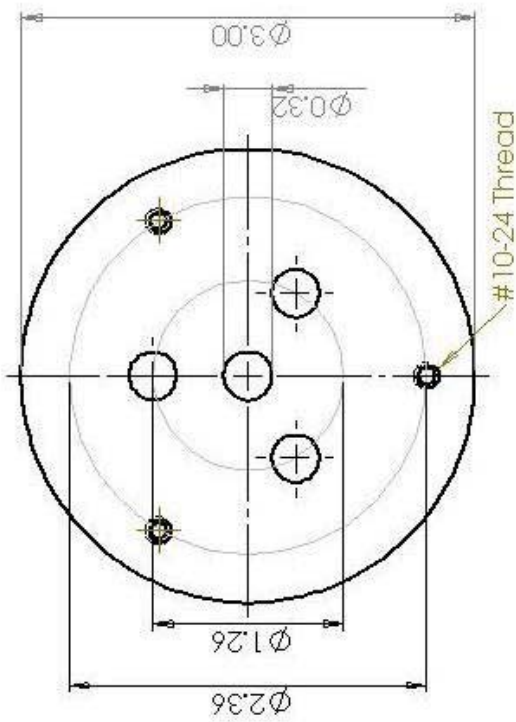
To move forward in this project, improvements can be made on the generation 3 design on the following:

- Redesign the fixture so that components such as the return disc spring can be easily adjusted accurately.
- Fabricate the hydraulic amplifier with tolerances specified to prevent fluid from leaking. Possibly treat the hydraulic amplifier as a pressure vessel.
- Modify existing commercial hydraulic cylinder to avoid fabrication complexity.
- Obtain a piezoelectric actuator with larger displacement to verify whether problem exist due to insufficient displacement generated by short actuator.
- Verify the fuel pressure balance idea to make sure that it helps lessen the fuel force on the needle.
- Proceed to static and dynamic testing.

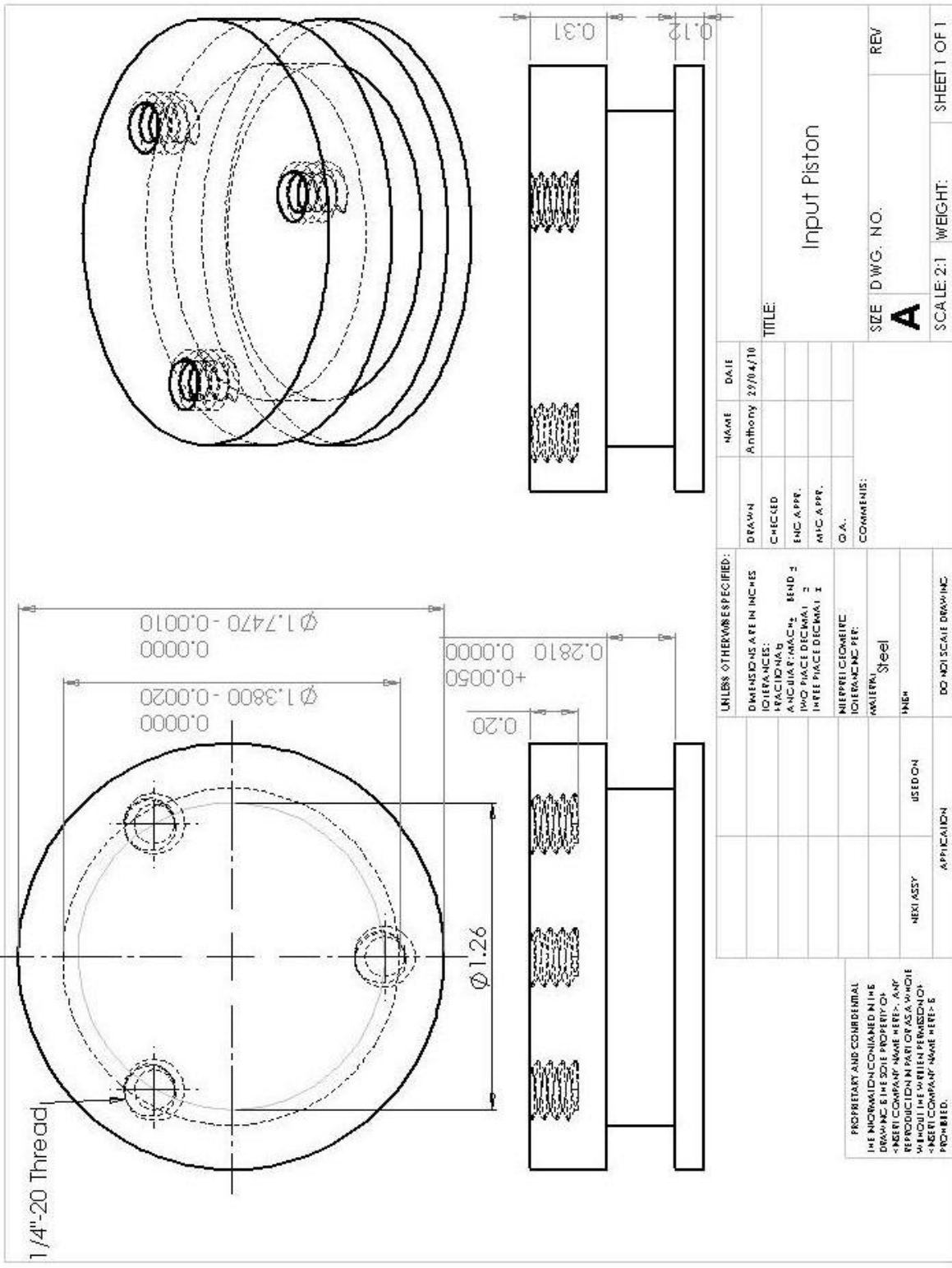
# Appendix A Technical Drawings

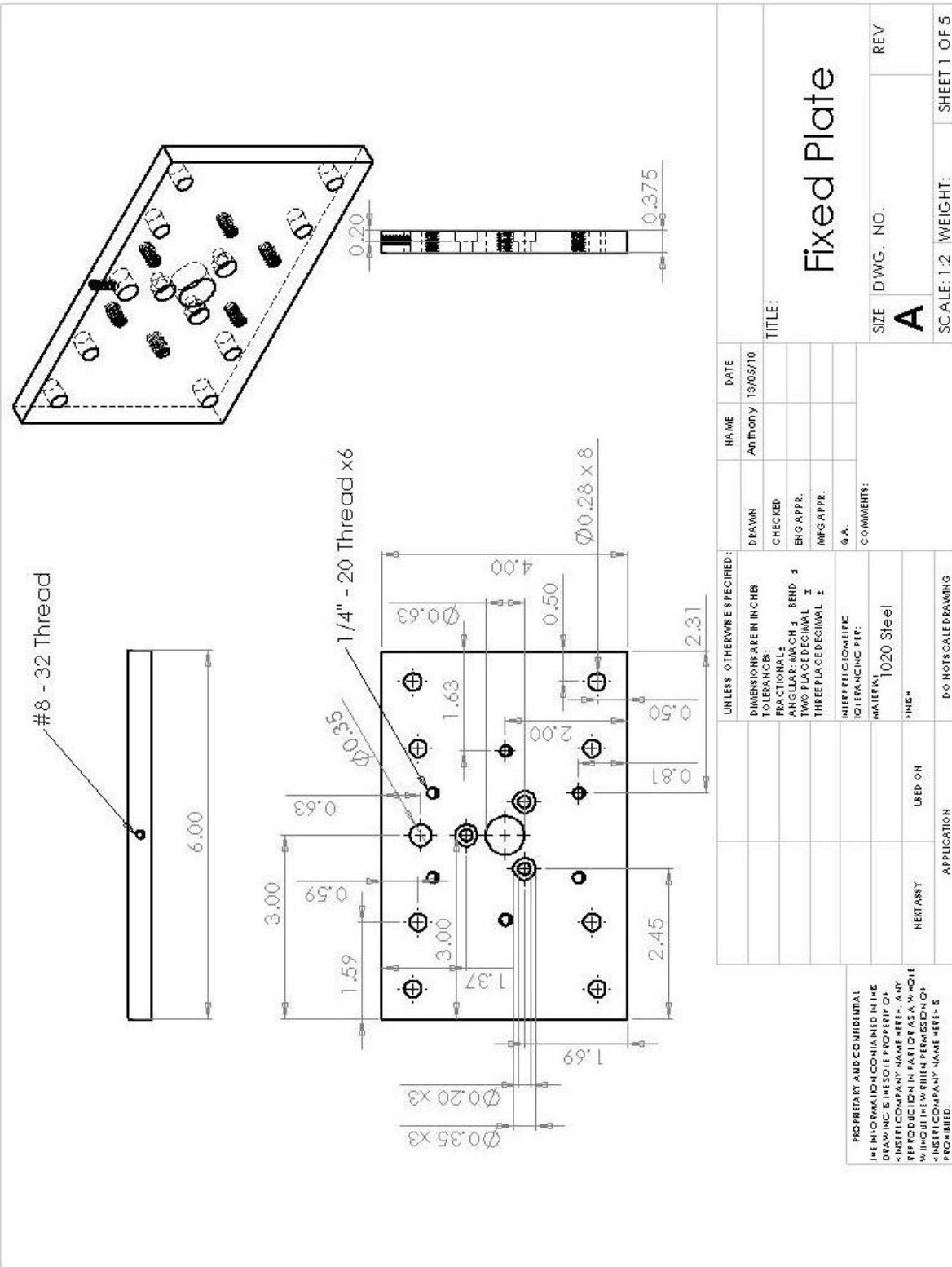


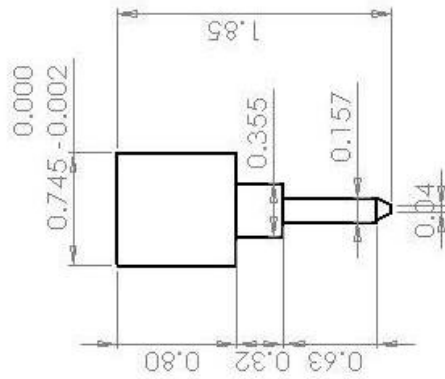
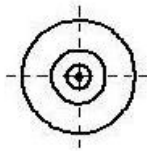
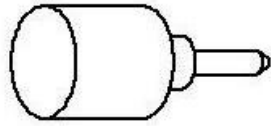




UNLESS OTHERWISE SPECIFIED:		NAME	DATE
DIMENSIONS ARE IN INCHES		Anthony	2/20/10
FRACTIONS:		DRAWN	
ANGULAR DIMENSIONS BEND 3		CHECKED	
TWO PLACE DECIMAL 1		ENG APPR.	
THREE PLACE DECIMAL 3		MTC APPR.	
MATERIAL:		D.A.	
FINISH:		COMMENTS:	
STEEL			
DO NOT SCALE DRAWING			
PROPRIETARY AND CONFIDENTIAL			
THE INFORMATION CONTAINED IN THIS			
DRAWING IS THE SOLE PROPERTY OF			
AMERICAN COMPANY NAME HERE - ANY			
REPRODUCTION IN PART OR AS A WHOLE			
WITHOUT THE WRITTEN PERMISSION OF			
AMERICAN COMPANY NAME HERE - IS			
PROHIBITED.			
NEXT ASSEMBLY	APPLICATION	USED ON	
TITLE: Connecting Plate		SIZE	DWG. NO.
		<b>A</b>	
		SCALE: 1:1	WEIGHT:
			SHEET 1 OF 1



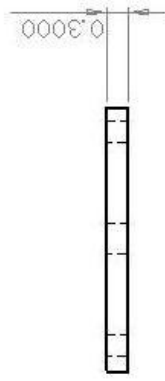
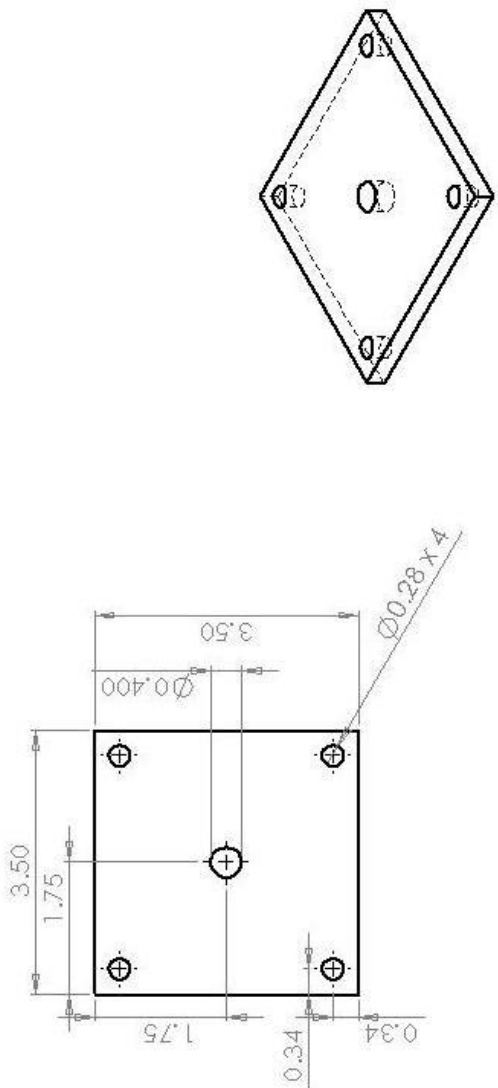




UNLESS OTHERWISE SPECIFIED:		DRAWN		NAME	DATE
DIMENSIONS ARE IN INCHES		CHECKED		Anthony	03/06/10
TOLERANCES:		ENG APPR.			
FRACTIONAL		MFG APPR.			
ANGULAR: MACH ±		Q.A.			
BEND ±		COMMENTS:			
TWO PLACE DECIMAL ±		INTERPRETOMETRIC			
THREE PLACE DECIMAL ±		OVER-MIN. PER:			
		MATERIAL: 1020 Steel			
		FINISH:			
		NEXT ASSY		USED ON	
		APPLICATION			
		DO NOT SCALE DRAWING			
PROPRIETARY AND CONFIDENTIAL THE INFORMATION CONTAINED IN THIS DRAWING IS THE SOLE PROPERTY OF INTERCOMPANY NAME HERE. ANY REPRODUCTION IN PART OR AS A WHOLE WITHOUT THE WRITTEN PERMISSION OF INTERCOMPANY NAME HERE IS PROHIBITED.		TITLE:		Needle	
		SIZE		DWG. NO.	
		A		REV	
		SCALE: 1:1		WEIGHT:	
				SHEET 6 OF 6	







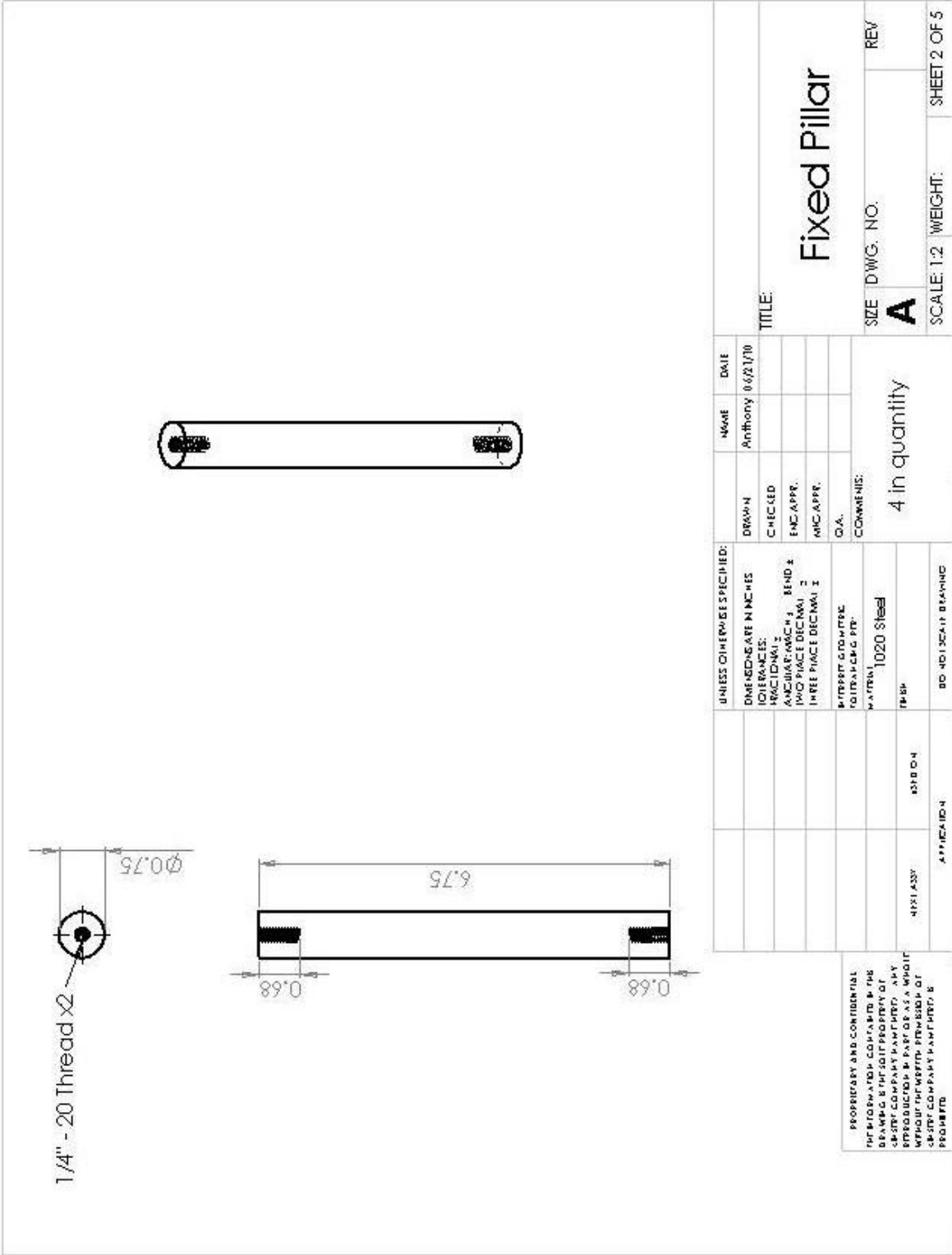
UNLESS OTHERWISE SPECIFIED:		NAME	DATE
DIMENSIONS ARE IN INCHES		Anthony	10/05/10
TOLERANCES:			
FRACTIONAL		DRAWN	
DECIMAL		CHECKED	
ANGULAR: MAX CH 1 BEND 1		ENG APPR.	
TWO PLACE DECIMAL 2		MFG APPR.	
THREE PLACE DECIMAL 3		Q.A.	
INTERFEROMETRIC		COMMENTS:	
TOLERANCES PER:			
MATERIAL: 1020 Steel			
FINISH:			
NEW ASSY	USED ON		
APPLICATION			
DO NOT SCALE DRAWING			

# Return Plate

SIZE DWG. NO. REV  
**A**

SCALE: 1:2 WEIGHT: SHEET 4 OF 5

PROPRIETARY AND CONFIDENTIAL  
 THE INFORMATION CONTAINED IN THIS  
 DRAWING IS THE SOLE PROPERTY OF  
 ELECTRIC COMPANY. MAKE REPLICAS, COPY  
 OR DISSEMINATE THIS INFORMATION  
 WITHOUT THE WRITTEN PERMISSION OF  
 ELECTRIC COMPANY. NAME HERE: 5  
 PROHIBITED.



1/4" - 20 Thread x2

Ø0.75

6.75

0.68

0.68

PROPRIETARY AND CONFIDENTIAL  
 THIS DRAWING CONTAINS THE  
 DESIGN & THE SOLE PROPERTY OF  
 CRYSTAL COMPANY. ANY REPRODUCTION,  
 REPRODUCTION IN PART OR AS A WHOLE,  
 WITHOUT THE WRITTEN PERMISSION OF  
 CRYSTAL COMPANY IS PROHIBITED.

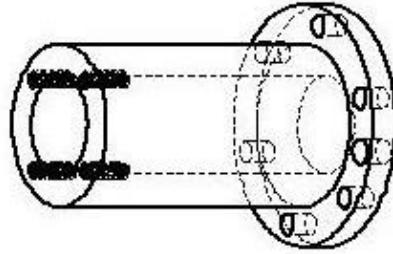
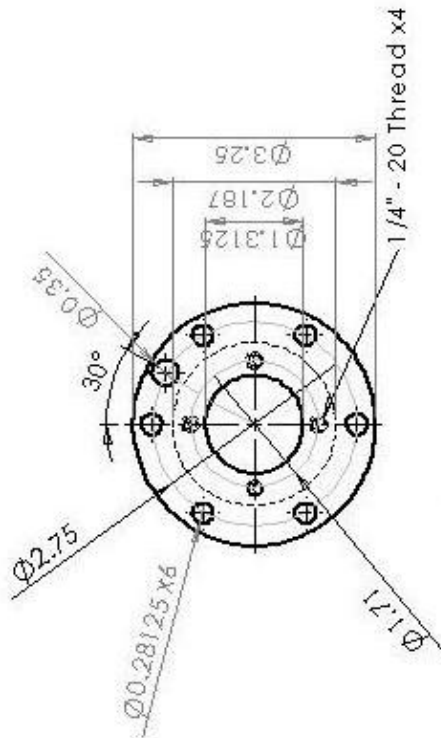
UNLESS OTHERWISE SPECIFIED:	NAME	DATE
DIMENSIONS ARE IN INCHES	Anthony	06/21/10
TOLERANCES:		
FRACTIONS: 1/16, 1/8, 1/4, 3/8, 1/2, 5/8, 3/4, 7/8		
DECIMALS: 0.0005, 0.001, 0.002, 0.005, 0.01, 0.015, 0.03, 0.05, 0.1, 0.15, 0.3, 0.5		
ANGLES: MINIMUM 1/8" RADIUS		
FINISH: UNLESS OTHERWISE SPECIFIED		
THREADS: PER ANSI B1.1		
WELDING: PER AWS D1.1		
SPRINGS: PER ASME Y14.3		
WELDED JOINTS: PER ASME B31.1		
WELDED JOINTS: PER ASME B31.3		
WELDED JOINTS: PER ASME B31.9		
WELDED JOINTS: PER ASME B31.11		
WELDED JOINTS: PER ASME B31.12		
WELDED JOINTS: PER ASME B31.13		
WELDED JOINTS: PER ASME B31.14		
WELDED JOINTS: PER ASME B31.15		
WELDED JOINTS: PER ASME B31.16		
WELDED JOINTS: PER ASME B31.17		
WELDED JOINTS: PER ASME B31.18		
WELDED JOINTS: PER ASME B31.19		
WELDED JOINTS: PER ASME B31.20		
WELDED JOINTS: PER ASME B31.21		
WELDED JOINTS: PER ASME B31.22		
WELDED JOINTS: PER ASME B31.23		
WELDED JOINTS: PER ASME B31.24		
WELDED JOINTS: PER ASME B31.25		
WELDED JOINTS: PER ASME B31.26		
WELDED JOINTS: PER ASME B31.27		
WELDED JOINTS: PER ASME B31.28		
WELDED JOINTS: PER ASME B31.29		
WELDED JOINTS: PER ASME B31.30		
WELDED JOINTS: PER ASME B31.31		
WELDED JOINTS: PER ASME B31.32		
WELDED JOINTS: PER ASME B31.33		
WELDED JOINTS: PER ASME B31.34		
WELDED JOINTS: PER ASME B31.35		
WELDED JOINTS: PER ASME B31.36		
WELDED JOINTS: PER ASME B31.37		
WELDED JOINTS: PER ASME B31.38		
WELDED JOINTS: PER ASME B31.39		
WELDED JOINTS: PER ASME B31.40		
WELDED JOINTS: PER ASME B31.41		
WELDED JOINTS: PER ASME B31.42		
WELDED JOINTS: PER ASME B31.43		
WELDED JOINTS: PER ASME B31.44		
WELDED JOINTS: PER ASME B31.45		
WELDED JOINTS: PER ASME B31.46		
WELDED JOINTS: PER ASME B31.47		
WELDED JOINTS: PER ASME B31.48		
WELDED JOINTS: PER ASME B31.49		
WELDED JOINTS: PER ASME B31.50		
WELDED JOINTS: PER ASME B31.51		
WELDED JOINTS: PER ASME B31.52		
WELDED JOINTS: PER ASME B31.53		
WELDED JOINTS: PER ASME B31.54		
WELDED JOINTS: PER ASME B31.55		
WELDED JOINTS: PER ASME B31.56		
WELDED JOINTS: PER ASME B31.57		
WELDED JOINTS: PER ASME B31.58		
WELDED JOINTS: PER ASME B31.59		
WELDED JOINTS: PER ASME B31.60		
WELDED JOINTS: PER ASME B31.61		
WELDED JOINTS: PER ASME B31.62		
WELDED JOINTS: PER ASME B31.63		
WELDED JOINTS: PER ASME B31.64		
WELDED JOINTS: PER ASME B31.65		
WELDED JOINTS: PER ASME B31.66		
WELDED JOINTS: PER ASME B31.67		
WELDED JOINTS: PER ASME B31.68		
WELDED JOINTS: PER ASME B31.69		
WELDED JOINTS: PER ASME B31.70		
WELDED JOINTS: PER ASME B31.71		
WELDED JOINTS: PER ASME B31.72		
WELDED JOINTS: PER ASME B31.73		
WELDED JOINTS: PER ASME B31.74		
WELDED JOINTS: PER ASME B31.75		
WELDED JOINTS: PER ASME B31.76		
WELDED JOINTS: PER ASME B31.77		
WELDED JOINTS: PER ASME B31.78		
WELDED JOINTS: PER ASME B31.79		
WELDED JOINTS: PER ASME B31.80		
WELDED JOINTS: PER ASME B31.81		
WELDED JOINTS: PER ASME B31.82		
WELDED JOINTS: PER ASME B31.83		
WELDED JOINTS: PER ASME B31.84		
WELDED JOINTS: PER ASME B31.85		
WELDED JOINTS: PER ASME B31.86		
WELDED JOINTS: PER ASME B31.87		
WELDED JOINTS: PER ASME B31.88		
WELDED JOINTS: PER ASME B31.89		
WELDED JOINTS: PER ASME B31.90		
WELDED JOINTS: PER ASME B31.91		
WELDED JOINTS: PER ASME B31.92		
WELDED JOINTS: PER ASME B31.93		
WELDED JOINTS: PER ASME B31.94		
WELDED JOINTS: PER ASME B31.95		
WELDED JOINTS: PER ASME B31.96		
WELDED JOINTS: PER ASME B31.97		
WELDED JOINTS: PER ASME B31.98		
WELDED JOINTS: PER ASME B31.99		
WELDED JOINTS: PER ASME B31.100		

# Fixed Pillar

SIZE DWG. NO. **A** REV

SCALE: 1:2 WEIGHT: SHEET 2 OF 5

4 in quantity



PROPRIETARY AND CONFIDENTIAL  
 THE INFORMATION CONTAINED ON THIS  
 DRAWING IS THE SOLE PROPERTY OF  
 WESTERN COMPANY MANUFACTURING  
 CORPORATION & PART OF AS A WHOLE  
 WITHOUT THE WRITTEN PERMISSION OF  
 WESTERN COMPANY MANUFACTURING  
 CORPORATION

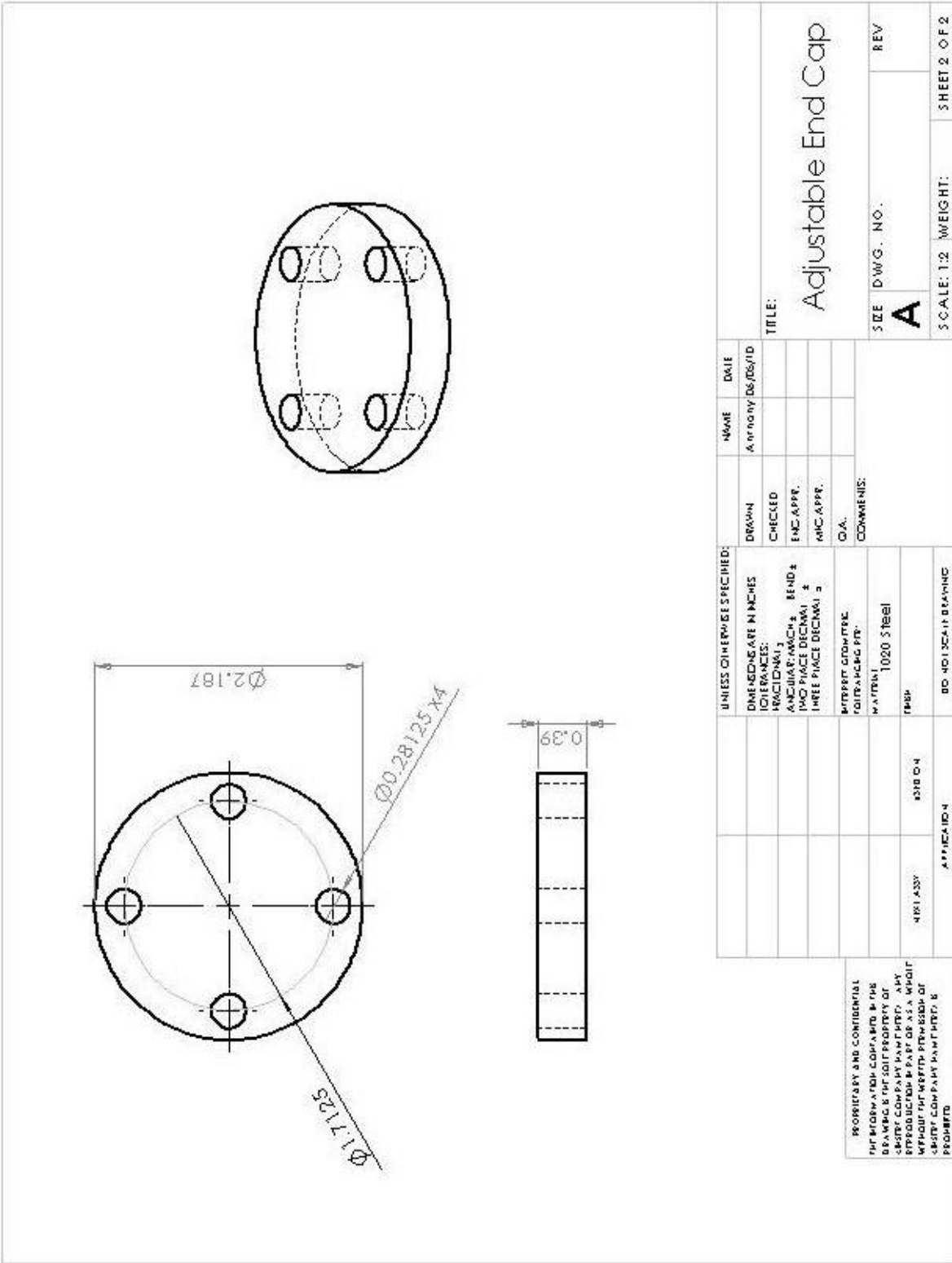
UNLESS OTHERWISE SPECIFIED:		NAME		DATE	
DIMENSIONS ARE IN INCHES	TOLERANCES:	DRAWN		A. HORNBY	05/05/10
FRACTIONAL	ANGULAR: ±0.004	CHECKED			
DECIMAL: ±0.0005	BEND: ±0.002	ENG. APPR.			
THREE PLACE DECIMAL: ±0.0005		MFG. APPR.			
		Q.A.			
		COMMENTS:			
		MATERIAL:			
		FINISH:			
		DR. NO. 134.11 DRAWING			
		APPLICATION			

# Actuator Housing

SIZE: DWG. NO. \_\_\_\_\_ REV \_\_\_\_\_

**A**

SCALE: 1:2 WEIGHT: \_\_\_\_\_ SHEET 1 OF 2



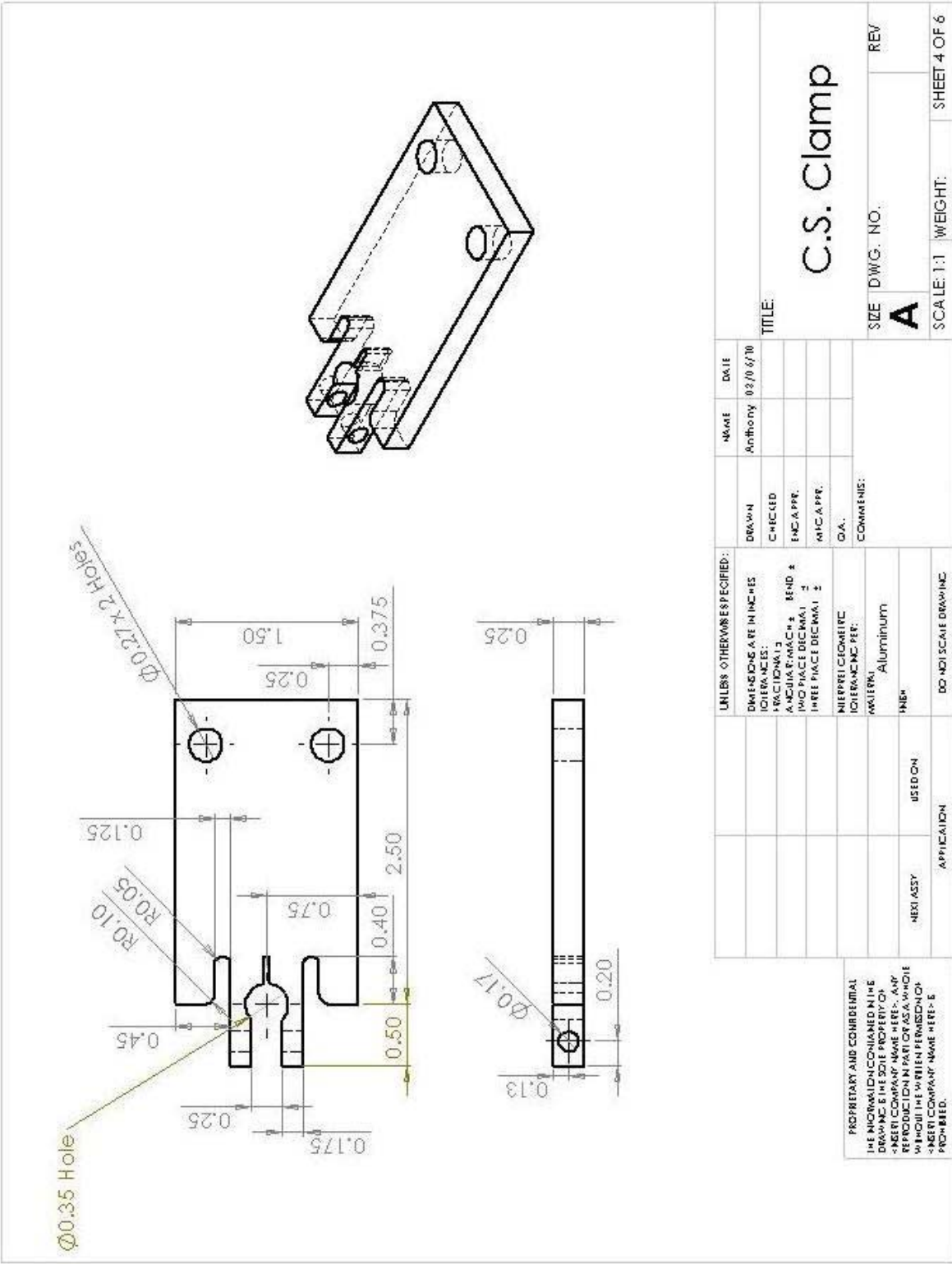
PROPRIETARY AND CONFIDENTIAL  
 THIS INFORMATION, COMPANY LOGO, AND THE  
 DESIGN ARE THE SOLE PROPERTY OF  
 CRYSTAL COMMUNICATIONS PART # 4331  
 WITHOUT THE WRITTEN PERMISSION OF  
 CRYSTAL COMMUNICATIONS PART # 4331  
 PROHIBITED

UNLESS OTHERWISE SPECIFIED:		NAME	DATE
DIMENSIONS ARE IN INCHES	DRAWN	A. HENRY	05/05/10
TOLERANCES:	CHECKED		
FRACTIONAL 1	ENG. APPR.		
ANGULAR: MACH 2 BEND 4	MFG. APPR.		
TWO PLACE DECIMAL 3	C.A.		
THREE PLACE DECIMAL 5	COMMENTS:		
MATERIAL: 1020 STEEL			
FINISH: BUSH			
4331-4331 4331 0-4	DO NOT SCALE DRAWING		
APPLICATION			

TITLE: Adjustable End Cap

SIZE: D/W/G. NO. A REV

SCALE: 1:2 WEIGHT: SHEET 2 OF 2



PROPRIETARY AND CONFIDENTIAL  
 THE INFORMATION CONTAINED IN THIS  
 DRAWING IS THE SOLE PROPERTY OF  
 INERTEC COMPANY. NAME HERE. ANY  
 REPRODUCTION IN PART OR AS A WHOLE  
 WITHOUT THE WRITTEN PERMISSION OF  
 INERTEC COMPANY IS PROHIBITED.

UNLESS OTHERWISE SPECIFIED:		DRAWN		NAME	DATE
DIMENSIONS ARE IN INCHES		CHECKED		Anthony	02/06/10
FRACTIONS 1/16		END APPR.			
DECIMALS 0.0004		MFG APPR.			
HOLE SIZE DECIMAL 1/16		D.A.			
HOLE SIZE DECIMAL 1/16		COMMENTS:			
MATERIAL: ALUMINUM		SIZE DWG. NO.			REV
FINISH:		A			
APPLICATION		SCALE: 1:1		WEIGHT:	SHEET 4 OF 6
USED ON		1			
NEXT ASSY		2			
APPLICATION		3			
USED ON		4			
NEXT ASSY		5			

# C.S. Clamp



## References

- [1] R. Mock and K. Lubitz, "Piezoelectric Injection Systems," *Springer Series in Materials Science*, vol. 114, pp. 299-310, 2008.
- [2] R. Bosch, *Diesel-Engine Management*, 4th ed. West Sussex: John Wiley & Sons Ltd., 2005.
- [3] G. Dober, S. Tullis, G. Greeves, N. Milovanovic, M. Hardy, and S. Zuelch, "The Impact of Injection Strategies on Emissions Reduction and Power output of Future Diesel Engines," *SAE International*, 2008.
- [4] M. Oki, S. Matsumoto, Y. Toyoshima, K. Ishisaka, and N. Tsuzuki, "180MPa Piezoelectric Common Rail System," *SAE International*, 2006.
- [5] "Sensor Product Overview," SensorTech, Ed.: Iron Media, 2008.
- [6] "Designing with Piezoelectric Transducers: Nanopositioning Fundamentals," P. Instrumente, Ed., 2005.
- [7] B. J. MacLachlan, N. Elvin, C. Blaurock, and N. J. Keegan, "Piezoelectric valve actuator for flexible diesel operation," *Smart Structures and Materials*, vol. 5388, pp. 167-178, 2004.
- [8] M. v. Schoor, E. Prechtel, B. Masters, B. MacLachlan, and P. Makar, "Innovative Technology for Clean, Lean, and Mean Diesel Fuel Injection," *SAE International*, 2002.
- [9] P. Bouchiloux, R. Le Letty, N. Lhermet, G. Patient, F. Claeysen, and M. Lang, "Application of Amplified Piezoelectric Actuators to the Construction of Gas Valves," *Proceedings of SPIE - The International Society for Optical Engineering*, vol. 5054, pp. 309-319, 2003.
- [10] M. P. Cooke, "Fuel Injector," U. S. P. a. T. Office, Ed.: Delphi Technologies, Inc., 2009.

- [11] M. P. Hardy, C. A. Goat, M. P. Cooke, A. J. Hargreaves, and J.-F. Berlemont, "System and Method for Operating A Piezoelectric Fuel Injector," U. S. P. a. T. Office, Ed.: Delphi Technologies, Inc., 2008.
- [12] A. E. Catania, A. Ferrari, and M. Manno, "Development and Application of a Complete Multijet Common-Rail Injection-System Mathematical Model for Hydrodynamic Analysis and Diagnostics," *Journal of Engineering for Gas Turbines and Power*, vol. 130, 2008.
- [13] M. Coppo, C. Dongiovanni, and C. Negri, "A Linear optical sensor for measuring needle displacement in common-rail diesel injectors," *Sensors and Actuators, A: Physical*, vol. 134, pp. 366-373, 2007.
- [14] A. Ficarella and D. Laforgia, "Injection Characteristics Simulation and Analysis in Diesel Engines," *Meccanica*, vol. 28, pp. 239-248, 1993.
- [15] P. W. Alexander, D. Brei, W. Miao, J. W. Halloran, R. L. Gentilman, G. E. Schmidt, P. T. McGuire, and J. R. Hollenbeck, "Fabrication and experimental characterization of d31 telescopic piezoelectric actuators," *Journal of Materials Science*, vol. 36, pp. 4231-4237, 2001.
- [16] S. Chakrabarti and M. J. Dapino, "Design and modeling of a hydraulically amplified magnetostrictive actuator for automotive engine mounts," *Proceedings of SPIE - The International Society for Optical Engineering*, vol. 7290, 2009.
- [17] H.-S. Yoon, G. Washington, P. Eyabi, M. Radhamohan, S. W. Woodard, and R. Dayton, "A millimeter-stroke piezoelectric hybrid actuator using hydraulic displacement amplification mechanism," *IEEE International Symposium on Industrial Electronics*, vol. 4, pp. 2809-2813, 2006.

- [18] "Handbook for Disc Springs," Schnorr Corporation, Ed., 2003.
- [19] G. Barillaro, A. Molfese, A. Nannini, and F. Pieri, "Analysis, simulation and relative performances of two kinds of serpentine springs," *Journal of Micromechanics and Microengineering*, vol. 15, pp. 736-746, 2005.
- [20] A. P. Boresi and R. J. Schmidt, *Advanced Mechanics of Materials*, 6 th ed.: John Wiley & Sons Ltd., 2003.
- [21] "McMaster-Carr Online Catalog," McMaster-Carr, Ed., 2010.
- [22] N.-H. Chung, B.-G. Oh, and M.-H. Sunwoo, "Modelling and injection rate estimation of common-rail injectors for direct-injection diesel engines," *Proceedings of the Institution of Mechanical Engineers, Part D: Journal of Automobile Engineering*, vol. 222, pp. 1089-1101, 2008.
- [23] R. R. Craig, *Mechanics of Materials*, 2nd ed.: John Wiley & Sons, Inc., 2000.
- [24] J. B. Heywood, *Internal Combustion Engine Fundamentals*: McGraw-Hill, Inc., 1988.
- [25] D. J. Inman, *Engineering Vibration*, 3rd ed.: Pearson Education, Inc., 2007.
- [26] J. W. Lee, K. D. Min, K. Y. Kang, C. S. Bae, E. Giannadakis, M. Gavaises, and C. Arcoumanis, "Effect of piezo-driven and solenoid-driven needle opening of common-rail diesel injectors on internal nozzle flow and spray development," *International Journal of Engine Research*, vol. 7, pp. 489-502, 2006.
- [27] S. W. Park, J. W. Kim, and C. S. Lee, "Effect of injector type on fuel-air mixture formation of high-speed diesel sprays," *Proceedings of the Institution of Mechanical Engineers, Part D: Journal of Automobile Engineering*, vol. 220, pp. 647-659, 2006.

- [28] F. Payri, J. M. Lujan, C. Guardiola, and G. Rizzoni, "Injection diagnosis through common-rail pressure measurement," *Proceedings of the Institution of Mechanical Engineers, Part D: Journal of Automobile Engineering*, vol. 220, pp. 347-357, 2006.
- [29] C. A. Randall, A. Kelnberger, G. Y. Yang, R. E. Eitel, and T. R. Shrout, "High Strain Piezoelectric Multilayer Actuators - A Material Science and Engineering Challenge," *Journal of Electroceramics*, vol. 14, pp. 177-191, 2005.
- [30] M. S. Senousy, F. X. Li, D. Mumford, M. Gadala, and R. K. N. D. Rajapakse, "Dynamic thermo-electro-mechanical performance of piezoelectric stack actuators," *Proceedings of SPIE - The International Society for Optical Engineering*, vol. 6526, 2007.
- [31] J. E. Shigley, R. G. Budynas, and C. R. Mischke, *Mechanical Engineering Design*, 7th ed.: McGraw-Hill College, 2003.
- [32] "Parker O-ring Handbook ORD 5700," Parker Hannifin Corporation, Ed., 2007.